FREAK WAVES IN CROSSING SEA WITH COUNTERPROPAGATING WAVE SYSTEMS

by

LISA BÆVERFJORD RYE

THESIS

for the degree of

MASTER OF SCIENCE

(Master i Anvendt matematikk og mekanikk)

Faculty of Mathematics and Natural Sciences
University of Oslo

May 2014

Det matematisk- naturvitenskapelige fakultet
Universitetet i Oslo

FREAK WAVES IN CROSSING SEA WITH COUNTERPROPAGATING WAVE SYSTEMS

by

LISA BÆVERFJORD RYE

Abstract

This work presents a theoretical and experimental investigation on the statistical properties of the surface elevation in a special case of crossing sea conditions. The special case considered is the case of two irregular wave trains propagating in opposite directions, with the same characteristic frequency ω_c and wave number k_c. The modulational instability of two crossing Stokes waves according to two coupled nonlinear Schrödinger equations describing the problem is investigated. Experiments are performed in the Hydrodynamic Laboratory at the University of Oslo, Blindern. The stability analysis shows that the unstable domain of the perturbation is reduced in the case of a crossing sea compared to a non-crossing sea, at the same time as the growth rates are reduced. Such behaviour is usually interpreted as an indication that the occurrence of extreme events is reduced. Experimental results show that the kurtosis, a measure of the probability of the occurrence of extreme events, is generally lower for crossing sea than non-crossing sea.

Acknowledgement

I would like to thank the Department of Mathematics at the University of Oslo, for providing me with the opportunity of carrying out this Master thesis.

I would like to express my appreciation to my supervisor, Professor Karsten Trulsen, for introducing me to the field of freak waves, and being my mentor in this exciting and challenging field of study. Thank you for inspiration, advice and endless enthusiasm during the work on this thesis.

Furthermore, I would like to thank Tore Magnus Taklo for invaluable help and instruction in the laboratory, and Jostein Kolaas for advice regarding post-processing of experimental data. I would also like to thank Odin Gramstad for enlightening me on important literature for my analysis of modulational instability.

I thank my parents, Grete Bæverfjord and Morten Rye, for their faith in me and all the moral support they have given me over the years. You have taught me that nothing is impossible, this is something I will always keep in mind. Also, thank you for invaluable help in the completion of this work.

Finally, I would like to thank my fellow student Anne Raustøl for valuable cooperation during the last year, and particularly the last few months working on this thesis. You made long and challenging days less tiring by laughing at my bad jokes and joining me in the consumption of way too much chocolate and Pepsi Max (PM). I would not have gotten this far without you.

This work has been supported by the Research Council of Norway (RCN) grant 214556/F20 for the activities in the laboratory.

Lisa Bæverfjord Rye
Oslo, May 2014

Contents

Chapter 1

Introduction

A freak wave is an abnormally large wave, in the extreme tail of a probability distribution. A classic criterion is that the wave height is more than two times the significant wave height H_s (Dysthe *et al.*, 2008), which means that a freak wave is very large compared to the other waves in a given sea state.

Crossing sea has traditionally been considered to have a larger occurrence of freak waves than non-crossing sea. It has been speculated in whether or not a freak wave due to crossing sea might have caused the sinking of the oil tanker Prestige off the coast of Spain in 2002 (Lechuga, 2006; Osborne, 2015). The cruise ship Louis Majesty was hit by a freak wave in 2010, and two people were killed. Following this accident it has been speculated in whether or not the freak wave occurred due to a crossing sea state (Cavaleri *et al.*, 2012). In light of these two recent disasters it has become clear that more knowledge is required, on freak waves generally, and crossing sea especially. The lack of such knowledge may have an impact on legal aspects, as well as economical and safety considerations of maritime industries.

The existence of two simultaneous wave systems on the sea surface is well documented by buoy measurements (Guedes Soares, 1984, 1991) and by hindcast data (Boukhanovsky & Guedes Soares, 2009). Over the last decade there has been a special attention on that a crossing sea state can be a source of increased modulational instability. Modulational instability, the exponential growth of unstable sidebands (or perturbations) such that a steady-state wave (such as a Stokes wave) is broken, is known as a mechanism that can produce freak waves. It has been shown that a two-wave system is more subject to modulational instability than a one-wave system (Okamura, 1984; Onorato *et al.*, 2006; Gramstad & Trulsen, 2011), and therefore might have especially large occurrence of freak waves. Increased modulational instability for crossing Stokes waves is often taken to be an indicator that freak waves might occur in a realistic ocean wave spectrum, despite the fact that a stability analysis of Stokes waves may not be relevant for a finite-width spectrum like the JONSWAP spectrum.

Apparently it is believed (personal communication, Karsten Trulsen), by some wave forecasters with experience from areas where crossing seas often occur, that realistic crossing seas likely have fewer freak wave occurrences than comparable non-crossing seas. This does not exclude, however, the possibility that crossing seas are dangerous in the sense that waves have unexpected (e.g. pyramidical)

shapes and arrive from unexpected locations. Theoretical studies of crossing Stokes waves have on the other hand shown that crossing sea is more subject to modulational instability (Okamura, 1984; Onorato *et al.*, 2006; Gramstad & Trulsen, 2011), thus the freak wave activity might be enhanced. These two opinions are unquestionably contradicting.

By studying a special case of crossing sea, both theoretically and experimentally, we wish to contribute to the understanding of whether or not crossing sea has a higher occurrence of freak waves than a non-crossing sea. The special case considered is two wave trains propagating in opposite directions, with the same characteristic wave frequency ω_c and wave number k_c. For the experiments, waves are generated from a JONSWAP spectrum, which allows us to consider realistic ocean waves which are not particularly subject to modulational instability (Alber, 1978).

1.1 Deterministic description of crossing sea

If we use a characteristic steepness ϵ as an ordering parameter we can imagine that the surface elevation of the wave train consists of contributions to different (relative) orders

$$\eta = \eta_1 + \epsilon\eta_2 + \epsilon^2\eta_3 + ...$$

where the first order linear part of the wave train consists of two wave trains propagating to the right and to the left

$$\eta_1 = \eta_{1,h} + \eta_{1,v}$$

where

$$\eta_{1,h} = \frac{1}{2}B_h \mathrm{e}^{\mathrm{i}(k_c x - \omega_c t)} + c.c.$$

and

$$\eta_{1,v} = \frac{1}{2}B_v \mathrm{e}^{\mathrm{i}(-k_c x - \omega_c t)} + c.c.$$

where c.c. denotes the complex conjugate. Up to second order the wave field looks something like this, where $B_{2,?}$ are complex amplitudes except $B_{2,0}$ which is real

$$\begin{aligned}\eta_2 = B_{2,0} + \frac{1}{2}\big(&B_{2,h}\mathrm{e}^{\mathrm{i}(k_c x - \omega_c t)} + B_{2,v}\mathrm{e}^{\mathrm{i}(-k_c x - \omega_c t)} + B_{2,2h}\mathrm{e}^{2\mathrm{i}(k_c x - \omega_c t)} \\ &+B_{2,2v}\mathrm{e}^{2\mathrm{i}(-k_c x - \omega_c t)} + B_{2,2x}\mathrm{e}^{2\mathrm{i}k_c x} + B_{2,2t}\mathrm{e}^{-2\mathrm{i}\omega_c t} + c.c.\big)\end{aligned}$$

The complex conjugate applies to all $B_{2,?}$ inside the parenthesis.
We assume an irrotational velocity field, and we have similar expansions for the velocity potential ϕ.

If we take the analysis up to third order we find two coupled nonlinear Schrödinger equations for the complex amplitudes $B_?$, the equations look something like this:

$$\frac{\partial B_h}{\partial t} + \frac{\omega_c}{2k_c}\frac{\partial B_h}{\partial x} + \frac{i\omega_c}{8k_c^2}\frac{\partial^2 B_h}{\partial x^2} + \frac{i}{2}\omega_c k_c^2 |B_h|^2 B_h + \alpha |B_v|^2 B_h = 0$$
$$\frac{\partial B_v}{\partial t} - \frac{\omega_c}{2k_c}\frac{\partial B_v}{\partial x} + \frac{i\omega_c}{8k_c^2}\frac{\partial^2 B_v}{\partial x^2} + \frac{i}{2}\omega_c k_c^2 |B_v|^2 B_v + \beta |B_h|^2 B_v = 0$$

1.1.1 Pre-project

In a pre-project for this thesis perturbation analysis has already been performed to determine exactly all the 2nd order coefficients $B_{2,0}$, $B_{2,h}$, $B_{2,v}$, $B_{2,2h}$, $B_{2,2v}$, $B_{2,2x}$ and $B_{2,2t}$. It has also been established what the coupling coefficients α and β in the two coupled nonlinear Schrödinger equations look like. This was done by:

- Taking the perturbation analysis up to third order to derive the coupled nonlinear Schrödinger equations
- Reading relevant articles and explaining to which degree these equations have been derived and studied earlier

The pre-project was not conducted as a part of this master thesis, but must be considered as a separate work. The project was conducted from Dec 13, 2013 to Jan 20, 2014, and is here included as Appendix C. The appended version has been corrected, see notes in the Appendix.

1.2 Previous work and motivation

1.2.1 Modulational instability

Over the last decade, wave systems characterised by two different spectral peaks, also known as crossing sea states, have become of particular interest in the community of ocean waves. There has been special attention on that crossing sea can be a source of both increased modulational instability and probability of freak waves. Modulational instability is known for possibly causing freak waves, and it has been speculated in whether or not crossing sea therefore might have especially large occurrence of freak waves.

Okamura (1984) investigated the modulational instability of a standing wave consisting of two crossing Stokes waves. To investigate the stability of the standing wave, Okamura used the Zakharov equation formalism (Zakharov, 1968) to derive a set of two coupled nonlinear Schrödinger (CNLS) equations describing two wave systems propagating in opposite directions. The stability of the single Stokes wave (the Benjamin-Feir instability) was also investigated in terms of a nonlinear Schrödinger equation. He found that, for the standing wave, a new region of instability occured, and the growth rate of this new region was the largest. Hence, the standing wave was more subject to modulational instability than a single travelling Stokes wave.

Two coupled nonlinear Schrödinger equations were also derived by Onorato *et al.* (2006), with the same starting point as Okamura (1984). While Okamura (1984) considered the special case of two wave trains propagating in opposite directions, Onorato *et al.*'s analysis was more extensive as it considered different angles between the wave trains. A stability analysis was performed directly on the equations, by considering two plane wave solutions of the equations with the same wavenumber and frequency, given small perturbations in amplitude and phase. A nonlinear dispersion relation was obtained, and was solved numerically. Results showed that the instability region and the growth rates were larger when a two-wave system was considered.

Gramstad & Trulsen (2011) extended the coupled equations given in Onorato *et al.* (2006), by deriving a set of two coupled fourth-ordered NLS equations for the more general case of two two-dimensional wave systems with different wave numbers or directions. Stability analysis of two interacting Stokes waves with small perturbations demonstrated that new regions of instability appeared for the coupled system compared to the result of each of the wave systems alone.

1.2.2 Numerical simulations and laboratory experiments

The CNLS equations derived in Onorato *et al.* (2006) were studied further in Shukla *et al.* (2006*a*). A nonlinear dispersion relation was derived, and solved numerically to obtain the regions and associated growth rates of the modulational instability. Furthermore, the long-term evolution of the nonlinear instability was followed by means of computer simulations of the governing nonlinear equations. Two crossing Stokes waves with the same constant amplitude were considered, and the instability was seeded by a low-amplitude noise. This simulation revealed that two water waves can, when nonlinear interactions are taken into account, give rise to novel behaviour such as the formation of localised large-amplitude coherent wave packets. This behaviour was very different from that of a single Stokes-wave which experienced the standard Benjamin-Feir instability and dissolved into a wide spectrum of waves.

Grönlund *et al.* (2009) also studied the development of two interacting Stokes waves with constant amplitudes. To seed the instability and generate multiple realisations for each parameter setting, a small-amplitude noise was added. The dynamics of the two interacting waves was simulated using a pseudo-spectral method, with periodic boundary conditions and the fourth-ordered Runge-Kutta algorithm as time integrator. The conclusion from the simulations was that an increased probability of freak waves was observed in a two-wave system compared with an uncoupled system.

Onorato *et al.* (2010) included numerical tests to verify if, in more realistic conditions, the predictions of crossing sea being more unstable than crossing sea were reasonable. First, the modulational instability of two plane wave solutions travelling at an angle with the x-axis was investigated, for perturbations only along the x-axis of propagation. For the numerical simulations, two wave systems with the exact same frequency were considered. Each of the wave systems was characterised by a JONSWAP spectrum with random phases. Numerical simu-

lations were performed using a higher-order spectral method, for the two wave systems propagating with different angles to the x-axis. The results showed that the probability of freak waves, indicated by the kurtosis, i.e., the fourth order moment of the probability density function of the surface elevation, depends on the angle with the x-axis with which the two wave systems propagate.

Laboratory experiments and numerical simulations were performed by Toffoli *et al.* (2011), to investigate the statistical properties of the surface elevation in crossing sea conditions. For the experiments, irregular waves were mechanically generated according to an input directional spectrum composed by the sum of two identical JONSWAP spectra. The JONSWAP spectra described long-crested wave fields, propagating along two different directions. Each of the spectra had the same peak period and steepness. Due to limitations of the experimental facilities, only angles between the wave systems of up to 40° were considered. To support the experimental results qualitatively, numerical simulations with initial conditions nominally identical to the ones applied in the tank were performed. Fortunately, numerical computations for large angles did not present any limitations, and the numerical simulations were extended up to an angle of 90° between the wave systems. Both experimental and numerical results indicated that the kurtosis, a measure of the probability of occurrence of extreme waves, depended on the angle between the crossing systems. Numerical simulations furthermore suggested that a maximum value was achieved for an angle between the systems of 40° to 60°.

1.2.3 Study objectives

Modulational instability is commonly considered as a possible reason for the formation of freak waves. Experiments and numerical investigations in this field are scarce. Modulational instability, being something tangible, might give an indication of the probability of freak events, and has been used for this purpose by several authors. The main conclusion of the stability analysis for modulational instability, which all authors mentioned above agree on, is that both instability regions and growth rates have increased when considering a two-wave compared to a one-wave system. Hence, all authors have concluded that two crossing Stokes waves are more subject to modulational instability than a non-crossing system. The question is, however, how much does this have to do with real life? The ocean, unlike a Stokes wave, can be represented by a finite-width spectrum, which is less subject to Benjamin-Feir instability. Thus, considerations regarding modulational instability might be of less relevance than commonly anticipated. In contrast, experiments and numerical simulations using finite-width spectra are important tools for predicting the occurrence of freak waves under natural conditions.

In the pre-project, two coupled nonlinear Schrödinger (CNLS) equations were derived, for the special case of two wave systems, each described by a finite-width spectrum, crossing at an angle of 180°, i.e. travelling in opposite directions. A stability analysis of these CNLS equations was done to indicate whether or not crossing sea has a higher occurrence of freak waves than a non-crossing sea.

Previous experiments and numerical simulations (Onorato *et al.*, 2010; Toffoli *et al.*, 2011) show us that the kurtosis, a measure of the probability of the

occurrence of extreme events, depends on the angle between the two crossing systems. Experiments have not been conducted, however, in such a manner that one can compare a non-crossing sea to a crossing sea, to see under otherwise equal conditions how the kurtosis changes when going from a one-wave to a two-wave system. The wave tank in the hydrodynamic laboratory at the University of Oslo is suitable to study this special case experimentally. Irregular wave trains can be generated from a JONSWAP spectra, and their propagation along the wave tank can be studied. Crossing sea can be obtained by inserting a reflecting wall in the far end of the wave tank. This provides two irregular wave trains crossing at 180°, with the same characteristic frequency and wavenumber, but a slightly different amplitude. The surface elevation can be measured and the kurtosis can be calculated. This way, the probability of extreme events in both a non-crossing and crossing sea can be investigated.

Okamura (1984) studied the modulational instability of two Stokes waves crossing at an angle of 180°, others have had 180° as a limiting angle in their analysis. However, experimental studies were never conducted for such large angles. Thus, there is no literature to which this study can be compared directly. To support the experimental results qualitatively, numerical simulations would the best approach. However, these simulations fall outside the scope of this work.

The work for this master thesis was done in parallel with the master thesis of Anne Raustøl. While we both have been studying the occurrence of freak waves, Raustøl has investigated the freak waves over variable depth, whereas this thesis studies freak waves in the special case of crossing sea. I have worked closely with Raustøl for parts of this thesis, especially the experimental arrangements and performance of the experiments.

1.3 Research questions

This master thesis should be regarded as a part of a long-term research activity at the University of Oslo, aiming at enhancing the understanding of freak waves in crossing sea. The main purpose of the research is determining whether or not crossing sea is more dangerous than non-crossing sea. More dangerous in this case means the properties of the surface elevation being further from Gaussian statistics. To be able to say something about this, it is necessary to find suitable modifications of the probability distributions of wave crests, the Rayleigh distribution to first order and the Tayfun distribution to second order, for crossing sea. It is also necessary to investigate whether or not the Hilbert transform is an applicable tool for calculating wave height for crossing sea, as using it assumes zero bandwidth. This thesis was focused on the two following activities:

1.3.1 The behaviour of the coupled nonlinear Schrödinger equations

The modulational instability of two Stokes waves propagating in opposite directions was studied. This represents an extension of the Benjamin-Feir instability for the special case of crossing sea. In particular, the two complex amplitudes B_h

and B_v were allowed to have different magnitudes $a_?$ and phases $\psi_?$.

Our results were compared to previous works, to find out whether or not this stability analysis was performed earlier. It was of particular interest to find out whether or not previous works were limited to the special case when $B_h = B_v$.

1.3.2 Laboratory experiments

A wave tank with an absorbing beach in one end as well as an insertable reflecting wall was used to compare the case of an irregular wave field propagating in one direction (non-crossing sea) to the case of crossing sea. The surface elevation was recorded and statistical properties were calculated in order to describe the occurrence of freak waves.

1.4 Outline

In Chapter 2 selected theoretical concepts are presented and described, important for the analytical work in this thesis. These include stochastic description of the surface elevation, definition of a narrowbanded process, characteristics of wave spectra, et cetera.

Chapter 3 presents the statistics of a narrowband wave train. Starting from the deterministic description of the surface elevation presented in Section 1.1, and assuming a narrowbanded process, theoretical values for variance, skewness and kurtosis are derived.

In Chapter 4 the modulational instability for the special case of two wave trains propagating in opposite directions is investigated. Starting from the nonlinear Schrödinger equations found in the pre-project, and finding equilibrium solutions which are then perturbed, leads to a nonlinear dispersion relation which can be solved numerically. A literature study of previous works on this topic is also included.

Chapter 5 explains in detail preparation for experiments, the experimental setup, as well as the post processing of the data.

In Chapter 6, results of the experiments are presented, and in Chapter 7 they are discussed. A concluding remark is presented, regarding what was found in this study as well as possible future work.

Chapter 2

Theoretical framework

2.1 The surface elevation as a stochastic process

2.1.1 Fundamentals of stochastic variables

The most central concept in probability theory is that of a *random* (or *stochastic*) variable (Krogstad & Arntsen, 2006). A stochastic variable Z is a rule that assigns a number z^j to each result j. Example: throwing a dice. Every time j you throw the dice, you get a number z^j. The stochastic variable Z is the rule that tells you to throw the dice and get a number. So a random variable is actually a function, where we do not know anything about the input. All we can see is the output, and we need to deduce all properties of the function by observing this. We can say something about the distribution of the outcomes. The *cumulative distribution function* is defined as follows:

$$F_Z(z) = P\{Z \leq z\} \tag{2.1}$$

The notation $\{Z \leq z\}$ refers to the collection of all outcomes z_0 of the stochastic variable Z such that $z_0 \leq z$ (Trulsen, 2006). Special properties of F are

$$\begin{aligned} F_Z(-\infty) &= 0 \\ F_Z(\infty) &= 1 \end{aligned}$$

and F must be an increasing function. The derivative of the cumulative distribution function is called the *probability density*

$$\begin{aligned} f_Z(z) &= \frac{dF_Z(z)}{dx} \\ F_Z(z) &= \int_{-\infty}^{x} f_Z(\xi)\,\mathrm{d}\xi \end{aligned}$$

Note that

$$\begin{aligned} f_Z(z) &\geq 0 \\ \int_{-\infty}^{\infty} f_Z(z)\,\mathrm{d}x &= 1 \end{aligned}$$

The *expected value* μ of a stochastic variable Z is defined as the weighted average

$$\mu = E[Z] = \int_{-\infty}^{\infty} z f_Z(z)\,\mathrm{d}z \tag{2.2}$$

Similarly, for a function $g(Z)$, the expected value is

$$\mu = E[g(Z)] = \int_{-\infty}^{\infty} g(z) f_Z(z)\,\mathrm{d}z$$

Note that the expectation operator E is linear. Suppose we have two functions $g(Z)$ and $h(Z)$ and two constants α and β. Then,

$$E[\alpha g(Z) + \beta h(Z)] = \alpha E[g(Z)] + \beta E[h(Z)]$$

The *variance* σ^2 of a stochastic variable Z is defined by

$$\sigma^2 = Var[Z] = E[(Z-\mu)^2] = \int_{-\infty}^{\infty} (z-\mu)^2 f_Z(z)\,\mathrm{d}z \tag{2.3}$$

The square root of the variance of a stochastic variable is called the *standard deviation*, and is symbolised by σ. The *nth moment* of a stochastic variable Z is given by

$$m_n = E[Z^n] = \int_{-\infty}^{\infty} z^n f_Z(z)\,\mathrm{d}z$$

while the *nth centered moment* is

$$E[(Z-\mu)^n] = \int_{-\infty}^{\infty} (z-\mu)^n f(z)\,\mathrm{d}z$$

It can be shown that $\mu = m_1$ and $\sigma^2 = m_2 - m_1^2$.

The *skewness* γ of a stochastic variable is defined as the third centred moment normalised by the cube of the standard deviation

$$\gamma = \frac{E[(Z-\mu)^3]}{\sigma^3} = \frac{m_3 - 3\sigma^2\mu - \mu^3}{\sigma^3} \tag{2.4}$$

The skewness is a measure of the asymmetry of the probability distribution of a real-valued random variable about its mean. The skewness value can be positive or negative, or even undefined. The qualitative interpretation of the skewness is complicated. For a unimodal distribution, negative skewness indicates that the tail on the left side of the probability density function is longer or fatter than the right side - it does not distinguish these shapes. For instance, a zero value indicates that the tails on both sides of the mean balance out, which is the case

both for a symmetric distribution, and for asymmetric distributions where the asymmetries even out.

The *kurtosis* κ of a stochastic variable is defined as the fourth centered moment normalised by the square of the variance

$$\kappa = \frac{E[(Z-\mu)^4]}{\sigma^4} = \frac{m_4 - 4\gamma\sigma^3\mu - 6\sigma^2\mu^2 - \mu^4}{\sigma^4} \tag{2.5}$$

In a similar way to the concept of skewness, kurtosis is a descriptor of the shape of a probability distribution. It gives us information about the weight of the distribution compared to the standard deviation. A normal (Gaussian) distribution has $\kappa = 3$. If $\kappa > 3$, the distribution has more weight on the tails, and the occurrence of extreme events is higher than what is "normal". Both skewness and kurtosis will be useful tools for us when analysing surface elevation data measured in the lab.

2.1.2 Stochastic description of surface waves

We wish to account for the vertical displacement $\eta(\mathbf{r}, t)$ of the water surface as a function of horizontal position $\mathbf{r} = (x, y)$ and time t. It is our everyday experience that ocean waves are random and unpredictable, given otherwise identical conditions (wind, etc.). We may therefore think of the surface displacement as a *stochastic process* with several possible outcomes or *realisations* (Trulsen, 2006). All properties of a stochastic variable, given in the previous section, are also valid for a stochastic process. For instance, the expected value of a stochastic process $Z(t)$ is

$$\mu(t) = \mathrm{E}[Z(t)] = \int_{-\infty}^{\infty} z f(z;t)\,\mathrm{d}z$$

A stochastic process also has some additional properties compared with a stochastic variable. The *autocorrelation function* of the stochastic process $Z(t)$ is defined as

$$R(t_1, t_2) = \mathrm{E}[Z(t_1)Z(t_2)] = \int_{-\infty}^{\infty}\int_{-\infty}^{\infty} z_1 z_2 f(z_1, z_2; t_1, t_2)\,\mathrm{d}z_1\,\mathrm{d}z_2$$

A stochastic process is said to be *weakly stationary* if the expected value is constant with respect to time, $\mathrm{E}[Z(t)] = \mu$, and the autocorrelation function does not depend on t explicitly, but only depends on a time lag $\tau = t_2 - t_1$. Hence, for a weakly stationary process, $R(t_1, t_2) = \mathrm{E}[Z(t_1)Z(t_2)] = R(\tau)$.

The *frequency spectrum* of a weakly stationary process is defined as the Fourier transform of the autocorrelation function $R(\tau)$. Whereas the Fourier transform is in principle undetermined by a multiplicative constant, the spectrum becomes uniquely defined by the constraint that the integral of the spectrum over the domain of the frequency axis that is used, should be equal to the variance of the process. The desired Fourier transform pair is

$$S(\omega) = \frac{1}{\pi}\int_{-\infty}^{\infty} R(\tau)\mathrm{e}^{i\omega\tau}\,\mathrm{d}\tau \tag{2.6}$$

$$R(\tau) = \frac{1}{2}\int_{-\infty}^{\infty} S(\omega)\mathrm{e}^{-i\omega\tau}\,\mathrm{d}\omega \tag{2.7}$$

The j^{th} *moment* m_j of a frequency spectrum $S(\omega)$ is defined as (Ochi, 1998)

$$m_j = \int_0^\infty \omega^j S(\omega)\,\mathrm{d}\omega \tag{2.8}$$

A stochastic process $Z(t)$ is said to be *ergodic* if all statistical properties of the ensemble are equal to those for a single record $Z(t)$ taken for a sufficiently long period of time (Ochi, 1998). For the remainder of this master thesis it has been assumed, but not justified, that the surface elevation can be considered a weakly stationary, ergodic process.

2.1.3 Narrowbanded process

A stochastic process $Z(t)$ is said to be *narrowbanded* if the spectral density function (frequency spectrum) is sharply concentrated in the neighbourhood of a specified frequency ω_c (Ochi, 1998). An estimate of the bandwidth is

$$\delta = \frac{\hat{\sigma}}{\omega_c}$$

where $\hat{\sigma}$ is the standard deviation of the spectral density function. Hence, the magnitude of δ depends to a great extent on the frequency range where the dominant wave energy exists. A stochastic process is said to be narrowbanded when

$$\delta << 1$$

The surface elevation can be expressed as

$$\eta(t) = \sum_{n=1}^{\infty} a_n \cos(\omega_n t) + b_n \sin(\omega_n t) = \frac{1}{2} B(t) \mathrm{e}^{-i\omega_c t} + c.c.$$

where $B(t)$ is a complex amplitude

$$B(t) = \sum_{n=1}^{\infty} (a_n + i b_n) \mathrm{e}^{-i(\omega_n - \omega_c)t}$$

For an extremely narrowbanded process, the complex amplitude B(t) will have infinitesimal contributions from frequencies other than the ones very close to ω_c. This means $B(t)$ simplifies to

$$B(t) = a + ib$$

where a and b are Gaussian distributed with $\mu = 0$ and variance σ^2. Probability density functions for a and b are given as

$$f_a(a) = \frac{1}{\sqrt{2\pi}\sigma} \mathrm{e}^{-\frac{a^2}{2\sigma^2}}$$

and

$$f_b(b) = \frac{1}{\sqrt{2\pi}\sigma} \mathrm{e}^{-\frac{b^2}{2\sigma^2}}$$

We wish to show that the amplitude $A = |B|$ is Rayleigh distributed, by using the cumulative distribution function to find the probability density function for A.

$$\begin{aligned} F_A(z) &= P\{A = \sqrt{a^2 + b^2} \leq z\} \\ &= \iint\limits_{\sqrt{a^2+b^2} \leq z} \frac{1}{2\pi\sigma^2} \mathrm{e}^{-\frac{a^2+b^2}{2\sigma^2}} \, \mathrm{d}a \, \mathrm{d}b \end{aligned}$$

Transforming into polar coordinates, we have $a = r\cos\theta$, $b = r\sin\theta$, and the Jacobian determinant is

$$\frac{\partial(a,b)}{\partial(r,\theta)} = r$$

This leads to

$$\begin{aligned} F_A(z) &= \int_0^{2\pi} \int_0^z \frac{1}{2\pi\sigma^2} \mathrm{e}^{-\frac{r^2}{2\sigma^2}} r \, \mathrm{d}r \, \mathrm{d}\theta \\ &= \int_0^z \frac{r}{\sigma^2} \mathrm{e}^{-\frac{r^2}{2\sigma^2}} \, dr \\ \Rightarrow f_A(r) &= \frac{r}{\sigma^2} \mathrm{e}^{-\frac{r^2}{2\sigma^2}} \quad \text{for } r \geq 0 \end{aligned} \tag{2.9}$$

We have shown that the amplitude of the surface elevation for an extremely narrowbanded process is Rayleigh distributed.

2.1.4 Wave envelope process

For a narrowbanded process the magnitude of the amplitude varies slowly with time; its frequency is much smaller than the frequency of the carrier wave, ω_c (Ochi, 1998). This implies that upper and lower envelopes can be drawn by connecting peaks and troughs, respectively. Thereby the statistical properties of peaks and troughs may be evaluated through the envelope process instead of dealing directly with the amplitude. The *envelope process* is defined as a pair of symmetric curves which pass through the wave crests and troughs, and it represents a measure of change of wave amplitude in the time domain.

An estimate for the wave height H of a narrowbanded process is two times the amplitude, $H = 2A(t)$, or two times the envelope, $H = 2E(t)$. When the surface elevation is taken to be a narrowbanded stochastic process, the crests and troughs are assumed to occur at the same time. In the previous section we showed that the amplitude of the surface elevation in this case is Rayleigh distributed, (2.9).

In a similar manner it can be shown that an estimate of the wave height, given as $H = 2A$, also is Rayleigh distributed.

The envelope process for a given wave record $\eta(t)$ can be evaluated by applying the concept of the Hilbert transform. For a real-valued function $\eta(t)$ in the interval $-\infty < \eta < \infty$, the Hilbert transform of η, denoted $\tilde{\eta}$, is defined as

$$\tilde{\eta}(t) = \frac{1}{\pi} \int_{-\infty}^{\infty} \frac{\eta(\tau)}{t - \tau} \, \mathrm{d}\tau$$

and the envelope $E(t)$ is defined by Ochi (1998) as

$$E(t) = \sqrt{\{\eta(t)\}^2 + \{\tilde{\eta}(t)\}^2} \tag{2.10}$$

2.2 Characteristics of wave spectra

The shape of wave spectra, in general, varies considerably depending on the severity of wind velocity, time duration of wind blowing, fetch length, etc (Ochi, 1998). Consider the situation of winds blowing with constant velocity over the sea surface. The wave spectrum reaches an upper limit under a given constant wind velocity; namely, a state of energy saturation in which a balance is set up between the rate at which energy is gained from the wind and the rate at which it is lost either by breaking or by nonlinear wave-wave interaction. This situation is called a fully-developed sea. For a fully developed sea the spectrum is a function of dimensionless frequency only.

2.2.1 Wave spectral formulations

The *Pierson-Moskowitz* spectral formulation was developed from analysis of measured data obtained in the North Atlantic by wave recorders installed on weather ships, and is defined as:

$$S_{PM}(f) = Ae^{-\frac{B}{f^4}}/f^5$$

A and B are related to the main sea state parameters. One possibility is to set

$$A = \frac{5}{16} Hm0^2 f_p^4$$
$$B = \frac{5}{4} f_p^4$$

where

$$Hm0 = 4\sqrt{m_0}$$

and m_0 is the zeroth spectral moment, see equation (2.8). f_p is the peak frequency. Another popular form has been the *JONSWAP spectrum*, which is defined by

$$S(f) = S_{PM}(f)\gamma^{exp(-(f-f_p)^2/(2\sigma^2 f_p^2))}$$

The parameter γ is called the *peak-shape parameter*, and it represents the ratio of the maximum spectral energy density to the maximum of the corresponding Pierson-Moskowitz spectrum. The value of the peak-shape parameter is usually chosen to be 3.30. The JONSWAP formulation is based on an extensive wave measurement program known as the Joint North Sea Wave Project carried out in 1968 and 1969 (Hasselmann *et al.*, 1973). The spectrum represents wind-generated seas with fetch limitation, and wind speed and fetch length are input to the formulation (Ochi, 1998). The fetch length is the length of water over which a given wind has blown.

The JONSWAP spectrum with $\gamma = 3.30$ is not narrowbanded, but we still chose it for generating waves for the experiments in the wave tank. The reason why we chose to use the JONSWAP spectrum is that we aim at studying crossing sea conditions that are realistic for the ocean, and with this in mind, the JONSWAP spectrum is our best choice. Alber (1978) presented empirical estimates for two JONSWAP spectra with bandwidths close to 0.08, which suggested that the two spectra were not subject to modulational instability. He then used his theories to argue that a typical JONSWAP spectrum is stable. As described in Section 1.2, we will be conducting experiments where irregular waves are generated from a JONSWAP spectrum. This means that the waves we will be studying, according to Alber, are not subject to modulational instability. In Chapter 4, however, we will be conducting a stability analysis for the equations that describe our special case of crossing sea. The reason that we will be performing this stability analysis, regardless of Alber's conclusion, is that there is a large and well-established tradition of using the modulational instability as an indicator of the potential a sea state has to develop extreme events. Also, most of the literature on this topic includes such an analysis, and to a certain extent we wish to be able to compare our results with previous works.

2.3 Exceedance probability

One way of investigating the relative number of extreme waves in a time series, is studying the *exceedance probability*. This is done by comparing the wave heights H found from the time series with theoretical values for the wave height (Rayleigh distribution).

Exceedance probability Pe is defined as the complimentary function of the cumulative distribution function F

$$Pe(z) = 1 - F(z)$$

While the cumulative distribution function F (given in equation 2.1) tells us probability that the outcome of a stochastic process is *lower than* a given value, the exceedance probability tells us the probability that the outcome will *exceed* a given value. By the definition given in Dysthe *et al.* (2008), a wave is freak if

$$H > 2H_s = 8\sigma$$

where H_s is the significant wave height, here defined as four times the standard deviation of the surface elevation. The *freak wave probability*, the probability that

the time series has an occurrence of one or more freak waves, will be given by the exceedance probability for a threshold of 8σ.

In Section 2.1.4 we have already established that the wave height for a narrowbanded process is Rayleigh distributed. We also explained how the Hilbert transform can be used to compute the envelope of a real-valued function $\eta(t)$. To calculate exceedance probability for a measured surface elevation $\eta(t)$, we need to find the wave heights from the time series. For the remainder of this thesis the surface elevation is considered a narrowbanded, stochastic process, and we will use the MATLAB function *hilbert* to approximate the wave heights. The function takes a real sequence x_r as input, and returns a complex helical sequence $x = x_r + ix_i$ where x_i is the Hilbert transform of x_r. This means that taking the absolute value of the output x of the *hilbert* function in MATLAB, will correspond to finding the envelope as defined in equation (2.10). We can then estimate the wave height as $H = 2|x|$.

2.4 Confidence intervals using bootstrapping

In this master thesis we wish to use measurements of the surface elevation for a certain amount of time, to say something about the properties of a certain sea state. The measured data can be seen as a sample of the sea surface under certain conditions. To say something about the properties (population parameters) of the ocean, we can for instance use confidence intervals. A confidence interval gives an estimated range of values which is likely to include an unknown population parameter, the estimated range being calculated from a given set of sample data.

2.4.1 Confidence intervals

A point estimate, because it is a single number, by itself provides no information about the precision or reliability of the estimation (Devore & Berk, 2007). An alternative to reporting a single sensible value for the parameter being estimated is to calculate and report an entire interval of plausible values - a *confidence interval* (CI). A confidence interval is always calculated by first selecting a confidence level, which is a measure of the degree of reliability of the interval. A confidence level of 95% for instance, implies that 95% of all samples would give an interval that includes μ, or whatever other parameter is being estimated, and only 5% of all samples would yield an erroneous interval. The higher the confidence lever, the more strongly we believe that the value of the parameter being estimated lies within the interval.

Information about the precision of an interval estimate is conveyed by the width of the interval. If the confidence level is high and the resulting interval is relatively narrow, our knowledge of the value of the parameter is reasonably precise.

2.4.2 Bootstrap confidence intervals

How can we find a confidence interval for a population parameter if the population distribution is not normal and the sample size n is not large? The bootstrap allows

us to calculate estimates in situations where there is no adequate statistical theory.

Bootstrapping is based on two concepts: 1) The best information we have about the population is the sample, and 2) Resampling from the sample produces a distribution very similar to repeated sampling from the population. If we really need to know what the population parameter is, we need to measure the entire population. But we cannot usually do that, so we take a sample. Every sample we take is likely to be different. We need to know how different these samples from the population are likely to be, to work out how far off the mark we could be with our estimate of the population parameter. We could take repeated samples of the population and work it out from there, but actually if we could do that we might as well take one big sample, or measure the population. The point is that we have only the sample data, and we wish to get the best possible information we can from it. So we pretend that the sample is the population. It is the best information we have about the population. Then, we take a whole lot of samples of the same size from our sample. We need to sample with replacement, otherwise every sample will be identical. These are called resamples or bootstrap samples.

Example: apples in an orchard

We wish to say something about the expected weight of an apple from an orchard. We take a sample of M apples from the orchard, and weigh them. We can now find the mean weight of the apples in the sample. We take a bootstrap sample of size m from this, since we sample with replacement, some of the values appear more often than they did in the original sample, and some do not appear. We get the computer to take N bootstrap samples like this, and calculate the mean weight for each of them. We are interested in the distribution of these values, as they give us a very good idea of how actual samples from the population are distributed. This is called a bootstrap distribution, and we use it to determine a bootstrap confidence interval by using the central 95% of the values. The lowest and highest value for the mean from these 95% are now the lower and upper limits for our 95% confidence interval. It is a fairly safe bet that the true value of the mean is one of the values in this confidence interval.

Chapter 3

Statistics of a narrowbanded wave train

In Chapter 1 it was determined that to first and second order, the surface elevation for crossing sea looks something like this:

$$\begin{aligned}\eta_1 &= \eta_{1,h} + \eta_{1,v} = \frac{1}{2}B_h \mathrm{e}^{\mathrm{i}\psi_h} + \frac{1}{2}B_v \mathrm{e}^{\mathrm{i}\psi_v} + c.c. + \mathcal{O}(\epsilon^2) \\ \eta_2 &= B_{2,0} + \frac{1}{2}\left(B_{2,h}\mathrm{e}^{\mathrm{i}\psi_h} + B_{2,v}\mathrm{e}^{\mathrm{i}\psi_v} + B_{2,2h}\mathrm{e}^{2\mathrm{i}\psi_h}\right. \\ &\quad \left. + B_{2,2v}\mathrm{e}^{2\mathrm{i}\psi_v} + B_{2,2x}\mathrm{e}^{2\mathrm{i}k_c x} + B_{2,2t}\mathrm{e}^{-2\mathrm{i}\omega_c} + c.c.\right) + \mathcal{O}(\epsilon^3)\end{aligned}$$

where $B_?$ are complex amplitudes, c.c. denotes the complex conjugate, and

$$\begin{aligned}\psi_h &= k_c x - \omega_c t \\ \psi_v &= -k_c x - \omega_c t\end{aligned}$$

In the pre-project, found in Appendix C, all the 2nd order coefficients $B_{2,0}$, $B_{2,h}$, $B_{2,v}$, $B_{2,2h}$, $B_{2,2v}$, $B_{2,2x}$ and $B_{2,2t}$ were determined exactly, and in section C.2.4 we ended up with

$$\eta_2 = \frac{1}{4}k_c\left(B_h^2 e^{2i\psi_h} + B_v^2 e^{2i\psi_v}\right) + c.c. + \mathcal{O}(\epsilon^3) \tag{3.1}$$

and similarly for the velocity potential

$$\begin{aligned}\phi_2 = a_{2,0} &- \frac{i}{2}\omega_c B_h B_v^* e^{2i\omega_c t_0} - \frac{1}{2k_c}\left(\frac{\partial B_h}{\partial t_1} + \omega_c \frac{\partial B_h}{\partial x_1} z\right) e^{i\psi_h + k_c z} \\ &- \frac{1}{2k_c}\left(\frac{\partial B_v}{\partial t_1} + \omega_c \frac{\partial B_v}{\partial x_1} z\right) e^{i\psi_v + k_c z} + c.c. + \mathcal{O}(\epsilon^3)\end{aligned}$$

$B_{2,h}$ and $B_{2,v}$ in the expression for the surface elevation have been set to zero by imposing certain demands on the corresponding velocity.

The formulations above are not limited to Stokes waves, but can be made more general by allowing the amplitudes and phases B_h, B_v, ψ_h and ψ_v to be slowly varying functions of time and space. In the following, analysis of a narrowband

wave train, which includes both Stokes waves and slowly modulating wave trains, is performed. The exact expression for the surface elevation to second order, (3.1), is used to find theoretical values for statistical properties like variance, skewness and kurtosis, which will later be compared with experimental results.

3.1 Useful properties

For simplification, a non-crossing sea to first order is considered. The surface elevation is obtained by setting $B_{?,?v} = 0$, and looks like this

$$\eta_{1,h} = \frac{1}{2} B_h \mathrm{e}^{i\psi_h} + c.c. + \mathcal{O}(\epsilon^2)$$

where B_h is a complex amplitude. Assuming B_h takes the form

$$B_h = a + ib$$

$\eta_{1,h}$ can be written in the following form

$$\eta_{1,h} = \frac{1}{2} B_h \mathrm{e}^{i\psi_h} + c.c. + \mathcal{O}(\epsilon^2) = a\cos\psi_h - b\sin\psi_h + \mathcal{O}(\epsilon^2)$$

where a and b are statistically independent, Gaussian distributed with $\mu = 0$ and variance σ^2:

$$\begin{aligned} \mathrm{E}[a] &= \mathrm{E}[b] = 0 \\ \mathrm{Var}[a] &= \mathrm{Var}[b] = \sigma^2 \end{aligned}$$

The probability densities for a and b are then given as

$$f_a(a) = \frac{1}{\sqrt{2\pi\sigma^2}} \mathrm{e}^{-\frac{a^2}{2\sigma^2}}$$

and

$$f_b(b) = \frac{1}{\sqrt{2\pi\sigma^2}} \mathrm{e}^{-\frac{b^2}{2\sigma^2}}$$

Rewriting a and b in polar coordinates

$$\begin{aligned} a &= A\cos\theta \\ b &= A\sin\theta \end{aligned}$$

and remembering the Jacobian

$$\frac{\partial(a,b)}{\partial(r,\theta)} = r$$

the probability densities for A and θ can be found:

$$\begin{aligned}
\mathrm{P}\left[\{a,b\} \in I\right] &= \iint_I f_a(a) f_b(b)\, da\, db \\
&= \iint_I \frac{1}{2\pi\sigma^2} \mathrm{e}^{-\frac{a^2+b^2}{2\sigma^2}}\, da\, db \\
&= \iint_I \frac{A}{2\pi\sigma^2} \mathrm{e}^{-\frac{A^2}{2\sigma^2}}\, dA\, d\theta \\
&= \iint_I \left(\frac{A}{\sigma^2} \mathrm{e}^{-\frac{A^2}{2\sigma^2}}\, dA\right)\left(\frac{1}{2\pi}\, d\theta\right)
\end{aligned} \tag{3.2}$$

The probability density in the first parenthesis corresponds to the Rayleigh distribution, and the latter corresponds to a uniform distribution. Hence, it has been shown that A is Rayleigh distributed and θ is uniformly distributed. Since the probability density can be factorized like this

$$f_{A\theta}(A,\theta) = f_A(A) f_\theta(\theta)$$

A and θ are statistically independent. Some integrals that will be useful in the following are:

$$\begin{aligned}
\mathrm{E}[A^n] &= \int_0^\infty A^n f_A(A)\, dA \\
\Rightarrow \mathrm{E}[A^2] &= \int_0^\infty A^2 \frac{A}{\sigma^2} \mathrm{e}^{-\frac{A^2}{2\sigma^2}}\, dA
\end{aligned}$$

Using partial integration leads to

$$\mathrm{E}[A^2] = 2\sigma^2 \tag{3.3}$$

and similarly for calculating

$$\mathrm{E}[A^4] = \int_0^\infty A^4 \frac{A}{\sigma^2} \mathrm{e}^{-\frac{A^2}{2\sigma^2}}\, dA$$

partial integration twice gives

$$\mathrm{E}[A^4] = 8\sigma^4 \tag{3.4}$$

Note that

$$\mathrm{E}[\mathrm{e}^{ni\theta}] = 0 \quad \text{for } n = \pm 1, \pm 2, \pm 3, \ldots \tag{3.5}$$

$$\mathrm{E}[\mathrm{e}^{0}] = 1 \tag{3.6}$$

3.2 First order

The expression for the surface elevation for non-crossing sea to first order is remembered to be

$$\begin{aligned}\eta_{1,h} &= a\cos\psi_h - b\sin\psi_h + \mathcal{O}(\epsilon^2) = A\cos\theta\cos\psi_h - A\sin\theta\sin\psi_h + \mathcal{O}(\epsilon^2)\\ &= A\cos(\theta+\psi_h) + \mathcal{O}(\epsilon^2) = \frac{1}{2}A\mathrm{e}^{i(\theta+\psi_h)} + c.c. + \mathcal{O}(\epsilon^2)\\ &= \frac{1}{2}B\mathrm{e}^{i\psi_h} + c.c. + \mathcal{O}(\epsilon^2)\end{aligned}$$

and the expected value of $\eta_{1,h}$ (given in section 2.1.1) can easily be computed:

$$\mu_{1,h} = \mathrm{E}[\eta_{1,h}] = \frac{1}{2}\mathrm{E}[A]\mathrm{E}[\mathrm{e}^{i\theta}]\mathrm{e}^{i\psi_h} + c.c. + \mathcal{O}(\epsilon^2) = 0 + \mathcal{O}(\epsilon^2) \tag{3.7}$$

because of (3.5). The variance to first order can be computed

$$\begin{aligned}\mathrm{Var}[\eta_{1,h}] &= \mathrm{E}[(\eta_{1,h}-\mu_{1,h})^2] = \mathrm{E}[\eta_{1,h}^2] = \mathrm{E}\left[\frac{1}{4}B_h^2\mathrm{e}^{2i\psi_h} + \frac{1}{2}|B_h|^2 + \frac{1}{4}(B_h^*)^2\mathrm{e}^{-2i\psi_h} + \mathcal{O}(\epsilon^3)\right]\\ &= \frac{1}{4}\mathrm{E}[A^2]\mathrm{E}[\mathrm{e}^{2i\theta}]\mathrm{e}^{2i\psi_h} + \frac{1}{2}\mathrm{E}[A^2] + \frac{1}{4}\mathrm{E}[A^2]\mathrm{E}[\mathrm{e}^{-2i\theta} + \mathcal{O}(\epsilon^3)]\mathrm{e}^{-2i\psi_h}\end{aligned}$$

Because of (3.5) the first and last terms vanish, and for the middle term (3.3) gives us

$$\mathrm{Var}[\eta_{1,h}] = \sigma^2 + \mathcal{O}(\epsilon^3) \tag{3.8}$$

Other properties that are of interest are the skewness and kurtosis. These are also defined in section 2.1.1:

$$\begin{aligned}\gamma &= \frac{E[(Z-\mu)^3]}{\sigma^3} = \frac{m_3 - 3\sigma^2\mu - \mu^3}{\sigma^3}\\ \kappa &= \frac{E[(Z-\mu)^4]}{\sigma^4} = \frac{m_4 - 4\gamma\sigma^3\mu - 6\sigma^2\mu^2 - \mu^4}{\sigma^4}\end{aligned}$$

For a zero-mean process (3.7) these expressions simplify to

$$\begin{aligned}\gamma_{1,h} = \frac{\mathrm{E}[\eta_{1,h}^3]}{\sigma^3} &= \frac{1}{\sigma^3}\mathrm{E}\left[\frac{1}{8}A^3\mathrm{e}^{3i(\theta+\psi)} + \frac{3}{8}A^3\mathrm{e}^{i(\theta+\psi)}\frac{3}{8}A^3\mathrm{e}^{-i(\theta+\psi)} + \frac{1}{8}A^3\mathrm{e}^{-3i(\theta+\psi)} + \mathcal{O}(\epsilon^4)\right]\\ &= 0 + \mathcal{O}(\epsilon)\end{aligned} \tag{3.9}$$

and

$$\begin{aligned}\kappa_{1,h} = \frac{\mathrm{E}[\eta_{1,h}^4]}{\sigma^4} &= \frac{1}{\sigma^4}\mathrm{E}\left[\frac{1}{16}A^4\mathrm{e}^{4i(\theta+\psi)} + \frac{4}{16}A^4\mathrm{e}^{2i(\theta+\psi)} + \mathcal{O}(\epsilon^4)\right]\\ &\quad + \frac{1}{\sigma^4}\mathrm{E}\left[\frac{6}{16}A^4\mathrm{e}^{0} + \frac{4}{16}A^4\mathrm{e}^{-2i(\theta+\psi)} + \frac{1}{16}A^4\mathrm{e}^{-4i(\theta+\psi)} + \mathcal{O}(\epsilon^4)\right]\\ &= \frac{1}{\sigma^4}\frac{6}{16}\mathrm{E}[A^4] + \mathcal{O}(\epsilon)\\ &= 3 + \mathcal{O}(\epsilon)\end{aligned} \tag{3.10}$$

using (3.4) and (3.5).

3.3 Second order

In (3.1) the surface elevation for crossing sea to second order is given. For simplification, non-crossing sea to second order is considered. Non-crossing sea is obtained by taking $B_{?,?v}$ to be zero. The surface elevation can be expressed more generally in the following form

$$\begin{aligned}\eta_{2,h} &= \frac{1}{2}B_h \mathrm{e}^{i\psi_h} + \frac{1}{2}\alpha B_h^2 \mathrm{e}^{2i\psi_h} + c.c. + \mathcal{O}(\epsilon^3) \\ &= \frac{1}{2}A\mathrm{e}^{i(\theta+\psi_h)} + \frac{1}{2}\alpha A^2 \mathrm{e}^{2i(\theta+\psi_h)} + c.c. + \mathcal{O}(\epsilon^3)\end{aligned}$$

where α is a complex number. The expected value of $\eta_{2,h}$ can be found using (3.5)

$$\begin{aligned}\mathrm{E}[\eta_{2,h}] &= \frac{1}{2}\mathrm{E}[A]\mathrm{E}[\mathrm{e}^{i\theta}]\mathrm{e}^{i\psi_h} + \frac{1}{2}\alpha \mathrm{E}[A^2]\mathrm{E}[\mathrm{e}^{2i\theta}]\mathrm{e}^{2i\psi_h} + c.c. + \mathcal{O}(\epsilon^3) \\ &= 0 + \mathcal{O}(\epsilon^3)\end{aligned} \tag{3.11}$$

The variance to second order is given as

$$\begin{aligned}\mathrm{Var}[\eta_{2,h}] = \mathrm{E}[\eta_{2,h}^2] &= \mathrm{E}\left[\frac{1}{4}A^2\mathrm{e}^{2i(\theta+\psi_h)} + \frac{1}{2}A^2 + \frac{1}{4}A^2\mathrm{e}^{-2i(\theta+\psi_h)}\right] \\ &+ \mathrm{E}\left[\frac{1}{4}\alpha A^3\mathrm{e}^{3i(\theta+\psi_h)} + \frac{1}{4}\alpha^* A^3\mathrm{e}^{-i(\theta+\psi_h)}\right] \\ &+ \mathrm{E}\left[\frac{1}{4}\alpha^* A^3\mathrm{e}^{-3i(\theta+\psi_h)} + \frac{1}{4}\alpha A^3\mathrm{e}^{i(\theta+\psi_h)} + \mathcal{O}(\epsilon^4)\right] \\ &= \sigma^2 + \mathcal{O}(\epsilon^4)\end{aligned} \tag{3.12}$$

For the calculation of skewness and kurtosis, contributions only come from terms that are not subject to (3.5)

$$\begin{aligned}\gamma_{2,h} = \frac{\mathrm{E}[\eta_{2,h}^3]}{\sigma^3} &= \frac{1}{\sigma^3}\mathrm{E}\left[\frac{3}{8}\alpha^* A^4 + \frac{3}{8}\alpha A^4 + \text{terms with } \mathrm{e}^{ni(\theta+\psi_h)} + \mathcal{O}(\epsilon^5)\right] \\ &= \frac{1}{\sigma^3}\left(3\alpha^*\sigma^4 + 3\alpha\sigma^4\right) + \mathcal{O}(\epsilon^2) \\ &= 6\sigma\mathrm{Re}(\alpha) + \mathcal{O}(\epsilon^2)\end{aligned} \tag{3.13}$$

$$\begin{aligned}\kappa_{2,h} = \frac{\mathrm{E}[\eta^4]}{\sigma^4} &= \frac{1}{\sigma^4}\mathrm{E}\left[\frac{6}{16}A^4 + \text{terms with } \mathrm{e}^{ni(\theta+\psi_h)} + \mathcal{O}(\epsilon^6)\right] \\ &= \frac{1}{\sigma^4}\frac{6}{16}\left(8\sigma^4\right) + \mathcal{O}(\epsilon^2) \\ &= 3 + \mathcal{O}(\epsilon^2)\end{aligned} \tag{3.14}$$

Comparing (3.9) and (3.13), it can be seen that the skewness becomes nonzero when taking the analysis up from first to second order. The expressions for mean, variance and kurtosis do not change, however. The expression for the surface elevation to second order, (3.1), tells us that $\alpha = \frac{1}{2}k_c$, when setting $B_{?,?v}$ to zero. In this case, the skewness to second order is $\gamma_{2,h} = 3\sigma k_c$.

It is interesting to compare the theoretical result for the skewness to the one found in Srokosz & Longuet-Higgins (1986). Equation (2.16) in this article states that for a narrowband process, the skewness to second order is given as

$$\lambda_3 = 6\pi s$$

where s is given in (2.15) in the same article as

$$s = \frac{\bar{a}k}{2\sqrt{2}\pi} \tag{3.15}$$

From the expression for the Rayleigh distribution, equation (2.3) in Srokosz & Longuet-Higgins (1986), it is seen that

$$\bar{a} = \sqrt{2}\sigma \tag{3.16}$$

and by inserting (3.16) into (3.15) the following is obtained:

$$s = \frac{\sigma k}{2\pi} \tag{3.17}$$

Finally, inserting (3.17) into (2.16) in the same article gave the same as (3.13) for the case studied in this work with $\alpha = \frac{1}{2}k_c$:

$$\lambda_3 = 3\sigma k_c \tag{3.18}$$

In Chapter 6, Figure (6.2), the theoretical values for the skewness of non-crossing sea are plotted together with the skewness found from experiments.

3.4 Third order

As shown in the previous section, the kurtosis to second order has a correction term of order ϵ^2. When taking the analysis up to third order, equation (32) in Mori & Janssen (2006) shows that this correction term for a narrowband process takes the following form

$$\kappa_{40} = 24\tilde{\epsilon}^2 \tag{3.19}$$

where $\tilde{\epsilon} = k_0\sqrt{m_0}$ and m_0 is the surface elevation variance. In this thesis, steepness is defined a little bit differently, with $\epsilon = k_c a_c$, where k_c is a characteristic wavenumber (for instance the peak wavenumber), and a_c is a characteristic amplitude. The characteristic amplitude is for this work chosen to be $a_c = \sqrt{2}\sigma$. This gives

$$\epsilon = k_c a_c = \sqrt{2}k_c\sigma = \sqrt{2}\tilde{\epsilon} \tag{3.20}$$

and the correction term ends up as

$$\kappa_{40} = 12\epsilon^2$$

This means that the kurtosis to third order is

$$\kappa = 3 + 12\epsilon^2 \tag{3.21}$$

As mentioned above, (3.19) is the correction term assuming a narrowband process. Mori & Janssen (2006) also define another version of this correction term, which considers a non-zero bandwidth

$$\kappa_{40} = \frac{\pi}{\sqrt{3}}\mathrm{BFI}^2 \tag{3.22}$$

This would give a kurtosis to third order

$$\kappa = 3 + \frac{\pi}{\sqrt{3}}\mathrm{BFI}^2 \tag{3.23}$$

The correction term is in this case a function of the Benjamin-Feir Index (BFI), which depends on the steepness and bandwidth of the wave field.

In Chapter 6, Figure (6.3), the theoretical values for the kurtosis of non-crossing sea are plotted together with the kurtosis found from experiments. Even though the process is not narrowbanded, due to the choice of the JONSWAP spectrum, the theoretical kurtosis from equation (3.21) is used for comparison with experimental results. This expression for the theoretical values of the kurtosis depends only on the steepness of the wave field, and assumes that the process is narrowbanded. The theoretical kurtosis in equation (3.23) would probably be a better approximation, but cannot be used because the bandwidth of the wave spectrum used for the experiments is not known.

3.5 Crossing sea

To be able to say something about the theoretical values for skewness and kurtosis of crossing sea, it would be necessary to say something about how much of the measured surface elevation that comes from right-going and left-going waves. When doing experiments in the lab the measured surface elevation η will consist of contributions to all orders. For experiments with reflecting wall, crossing sea is obtained, and η will consist of wave components to different orders travelling both to the right and to the left. To find out how much energy is contained in each of the components (and determine A_h and A_v), a two-dimensional Fourier analysis is necessary, which would allow us to study the dispersion relation for the surface elevation in the (k, ω)-plane. Such an analysis falls outside the scope of this master thesis, and therefore only theoretical values for the skewness and kurtosis of non-crossing sea will be compared to experimental results.

Chapter 4

Modulational Instability

Modulational instability, the exponential growth of unstable sidebands (or perturbations) such that a steady-state wave (such as a Stokes wave) is broken, is known as a mechanism that can produce freak waves. Over the last decade there has been a special attention on that a crossing sea state can be a source of increased modulational instability, and it has been speculated in whether or not crossing sea therefore might have especially large occurrence of freak waves.

The phenomenon was first discovered in 1967 by T. Brooke Benjamin and Jim E. Feir, for surface gravity waves on deep water. Therefore, it is also known as the Benjamin-Feir instability.

4.1 Modulational instability of NLS

The nonlinear Schrödinger equation (NLS) describes the evolution of the envelope of modulated wave groups, and it is thought to be important for explaining the formation of freak waves.

$$\frac{\partial B}{\partial t} + \frac{\omega_c}{2k_c}\frac{\partial B}{\partial x} + \frac{i\omega_c}{8k_c}\frac{\partial^2 B}{\partial x^2} - \frac{i\omega_c}{4k_c^2}\frac{\partial^2 B}{\partial y^2} + \frac{ik_c^2\omega_c}{2}|B|^2 B = 0 \tag{4.1}$$

A stability analysis of this equation was performed, with respect to spacial perturbations. An equilibrium solution was found, by assuming that the solution B of the equation did not vary in space (hence was not a function of x or y). This led to the simplified equation

$$\frac{\partial B}{\partial t} + \frac{ik_c^2\omega_c}{2}|B|^2 B = 0$$

A solution of the form

$$B = |B|e^{iarg(B)} = Re^{i\Psi}$$

was assumed. Inserted into the equation, this gave

$$\frac{\partial B}{\partial t} = \frac{\partial R}{\partial t}e^{i\Psi} + Ri\frac{\partial \Psi}{\partial t}e^{i\Psi} = -\frac{ik_c\omega_c^2}{2}|B|^2 B$$

The real part of this equation gave

$$\frac{\partial R}{\partial t} = 0$$
$$\Rightarrow R = C_1$$

which means R is a constant. The imaginary part of the equation gave

$$R\frac{\partial \Psi}{\partial t}e^{i\Psi} = -\frac{k_c^2\omega_c}{2}R^2 Re^{i\Psi}$$

B was eliminated from each side of the equation, and resulted in

$$\frac{\partial \Psi}{\partial t} = -\frac{k_c^2\omega_c}{2}R^2$$
$$\Rightarrow \Psi = -\frac{k_c^2\omega_c}{2}R^2 t + C_2$$

An expression for the equilibrium solution of (4.1) had now been found:

$$B = Re^{-\frac{i}{2}k_c^2\omega_c R^2 t}$$

The solution where $|B| = a$, and a is a real number, was chosen. Since $\epsilon = ak_c$

$$B_s = ae^{-\frac{i}{2}\epsilon^2\omega_c t}$$

Further simplification, by assuming $k_c = 1$, $\omega_c = 1$, yielded

$$B_s = ae^{-\frac{i}{2}a^2 t} \tag{4.2}$$

This is a Stokes wave, since it is a solution of the NLS equation under assumption of no modulation in space. The goal was to consider modulational instability of the Stokes wave in two horizontal dimensions. The Stokes wave B_s was given an infinitesimal perturbation $(\alpha(x,y,t), \beta(x,y,t))$:

$$B = B_s(1 + \alpha + i\beta)$$

The perturbed equilibrium solution was inserted into the simplified nonlinear Schrödinger equation

$$\frac{\partial B}{\partial t} + \frac{1}{2}\frac{\partial B}{\partial x} + \frac{i}{8}\frac{\partial^2}{\partial x^2} - \frac{i}{4}\frac{\partial^2 B}{\partial y^2} + \frac{i}{2}|B|^2 B = 0 \tag{4.3}$$

and this led to

$$-\frac{i}{2}a^3 e^{-\frac{i}{2}a^2 t}(1 + \alpha + i\beta) + ae^{-\frac{i}{2}a^2 t}\left(\frac{\partial \alpha}{\partial t} + i\frac{\partial \beta}{\partial t}\right)$$
$$+\frac{1}{2}ae^{-\frac{i}{2}a^2 t}\left(\frac{\partial \alpha}{\partial x} + i\frac{\partial \beta}{\partial x}\right) + \frac{i}{8}ae^{-\frac{i}{2}a^2 t}\left(\frac{\partial^2 \alpha}{\partial x^2} + i\frac{\partial^\beta}{\partial x^2}\right)$$
$$-\frac{i}{4}ae^{-\frac{i}{2}a^2 t}\left(\frac{\partial^2 \alpha}{\partial y^2} + i\frac{\partial^2 \beta}{\partial y^2}\right) + \frac{i}{2}a^3 e^{-\frac{i}{2}a^2 t}\left(\left((1+\alpha)^2 + \beta^2\right)(1 + \alpha + i\beta)\right) = 0$$

$B_s = ae^{-\frac{i}{2}a^2t}$ was eliminated from all terms, and the equation was linearised in α and β. After some calculation, the equation looked like

$$\begin{aligned}&\frac{\partial\alpha}{\partial t} + i\frac{\partial\beta}{\partial t} + \frac{1}{2}\frac{\partial\alpha}{\partial x} + \frac{i}{2}\frac{\partial\beta}{\partial x}\\ &\quad + \frac{i}{8}\frac{\partial^2\alpha}{\partial x^2} - \frac{1}{8}\frac{\partial^2\beta}{\partial x^2} - \frac{i}{4}\frac{\partial^2}{\partial y^2}\\ &\quad + \frac{1}{4}\frac{\partial^2\beta}{\partial y^2} + \frac{3i}{2}a^2\alpha = 0\end{aligned} \tag{4.4}$$

This equation was split up into real and imaginary parts, and the following pair of equations was obtained:

$$\frac{\partial\alpha}{\partial t} + \frac{1}{2}\frac{\partial\alpha}{\partial x} - \frac{1}{8}\frac{\partial^2\beta}{\partial x^2} + \frac{1}{4}\frac{\partial^2\beta}{\partial y^2} = 0 \tag{4.5}$$

$$\frac{\partial\beta}{\partial t} + \frac{1}{2}\frac{\partial\beta}{\partial x} + \frac{1}{8}\frac{\partial^2\alpha}{\partial x^2} - \frac{1}{4}\frac{\partial^2\alpha}{\partial y^2} + a^2\alpha = 0 \tag{4.6}$$

Finally, the perturbations α and β were assumed to take the following form

$$\begin{bmatrix}\alpha\\ \beta\end{bmatrix} = \begin{bmatrix}\hat{\alpha}\\ \hat{\beta}\end{bmatrix} e^{i(K_x x + K_y y - \Omega t)}$$

where

$$K_x, K_y \in \mathbb{R}$$

and

$$\Omega \in \mathbb{R} \ \vee \ \Omega \in \mathbb{C}$$

When inserted into equations for real and imaginary parts, this led to the following system of two equations

$$\begin{bmatrix}-i\Omega + \frac{i}{2}K_x & \frac{1}{8}K_x^2 - \frac{1}{4}K_y^2\\ -\frac{1}{8}K_x^2 + \frac{1}{4}K_y^2 + a^2 & -i\Omega + \frac{i}{2}K_x\end{bmatrix}\begin{bmatrix}\hat{\alpha}\\ \hat{\beta}\end{bmatrix} = \begin{bmatrix}0\\ 0\end{bmatrix} \tag{4.7}$$

In order for this system to have a non-trivial solution, the determinant of the coefficient matrix has to be zero. Hence,

$$\begin{aligned}&\left(-i\Omega + \frac{i}{2}K_x\right)^2 + \left(\frac{1}{8}K_x^2 - \frac{1}{4}K_y^2 - a^2\right)\left(\frac{1}{8}K_x^2 - \frac{1}{4}K_y^2\right) = 0\\ &\Rightarrow \Omega = \frac{1}{2}K_x \pm \sqrt{\left(\frac{1}{8}K_x^2 - \frac{1}{4}K_y^2 - a^2\right)\left(\frac{1}{8}K_x^2 - \frac{1}{4}K_y^2\right)}\end{aligned} \tag{4.8}$$

The perturbations α and β will grow unboundedly if Ω has an imaginary part. Hence, the system is unstable if

$$\left(\frac{1}{8}K_x^2 - \frac{1}{4}K_y^2 - a^2\right)\left(\frac{1}{8}K_x^2 - \frac{1}{4}K_y^2\right) < 0 \tag{4.9}$$

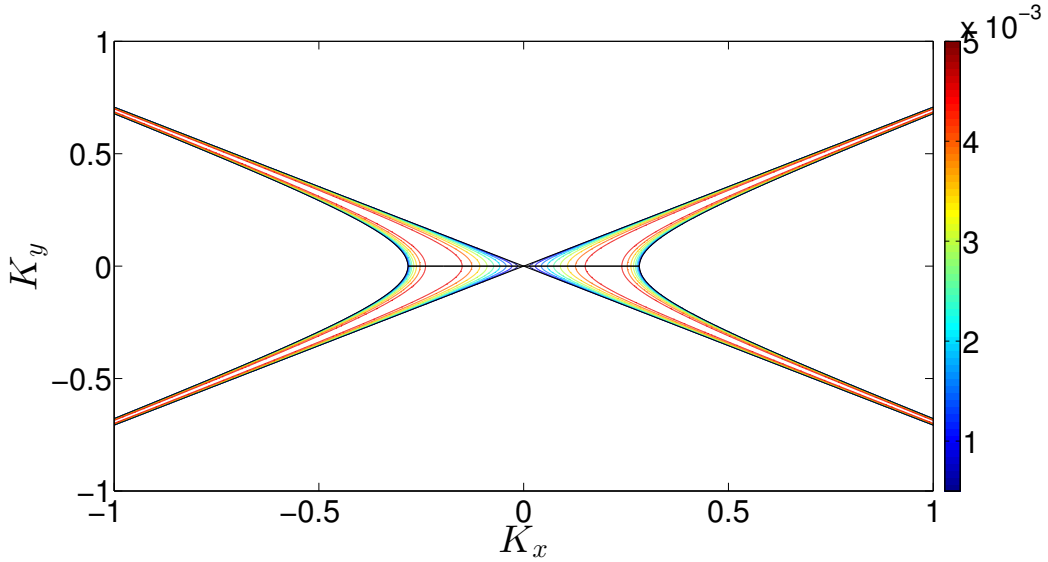

Figure 4.1: Growth rate for perturbation of Stokes wave.

The limits of the unstable region in the (K_x, K_y)-plane correspond to the two cases when

$$\begin{aligned} &\frac{1}{4}K_x^2 = \frac{1}{8}K_x^2 \\ &\Rightarrow K_y = \pm\frac{1}{\sqrt{2}}K_x \end{aligned} \tag{4.10}$$

which are straight lines, and

$$\frac{1}{8}K_x^2 - \frac{1}{4}K_y^2 = 0 \tag{4.11}$$

which is the equation for a hyperbola. The unstable region in the (K_x, K_y)-plane is plotted in Figure 4.1.

4.2 Coupled nonlinear Schrödinger equations

In the pre-project, found in Appendix C, coupled nonlinear Schrödinger (CNLS) equations were derived, which describe crossing sea in the special case of two wave trains with the same characteristic frequency ω_c and the same characteristic wave number k_c propagating in opposite directions:

$$\frac{\partial B_h}{\partial t} + \frac{\omega_c}{2k_c}\frac{\partial B_h}{\partial x} + \frac{i\omega_c}{8k_c^2}\frac{\partial^2 B_h}{\partial x^2} + \frac{i}{2}\omega_c k_c^2|B_h|^2 B_h + \frac{i}{4}\omega_c k_c^2|B_v|^2 B_h = 0$$
$$\frac{\partial B_v}{\partial t} - \frac{\omega_c}{2k_c}\frac{\partial B_v}{\partial x} + \frac{i\omega_c}{8k_c^2}\frac{\partial^2 B_v}{\partial x^2} + \frac{i}{2}\omega_c k_c^2|B_v|^2 B_v + \frac{i}{4}\omega_c k_c^2|B_h|^2 B_v = 0$$

These coupled equations were used to investigate the modulational instability of two Stokes waves propagating towards each other (an extension of the Benjamin-Feir instability) in the special case that the complex amplitudes B_h and B_v did not necessarily have same magnitudes and phases. First, equilibrium solutions for B_h and B_v were found. Like in section 4.1, the solutions were first assumed not to vary in space. The equations then simplifed to

$$\frac{\partial B_h}{\partial t} + \frac{i}{2}\omega_c k_c^2|B_h|^2 B_h + \frac{i}{4}\omega_c k_c^2|B_v|^2 B_h = 0 \tag{4.12}$$
$$\frac{\partial B_v}{\partial t} + \frac{i}{2}\omega_c k_c^2|B_v|^2 B_v + \frac{i}{4}\omega_c k_c^2|B_h|^2 B_v = 0 \tag{4.13}$$

The following was assumed:

$$B_{hs} = |B_{hs}|e^{iarg(B_{hs})} = R_h e^{i\Psi_h} \tag{4.14}$$
$$B_{vs} = |B_{vs}|e^{iarg(B_{vs})} = R_v e^{i\Psi_v} \tag{4.15}$$

Inserting (4.14) into (4.12) gave

$$\frac{\partial \Psi_h}{\partial t} = -\frac{1}{2}\left(R_h^2 + \frac{1}{2}R_v^2\right)$$
$$\Rightarrow B_{hs} = R_h e^{-\frac{i}{2}t\left(R_h^2 + \frac{1}{2}R_v^2\right)} \tag{4.16}$$

and similarly it was found that

$$B_{vs} = R_v e^{-\frac{i}{2}t\left(R_v^2 + \frac{1}{2}R_h^2\right)} \tag{4.17}$$

Now, modulational instability of the Stokes waves in one horizontal dimension was considered. B_{hs} and B_{vs} were assumed to have infinitesimal perturbations ($\alpha(x,t)$, $\beta(x,t)$, $\gamma(x,t)$, $\delta(x,t)$):

$$B_h = B_{hs}\left(1 + \alpha + i\beta\right) \tag{4.18}$$
$$B_v = B_{vs}\left(1 + \gamma + i\delta\right) \tag{4.19}$$

For simplification, $\omega_c = k_c = 1$ in the following, and the equilibrium solutions were inserted into the simplified NLS equations (4.12),(4.13). The following phases was defined:

$$\theta_1 = R_h^2 + \frac{1}{2}R_v^2 \tag{4.20}$$

$$\theta_2 = R_v^2 + \frac{1}{2}R_h^2 \tag{4.21}$$

Inserting (4.18), and (4.20) into (4.12):

$$\begin{aligned}
&-\frac{i}{2}\left(R_h^2 + \frac{1}{2}R_v^2\right) R_h e^{-\frac{i}{2}t\theta_1}\left(1+\alpha+i\beta\right) + R_h e^{-\frac{i}{2}t\theta_1}\left(\frac{\partial\alpha}{\partial t} + i\frac{\partial\beta}{\partial t}\right)\\
&+\frac{1}{2}R_h e^{-\frac{i}{2}t\theta_1}\left(\frac{\partial\alpha}{\partial x} + i\frac{\partial\beta}{\partial x}\right) + \frac{i}{8}R_h e^{-\frac{i}{2}t\theta_1}\left(\frac{\partial^2\alpha}{\partial x^2} + i\frac{\partial^2\beta}{\partial x^2}\right)\\
&+\frac{i}{2}R_h^2\left(\left(1+\alpha\right)^2+\beta^2\right)\left(1+\alpha+i\beta\right)R_h e^{-\frac{i}{2}t\theta_1}\\
&+\frac{i}{4}R_v^2\left(\left(1+\gamma\right)^2+\delta^2\right)\left(1+\alpha+i\beta\right)R_h e^{-\frac{i}{2}t\theta_1} = 0
\end{aligned}$$

Eliminating $B_{hs} = R_h e^{-\frac{i}{2}\theta_1 t}$ from all terms, linearising in (α,β) and splitting up into real and imaginary parts gave two equations

$$\frac{\partial\alpha}{\partial t} + \frac{1}{2}\frac{\partial\alpha}{\partial x} - \frac{1}{8}\frac{\partial^2\beta}{\partial x^2} = 0 \tag{4.22}$$

$$\frac{\partial\beta}{\partial t} + \frac{1}{2}\frac{\partial\beta}{\partial x} + \frac{1}{8}\frac{\partial^2\alpha}{\partial x^2} + R_h^2\alpha + \frac{1}{2}R_v^2\gamma = 0 \tag{4.23}$$

Similarly, inserting (4.19) and (4.21) into (4.13), eliminating, linearising and splitting up in real and imaginary parts gave two additional equations

$$\frac{\partial\gamma}{\partial t} - \frac{1}{2}\frac{\partial\gamma}{\partial x} - \frac{1}{8}\frac{\partial^2\delta}{\partial x^2} = 0 \tag{4.24}$$

$$\frac{\partial\delta}{\partial t} - \frac{1}{2}\frac{\partial\delta}{\partial x} + \frac{1}{8}\frac{\partial^2\gamma}{\partial x^2} + R_v^2\gamma + \frac{1}{2}R_h^2\alpha = 0 \tag{4.25}$$

Perturbations of the form

$$\begin{bmatrix}\alpha\\ \beta\\ \gamma\\ \delta\end{bmatrix} = \begin{bmatrix}\hat{\alpha}\\ \hat{\beta}\\ \hat{\gamma}\\ \hat{\delta}\end{bmatrix} e^{i(Kx-\Omega t)}$$

were assumed, where

$$K \in \mathbb{R}$$

and

$$\Omega \in \mathbb{R} \ \vee \ \Omega \in \mathbb{C}$$

When inserted into the 4x4 system constituted by (4.22) - (4.25), this led to the following system of four equations:

$$\begin{bmatrix} -i\Omega + \frac{i}{2}K & \frac{1}{8}K^2 & 0 & 0 \\ -\frac{1}{8}K^2 + R_h^2 & -i\Omega + \frac{i}{2}K & \frac{1}{2}R_v^2 & 0 \\ 0 & 0 & -i\Omega - \frac{i}{2}K & \frac{1}{8}K^2 \\ \frac{1}{2}R_h^2 & 0 & -\frac{1}{8}K^2 + R_v^2 & -i\Omega - \frac{i}{2}K \end{bmatrix} \begin{bmatrix} \hat{\alpha} \\ \hat{\beta} \\ \hat{\gamma} \\ \hat{\delta} \end{bmatrix} = \begin{bmatrix} 0 \\ 0 \\ 0 \\ 0 \end{bmatrix} \tag{4.26}$$

In order for this system to have a non-trivial solution, the determinant of the coefficient matrix has to be 0. This gives the dispersion relation

$$\begin{aligned} &\left[-\left(-\Omega + \frac{1}{2}K \right)^2 + \frac{1}{64}K^4 - \frac{1}{8}K^2 R_h^2 \right] * \\ &\left[-\left(\Omega + \frac{1}{2}K \right)^2 + \frac{1}{64}K^4 - \frac{1}{8}K^2 R_v^2 \right] - \frac{1}{256}R_h^2 R_v^2 K^4 = 0 \end{aligned} \tag{4.27}$$

which can be solved numerically.

Figure 4.2 shows the growth rates for the modulational instability as a function of k, for different amplitudes R_v of the reflected wave train. A double instability can be seen for all cases, i.e. the dispersion relation has two complex roots. Note that the mode with the highest growth rate has the same absolute value regardless of the amplitude of the reflected wave. Thus, the system is equally unstable for all cases.

It is interesting to compare this case of crossing sea with a single Stokes wave propagating in one direction. The energy density in a crossing sea with $R_v = R_h = a_c$ is $R_h^2 + R_v^2 = 2R_h^2 = 2a_c^2$. If only a single travelling Stokes wave is considered, and should have the same energy density as the crossing sea, it must have an amplitude $a_s = \sqrt{2}a_c$. Figure 4.3a shows the growth rate for this wave as well as for the crossing sea, in the case of $R_v = R_h = a_c$. The following is observed: For the crossing sea 1) the unstable domain is decreased, and 2) the growth rate is reduced. Hence, a conclusion can be drawn that a crossing sea which consists of two Stokes waves propagating in opposite directions is *less* subject to modulational instability than a single travelling Stokes wave with the same energy density.

In Figure 4.3b another case is considered. The two Stokes waves constituting the crossing sea each have the same amplitude a_c as the single Stokes wave a_s. This means the energy density is doubled for the crossing sea compared to the single travelling Stokes wave. In this case, the crossing sea and the non-crossing sea are equally unstable, we can see that the two curves overlap.

Finally, Figure 4.3c considers a case where the energy density is halved when going from a non-crossing to a crossing sea. The two Stokes waves constituting the crossing sea each have an amplitude $a_c = \frac{1}{2}a_s$, where a_s is the amplitude of the single travelling Stokes wave. This results in the energy density for the crossing sea being $2a_c^2 = 2(\frac{1}{2}a_s)^2 = \frac{1}{2}a_s^2$, which is half of the energy density of the non-crossing sea. Not surprisingly, when the energy density is lowered, the crossing

sea becomes less unstable than the non-crossing sea.

For Figure 4.3 a steepness of $\epsilon = 0.1$ is considered, Figure 4.4 shows the corresponding plots considering a steepness of $\epsilon = 0.06$.

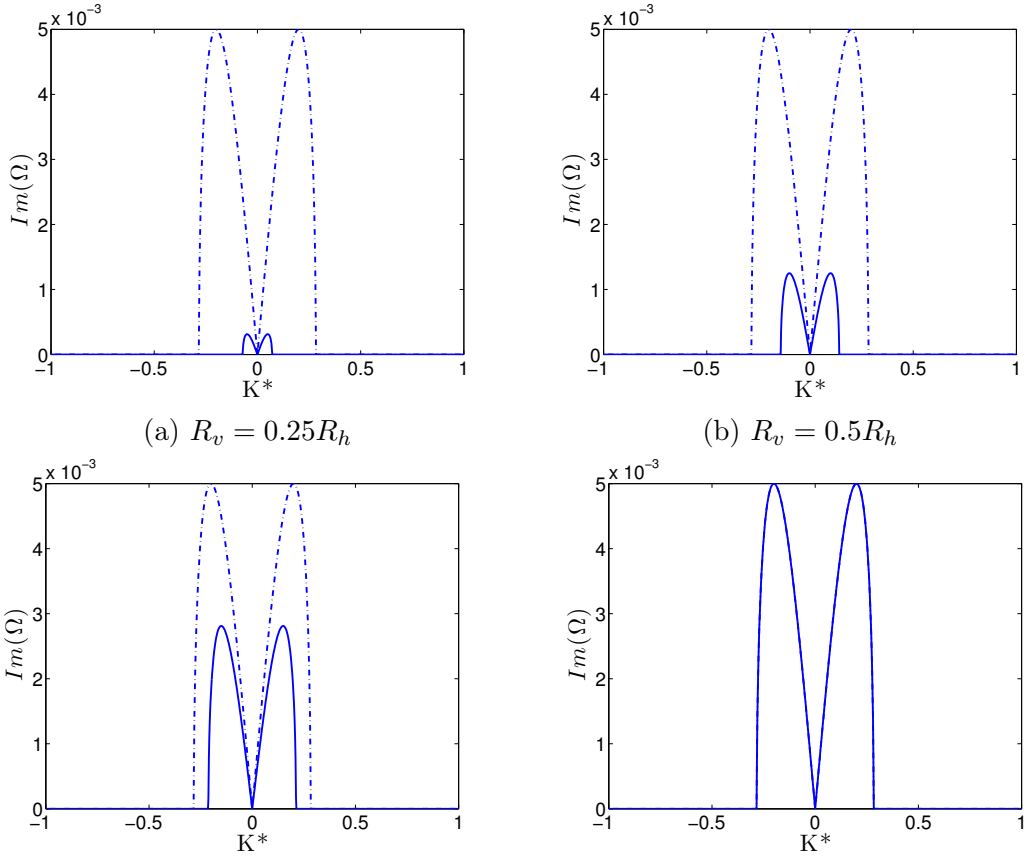

(a) $R_v = 0.25R_h$ (b) $R_v = 0.5R_h$

(c) $R_v = 0.75R_h$ (d) $R_v = R_h$

Figure 4.2: Growth rate for perturbation of two crossing Stokes waves. The instability has two modes, whereas the absolute value of the largest is the same regardless of the amplitude of the reflected wave R_v.

4.3 Previous works

It is of great interest to look into whether or not this stability analysis has been performed earlier, for the special case of counterpropagating Stokes waves.

4.3.1 Instabilities of weakly nonlinear standing gravity waves

Okamura (1984) was the first to compare the modulational instability of a travelling Stokes wave to the one of a standing wave. He compared resonant interaction among infinitesimal and carrier waves associated with the wave vectors $\mathbf{k_0}$ to the resonant interaction associated with wave vectors $\mathbf{k_0}$ and $-\mathbf{k_0}$. Okamura used the Zakharov equation formalism (Zakharov, 1968) to derive a set of two coupled nonlinear Schrödinger (CNLS) equations describing two wave systems propagating in

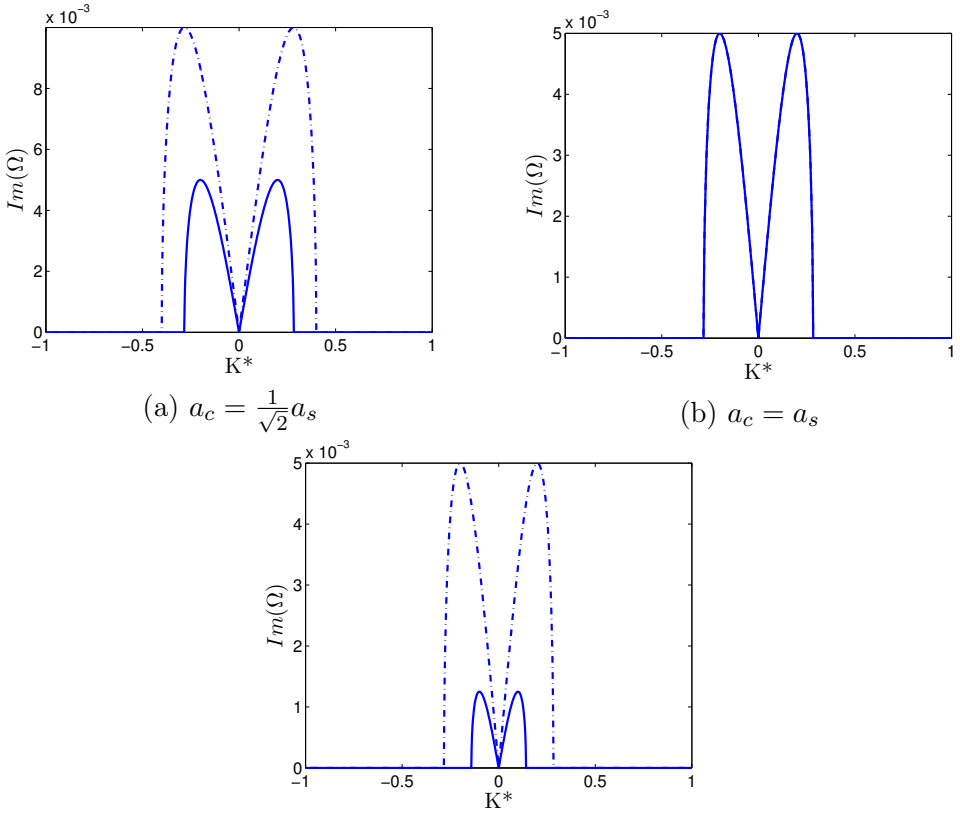

(a) $a_c = \frac{1}{\sqrt{2}} a_s$

(b) $a_c = a_s$

(c) $a_c = \frac{1}{2} a_s$

Figure 4.3: Case 1: $\epsilon \simeq 0.1$. Growth rate for perturbation of Stokes wave (dash-dotted line) and crossing sea (solid line) for different relationships between the amplitudes. a_s is the amplitude of the Stokes wave. The crossing sea is constituted of two Stokes waves travelling in opposite directions, each with an amplitude of a_c.

opposite directions. The stability of the single Stokes wave (the Benjamin-Feir instability) was also investigated in terms of a nonlinear Schrödinger equation. This is the same approach used in Section 4.2 for the stability analysis of the special case studied in this work.

The standing wave with infinitesimal amplitude a was by Okamura modelled by a superposition of two Stokes waves, each with an amplitude of $a/2$ and moving in opposite directions. This means that Okamura's standing wave had an energy density proportional to $2(\frac{a}{2})^2 = \frac{1}{2}a^2$, while the travelling Stokes wave had an energy density proportional to a^2. In other words, the energy of the system was halved in the case of the standing wave compared with the travelling Stokes wave. This corresponds to what was plotted in Figure 4.3c, for the dispersion relation found from the CNLS equations describing the special case studied in this thesis.

While Okamura found that, for the standing wave, a new region of instability occured, and the growth rate of this new region was the largest, the analysis in Section 4.2 showed that the crossing sea was less unstable than the corresponding non-crossing sea. These two results are obviously contradicting. It is peculiar that Okamura got the largest growth rate for crossing sea, even though the energy dens-

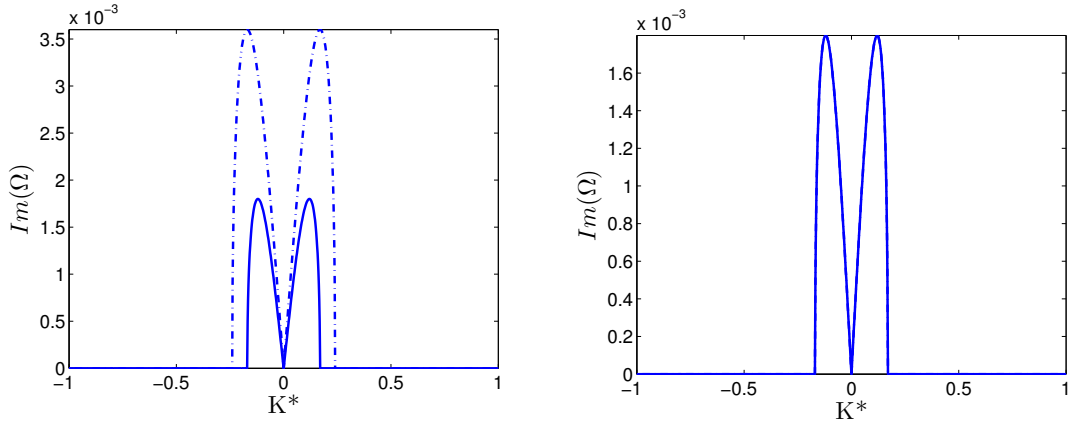

(a) $a_c = \frac{1}{\sqrt{2}} a_s$

(b) $a_c = a_s$

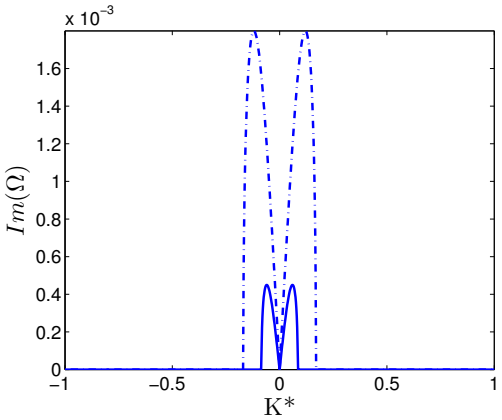

(c) $a_c = \frac{1}{2} a_s$

Figure 4.4: Case 2: $\epsilon \simeq 0.06$. Growth rate for perturbation of Stokes wave (dash-dotted line) and crossing sea (solid line) for different relationships between the amplitudes. a_s is the amplitude of the Stokes wave. The crossing sea is constituted of two Stokes waves travelling in opposite directions, each with an amplitude of a_c.

ity in the system was halved. The reason for this contradiction between Okamura's results and the results of the analysis in Section 4.2, is unknown. One factor might be that Okamura (1984) considers perturbations in two spatial directions, while the analysis in this work only considers perturbations in one direction. Also, while a narrow bandwidth was assumed for the analysis in Section 4.2, Okamura did not have the same limitations.

4.3.2 Modulational instability in crossing sea states

Onorato *et al.* (2006) discussed the case of waves propagating with wave number vectors $\mathbf{k}_a = (k, l)$ and $\mathbf{k}_b = (k, -l)$, see Figure 4.5. The opening angle between the two wave trains was $\beta = 2\theta = 2\arctan(l/k)$.

Stability analysis for perturbations along the k_x-axis was performed directly

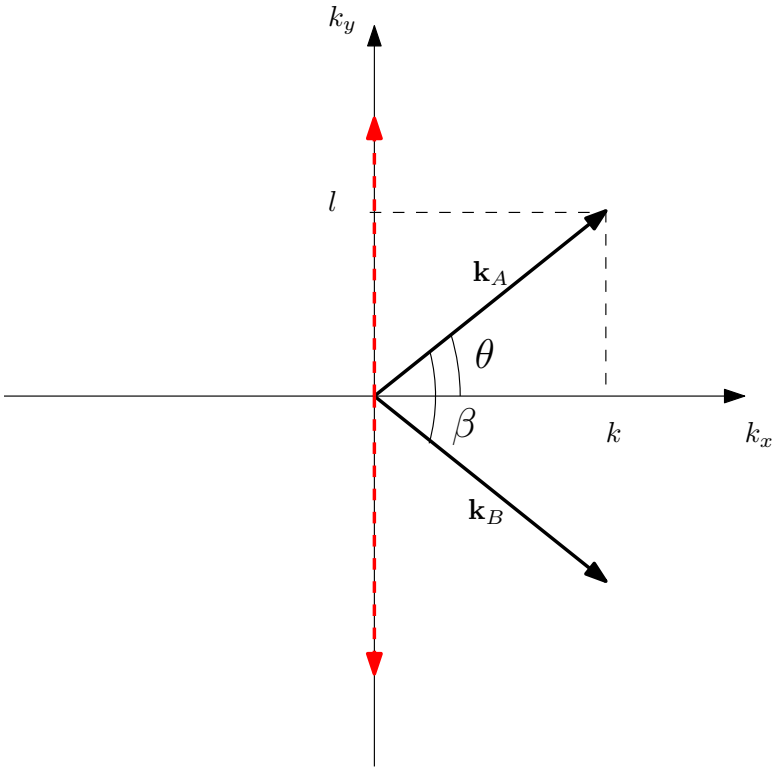

Figure 4.5: Wave number vectors $\mathbf{k}_A, \mathbf{k}_B$ for Onorato et al. The red vectors correspond to the special case with waves propagating in opposite directions.

on the following equations:

$$\frac{\partial A}{\partial t} - i\alpha\frac{\partial^2 A}{\partial x^2} + i\left(\xi|A|^2 + 2\zeta|B|^2\right)A = 0$$
$$\frac{\partial B}{\partial t} - i\alpha\frac{\partial^2 B}{\partial x^2} + i\left(\xi|B|^2 + 2\zeta|A|^2\right)A = 0$$

where

$$\xi = \frac{1}{2}\omega(\kappa)\kappa^2$$

and

$$\zeta = \frac{\omega(\kappa)}{2\kappa}\frac{k^5 - k^3l^2 - 3kl^4 - 2k^4\kappa + 2k^2l^2\kappa + 2l^4\kappa}{(k-2\kappa)\kappa}$$

There is something strange about the way the coefficients ξ and ζ were defined in Okamura's article. The interpretation used here is explained in Section C.4.3 in the pre-project found in Appendix C.

Compared with the CNLS equations derived in this thesis, the term containing the group velocity was removed by Onorato *et al.* from each equation by performing a Galilean transformation of the form $x' = x - C_x t$. A plane wave solution was found for each of the coupled equations, and then small perturbations in amplitude and phase were assumed. By linearising and assuming the same form of the

perturbations as in my analysis, the following dispersion relation was obtained:

$$\Omega = \pm\sqrt{\alpha K^2\left[\left(\xi\left(A_0^2+B_0^2\right)+\alpha K^2\right)\pm\sqrt{\xi^2\left(A_0^2-B_0^2\right)^2+16\zeta^2A_0^2B_0^2}\right]}$$

Figures 1 and 2 in Onorato *et al.* (2006) show the imaginary part of Ω'. The growth rate $Im[\Omega']$ and wave number K' reported in the figures are non-dimensional ($\Omega' = \Omega/\sqrt{g\kappa}$ and $K' = K/\kappa$ where $\kappa = |\mathbf{k}|$). Growth rates are presented in gray scale: white regions correspond to zero growth rates (stability) and the darker regions to instability.

The evolution of the perturbation along the k_x-axis is considered, and not along the direction of propagation of the wave. θ is ranging from 0° to 90°. For the case of one carrier wave with steepness $\epsilon = 0.1$, Fig. 1 in Onorato *et al.* (2006) shows an unstable region for angles θ from 0° to 35°. For angles larger than 35° any perturbation is stable. For the case of two carrier waves with the same steepness, Fig. 2 shows that the growth rate has increased, and an additional unstable region can be seen for large angles of 68° to 90°. This shows that *both the instability region and the growth rates are larger when two-wave systems are considered.* Hence, the two-wave system is more subject to modulational instability than a one-wave system.

When Onorato *et al.* consider an angle of $\theta = 90°$, this corresponds to the special case considered in this work with wave trains travelling in opposite directions, as the angle between the wave trains in this case is $180° = \pi$ rad. From Figure 4.5, it can be seen that perturbations along the k_x-axis would correspond to perturbations perpendicular to our waves' direction of propagation. Even though there might be perturbations of this kind in the wave tank, they would have a component k_x which is a multiple of $\frac{\pi}{d}$, where $d = 0.5$ m is the width of the tank. So for the perturbations, $k_x = 2\pi n\text{m}^{-1}$, where n is an integer. Experiments with a water depth of $h = 0.5$ m and a peak period of $T_p = 0.7$ s are planned to be conducted for this work. It can be found that, for this case, $k = 8.2$ m^{-1}, which means that the peak wave length is $\lambda = \frac{2\pi}{k} = 0.77$ m. This gives $K' = \frac{2\pi}{\kappa} = 0.77$. Hence, the experiments conducted for this thesis will fall far outside the unstable region in Figure 2 in Onorato *et al.* (2006).

It is interesting to discuss: Which wavelengths would have had to be considered for the experiments in this work, in order to fall inside the unstable region for $\beta = \pi$ rad in Onorato *et al.* (2006)? $K' = 0.16$ corresponds to $\kappa = 39.3$ which again corresponds to $\lambda = 0.16$ m. A numerical algorithm (iteration) tells us that this corresponds to a peak period $T_p = 0.32$ s. Hence $T_p = 0.32$ s and $\lambda = 0.16$ m would allow us to fall into the unstable region in FIG 2 in Onorato *et al.* (2006).

4.3.3 Others

Gramstad & Trulsen (2011) started from the Zakharov equation, and derived two fourth-ordered CNLS equations for the more general case of two two-dimensional wave systems with different wave numbers or directions. The stability of two interacting uniform wave trains was investigated by assuming small sideband perturbations of the Stokes wave solutions of the governing equations. Thus, the

analysis was of the same character as the stability analysis of the third ordered CNLS equations describing the special case considered in this work. Gramstad & Trulsen (2011) defined the angle between the two wave trains as θ (this corresponds to β in Onorato *et al.* (2006)'s case). Opening angles of $\theta = \frac{\pi}{4}, \frac{\pi}{2}, \frac{3\pi}{4}$ were considered, while the special case considered in this work corresponds to an opening angle of π. This means that even though the stability analysis performed in Gramstad & Trulsen (2011) is of the same character as the one in this thesis, results cannot be compared directly, as different configurations of crossing sea have been considered.

Shukla *et al.* (2006*a*) had the same approach as Onorato *et al.* (2006), and the angles between the wave trains were the same as in Gramstad & Trulsen (2011). Hence this article is not relevant for comparison with results found in this work.

Shukla *et al.* (2006*b*) had a different approach. The modulational instability of incoherent crossing sea states was investigated by applying a Wigner transform to the wave amplitudes A and B. Two coupled wave kinetic equations (von Neumann equations) were obtained, and then analysed to obtain a nonlinear dispersion relation for background sea states that had broad banded spectra. It was found that the growth rate of the modulational instability was suppressed. Hence, random phased nonlinearly interacting waves could propagate over long distances without being much affected by the modulational instability, and for a wide enough spectral distribution, the formation of freak waves was completely suppressed.

4.4 Discussion

This analysis of crossing Stokes waves will not necessarily have anything to do with the experiments which will be conducted as a part of this thesis. In our experimental work we will not be looking at Stokes waves, but irregular waves with a spectral distribution based on a JONSWAP spectrum, which has a non-zero bandwidth. These are two completely different cases which can not be compared directly. We do however have a hope that this analysis can give us an indication of whether or not crossing sea has an increased modulational instability compared to non-crossing sea.

In this chapter it was shown that a Stokes wave propagating in one direction has a higher modulational instability than two counterpropagating Stokes waves in the case that the energy density is conserved. It is common to look only at the size of the unstable domain in the (K_x, K_y)-plane; if the area is increased one concludes that the modulational instability is also increased. The analysis of the CNLS equations in Section 4.2 showed that both the instability domain as well as the values of the growth rate were decreased when going from non-crossing to crossing sea. Hence, it was shown that a crossing sea made up by two Stokes waves propagating in opposite directions is less subject to modulational instability than a single travelling Stokes wave.

Previous works were studied, for find out whether or not this special case had been studied previously. The only work that considered the same configuration of crossing sea as the one in this thesis, was Okamura (1984). Also, Onorato *et al.* (2006) had it as a limiting case, but was not directly comparable. The results

presented by Okamura and the results presented in this work, were contradicting. The reason for this contradiction is unknown, but some possible factors were discussed in Section 4.3.1.

Chapter 5

Experimental arrangements

In this chapter the experimental work for this thesis is presented in great detail. It includes preparation for, and setup of, the experiments. The post-processing of data is also explained here, while experimental conditions and results are included in Chapter 6.

5.1 Pre-lab activities

When working with statistics it is of great importance to make sure that one has enough data to say something significant about different statistical properties. To prepare for the planned experiments, two different cases were considered, *Draupner* and *Marin*. The goal was to determine how much experimental data was needed in order to say something significant about values of kurtosis. In particular, it was necessary to find out how long the time series would have to be.

5.1.1 New Year wave recorded at Draupner

The Draupner wave, or New Year's wave, is often believed to be the first freak wave to be detected by a measuring instrument, occurring at the Draupner platform in the North Sea off the coast of Norway on January 1, 1995, at 15.20. The measured data has been made accessible, and the statistical properties of the time series were studied here. The Draupner wave time series is 20 min long, and has $N = 2560$ points. It was interesting to investigate whether or not this time series was long enough in order for the statistical properties (in particular the kurtosis) to have converged. In Figure 5.1 the time series is shown, and the freak wave can easily be spotted around $t = 263$ s.

Point estimates

The n first points of the time series were considered, $n = 1, 2, ..., N$, and point estimates for mean, variance, skewness and kurtosis were calculated using the MATLAB functions *mean*, *var*, *skewness* and *kurtosis*. Figure 5.2 shows that the point estimates for variance, skewness and kurtosis have a jump around $t = 263$ s ($n \simeq 500$), which is the time the freak wave occurred. It can also be seen that the values for skewness and kurtosis have clearly not converged, since the curves

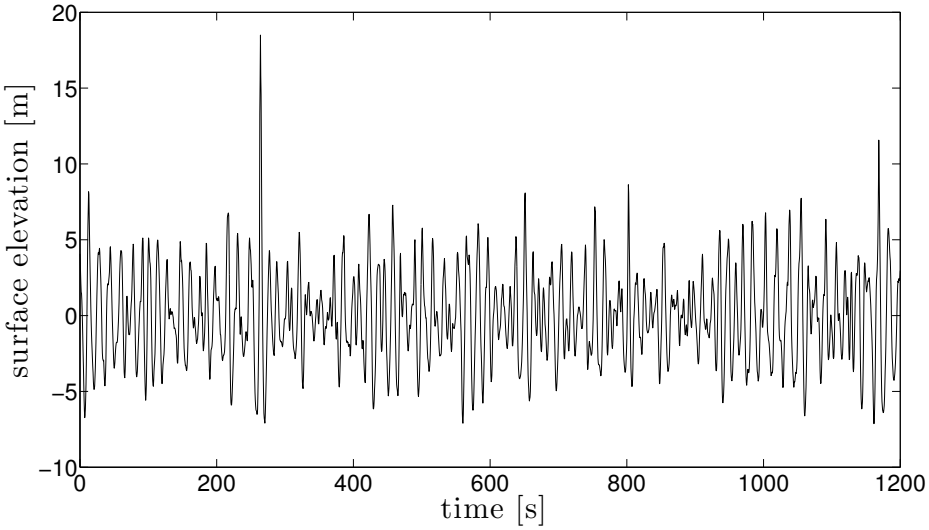

Figure 5.1: New Year's wave recorder at Draupner.

have a non-zero slope towards the end of the time series. Mean and variance however have converged as they have flattened towards the end of the time series. It makes sense that first and second order statistics (mean and variance) may have converged, while third and fourth order statistics (skewness and kurtosis). The higher the order of the statistics, the more data is required to get accurate estimates for statistical properties. In other words, a 20 min time series (1200 s) is not sufficient to say something about third and fourth order statistics of the surface elevation surrounding the Draupner platform on January 1, 1995.

The same exercise was repeated, calculating point estimates for statistical properties from an increasing number of points, but this time n points were drawn randomly from the time series, with replacement. Again, $n = 1, 2, ..., N$. The jump in values for variance, skewness and kurtosis because of the freak wave now occurs at different times for the different properties. When repeating the process, it was seen that there was no systematics in there the jumps occurred for the different properties and runs. This happened because the values for the surface elevation were drawn randomly, and the highest value corresponding to the freak wave was drawn at different times for each property and run. The different values could even be drawn more than once.

Bootstrapping

Even though the point estimates for skewness and kurtosis had not converged, it was interesting to investigate the width of a 95% confidence interval found from bootstrapping. As mentioned before, the time series has $N = 2560$ data points. K points were drawn randomly from the data set, with replacement. Point estimates for mean, variance, skewness and kurtosis were calculated from this selection, as described in the previous section. This was then repeated K times. The obtained values for the statistical properties were sorted in ascending order, and then the upper and lower 2.5% were removed. The 95% confidence interval was now the very right value minus the very left value. Point estimates with confidence intervals

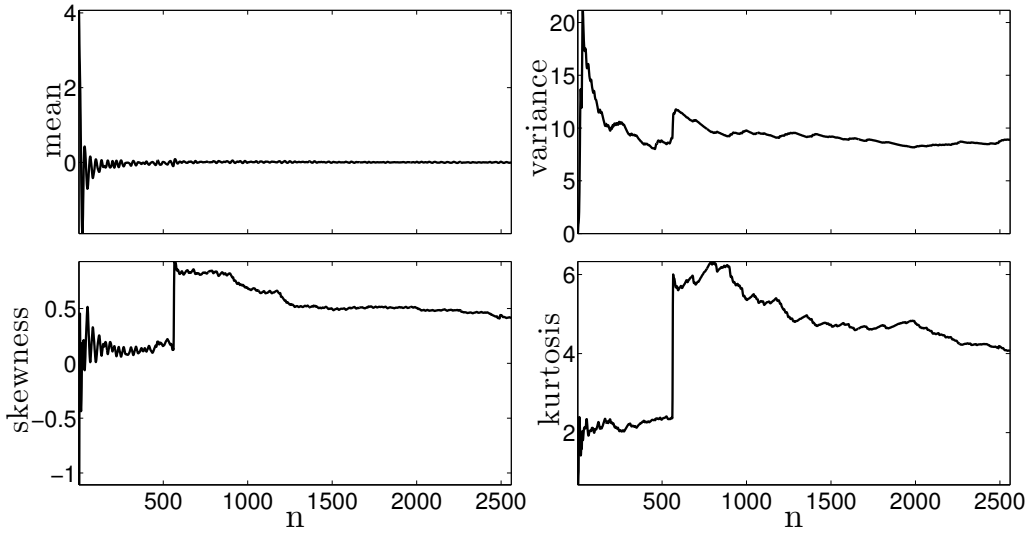

Figure 5.2: Convergence of statistical properties for the Draupner time series.

are shown in Figure 5.3 for different values of K. It can be seen that even though N data points in the Draupner time series have been used, and N repetitions in the bootstrapping, the width of the confidence intervals (especially for kurtosis) is relatively large. It is, however, interesting to see that the confidence interval for the point estimate for kurtosis is entirely located above $\kappa = 3$. This tells us that even though $N = 2560$ points is not enough for the kurtosis to have converged, it is sufficient for us to be able to say something significant about the kurtosis. We have shown that the surface elevation surrounding the Draupner platform on January 1, 1995, was definitely not Gaussian distributed.

5.1.2 MARIN

Experiments were performed at MARIN (Maritime Research Institute Netherlands) for a benchmark workshop on numerical wave modelling (Bunnik, 2010). Irregular long-crested waves were propagated over a 1:20 slope from water of constant depth 0.60 m (a "deeper" regime) to water of constant depth 0.30 m (a "shallower" regime). The surface elevation was measured by eight probes which were located at different distances from the wave generator.

Trulsen *et al.* (2012) addressed the question if the change of depth could provoke increased likelihood of freak waves. This article, as well as the experimental data from MARIN, were studied here in great detail, to determine how long the time series for the planned experiments had to be in order to say something significant about third and fourth order statistics. The goal was to also say something significant about the probability of freak waves, described by the exceedance probability. The article includes plots of variance, skewness and kurtosis with bootstrap intervals, as a function of the distance from the wave generator. The 95% confidence intervals were obtained from 10 000 bootstrap samples from the original dataset (the first 10 000 samples were neglected to exclude startup effects).

Three cases of long-crested irregular waves were employed, generated with con-

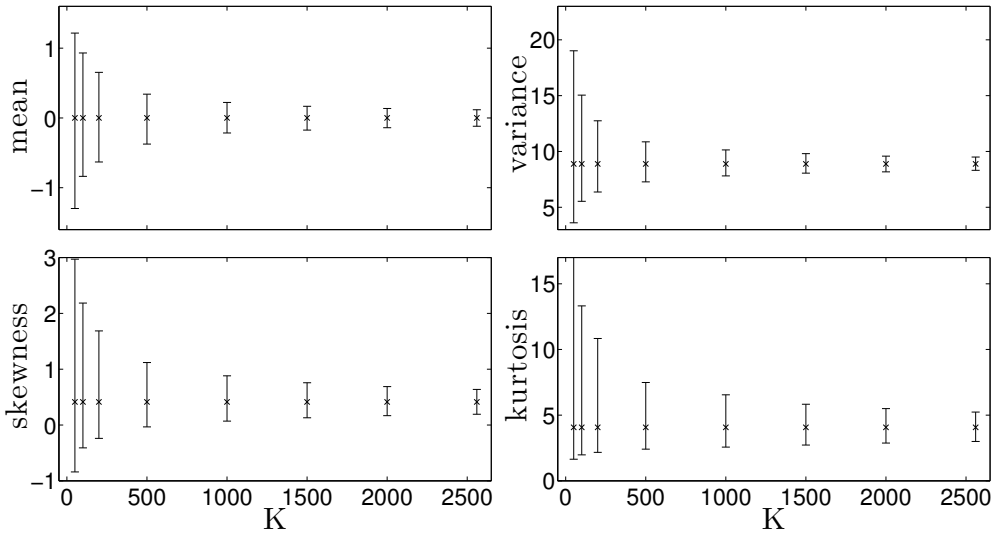

Figure 5.3: Convergence of width of bootstrap confidence intervals for the Draupner time series.

stant nominal significant wave height H_s and different nominal peak periods T_p. From Figure 8 in Trulsen *et al.* (2012) it can be seen that the widest confidence intervals for kurtosis occurs for case 3, which corresponds to a peak period of $T_p = 2.121$ s. Maximum width is $\simeq 0.12$, and it occurs for probe 15 located at the top of the step, exactly where the shallower regime begins. A width of 0.12 was chosen to be the starting point for the estimation of the duration of the time series for the experiments presented in this work.

Measured data from each probe consisted of a matrix with two columns, where the first column was the time and the second was the surface elevation measured by the probe. The time steps were $\Delta t = 0.02$ s, and the data for case 3 consisted of 92148 measurements. This means that the time series was about 1843 s long ($\sim$ 31 min), which corresponded to 869 peak periods T_p of 2.12 s. The goal for studying this data was to find out how many peak periods or significant wave periods are needed in order to say something significant about kurtosis and exceedance probability (deviation from Rayleigh).

Bootstrapping

The M first samples in the data set were considered, after the first 10000 samples had been removed, and confidence intervals were calculated using bootstrapping. M draws with replacement were made, and this was repeated M times. The first goal was to get a confidence interval for kurtosis which was max 0.2 units wide (this limit was set with background in what was explained in the previous section). By choosing $M = 20000$ the confidence interval for kurtosis was 0.225, which meant that the number of samples had to be increased. $M = 40000$ was the next guess, and the confidence interval for kurtosis was now 0.161. This means that by using only the first 40000 samples from the data set, something significant can be said about the kurtosis. The confidence intervals for $M = 20000$ and $M = 40000$ are shown in Figure 5.4.

Exceedance probability

The next goal was to make sure the time series were long enough so that deviations from the Rayleigh distribution for wave heights were at the same probability level as in Figure 9 in Trulsen *et al.* (2012). It was interesting to find out whether or not 40000 samples, which was sufficient with respect to the width of the bootstrap confidence intervals, is enough. Again, the M first samples in the data set were considered, after the first 10000 samples had been removed. The exceedance probability of the wave heights, $1 - P$, was calculated, where P was the cumulative distribution function of the wave heights. The wave heights were found under assumption of a narrowbanded process, using the Hilbert transform in MATLAB (see section 2.3). In Figure 5.5 the exceedance probability of the wave heights is plotted, together with the theoretical values found from the Rayleigh distribution. Figures 5.5a and 5.5b correspond to the exceedance probability of the first 40000 and 70000 samples respectively, while Figure 5.5c corresponds to all the 82148 samples being used. A significant difference can be observed between the curves in Figure 5.5a and Figure 5.5c, this indicates that 40000 samples is not enough. The curve in the Figure 5.5b, however, found from the first 70000 samples, seems to correspond well to the curve in Figure 5.5c, found using all the samples. This allowed a conclusion to be drawn that 70000 samples from the MARIN data were enough to be able to say something significant about exceedance probability (the probability of freak waves).

Conclusion from MARIN

70000 samples corresponds to 1400 s ($\sim$ 23 min). For a peak wave period of $T_p = 2.121$ s, this corresponds to 661 peak wave periods. For the experiments performed for this work, a peak period of $T_p = 0.7$ s was used. Other experiments were also conducted (in cooperation with Anne Raustøl), with a max peak period of 1.1 s. Hence, the time series needed to be 726 s ($\sim$ 12 min) in order to be able to say something significant about kurtosis as well as the probability of freak waves. A duration of 15 min was chosen for the time series, to be on the safe side.

5.2 Experiments

5.2.1 Setup

Experiments were performed in the long wave tank in the Hydrodynamic Laboratory at the University of Oslo, Blindern. The wave tank is 24.6 m long and 0.5 m wide, and was filled with 0.5 m of water for these experiments (see Figures 5.6a and 5.8). At the left end, $D = 0$, the wave tank has a hydraulic piston wave generator which induces surface waves into the tank. The wave generator is controlled by the computer software Wavelab©. The back and forth movement of the piston is given by input files in electrical voltage, generated using a MATLAB script which gives irregular wave fields with a spectral distribution based on a JONSWAP spectrum. See Appendix A.1 for more info on how the input files were created.

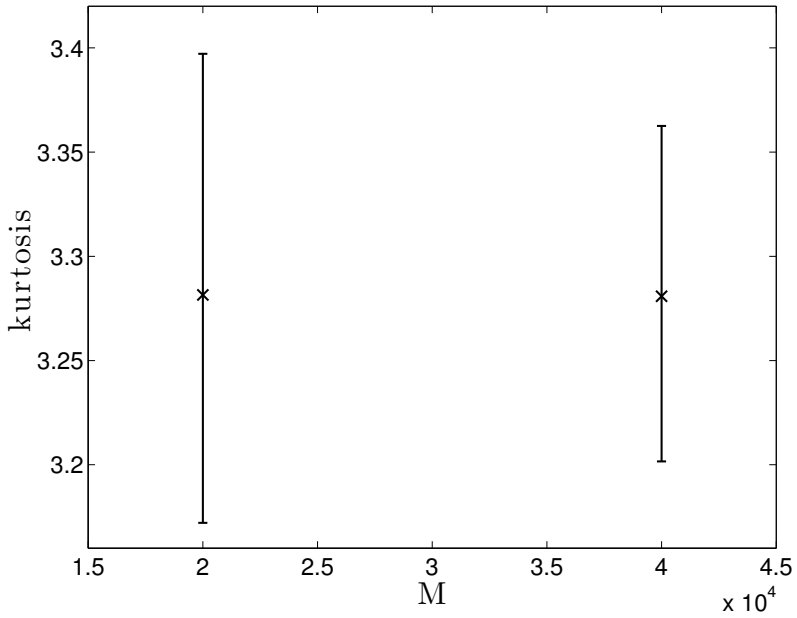

Figure 5.4: Convergence of width of bootstrap confidence intervals for kurtosis. MARIN data; case 3, probe 15.

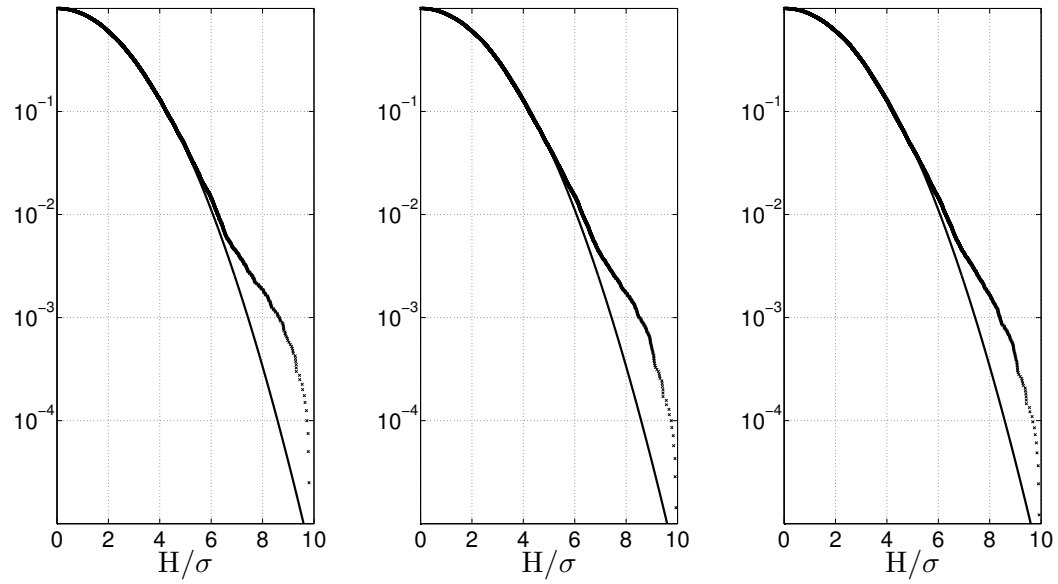

(a) M = 40000 (b) M = 70000 (c) M = 82148

Figure 5.5: Exceedance probability of the wave height H normalised by the standard deviation σ (crosses), compared with the exceedance probability of the Rayleigh distribution (solid line). MARIN data; case 3, probe 15.

The generated waves were long-crested, which means the crests and troughs extended over the entire width of the tank perpendicular to the propagation direction. The surface elevation was measured along the half-width of the tank, 0.25

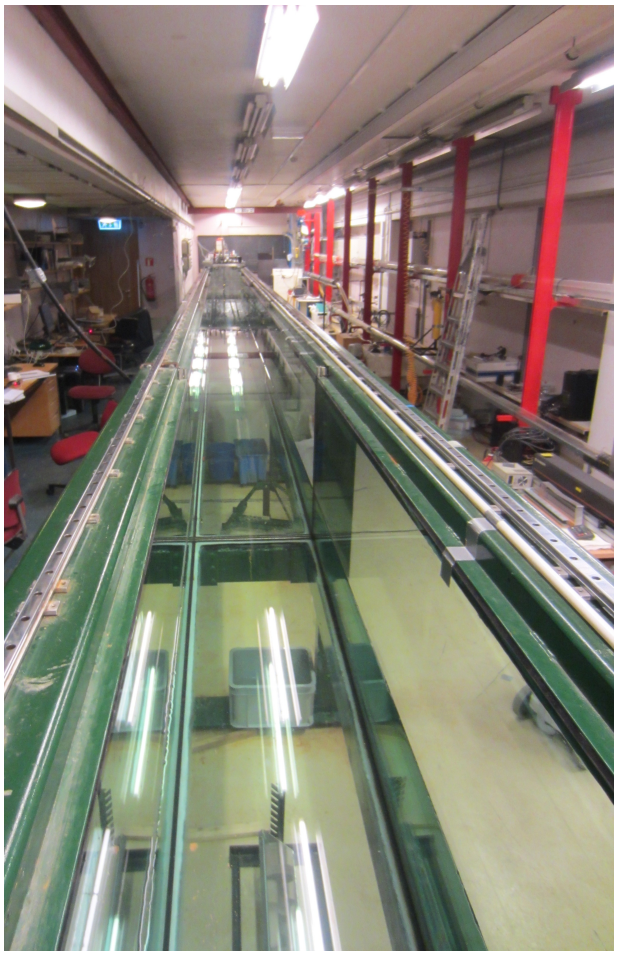

(a) The length of the wave tank

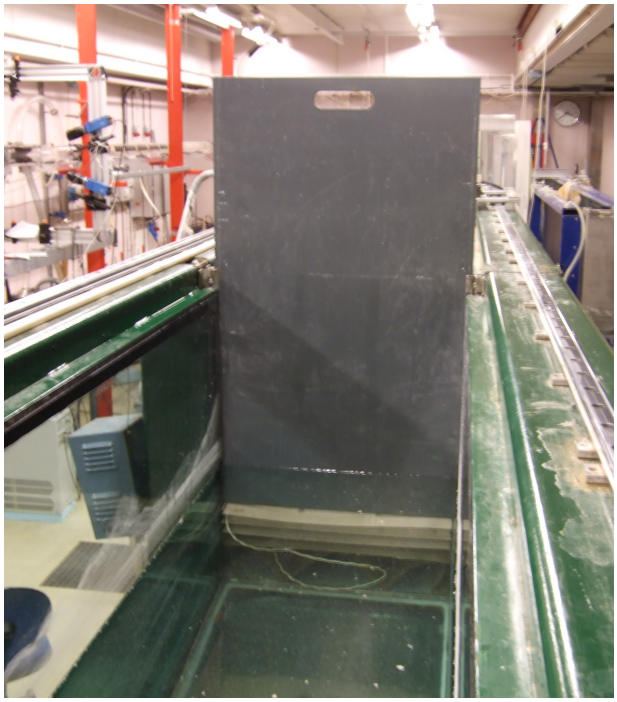

(b) The reflecting wall. Photo: Tore Magnus Taklo

Figure 5.6: The wave tank

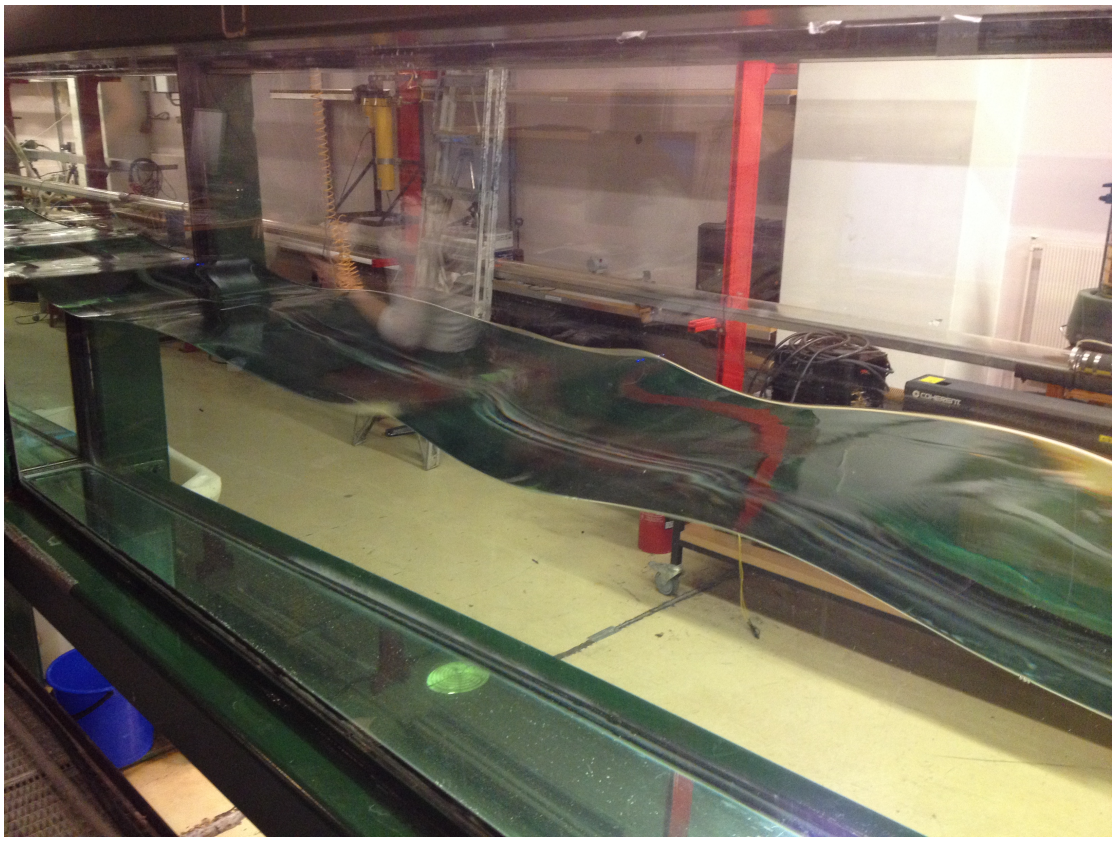

(a)

(b)

Figure 5.7: Surface elevation measured by ultrasonic probes

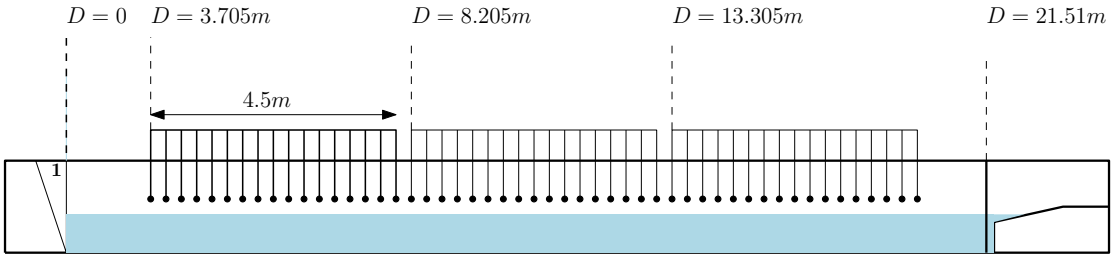

Figure 5.8: A model of the wave flume.

m, this allowed waves propagating along one axis to be considered. The x-axis was defined to be the longitudinal axis of the wave tank, and the z-axis was defined to be the vertical axis with the mean water level chosen to be at $z = 0$.

The wave tank has an absorbing beach at the right end, which reflects less than 3% of the amplitude of the incoming waves from the wave generator (Grue *et al.*, 2003). When the absorbing beach was in use, the waves were approximately unidirectional. For about half of the measurements the reflecting wall was inserted just in front of the absorbing beach, at $D = 21.51$ m. The wall can be seen in Figure 5.6b. This generated crossing sea, with wave trains crossing at an angle of $180° = \pi$ rad, i.e. opposite directioned wave trains. This is the most broad banded sea state that can be obtained in such a two-dimensional experiment.

5.2.2 Ultrasonic probes

The surface elevation was measured with a set of ultrasonic U-GAGE S18U probes from Banner®. A linear array with $M = 16$ equispaced probes placed $\Delta x = 0.3$ m apart could be moved along the tank. The probes were located 15 cm above mean water level at the half-width of the tank, looking vertically down at the surface. The surface elevation and probes are depicted in Figure 5.7. The ultrasonic probes did not affect the wave propagation, and they were controlled by a computer software, Labview©. The probes were initially set to measure the surface elevation in a window ranging from -5 cm to 5 cm, but this window turned out to be too small. It was observed that wave crests and troughs were cut off, hence the measuring window had to be increased to measure from -10 cm to 10 cm. This was done by calibrating the probes manually, and the calibration process is described in Appendix A.2. All experiments were performed with the ± 10 cm window.

The ultrasonic probes emit one or multiple pulses of ultrasonic energy, which travel through the air at the speed of sound (Banner, 2013). A portion of this energy reflects off the target and travels back to the sensor. The sensor measures the total time required for the energy to reach the target and return to the sensor, and the distance to the object is then calculated using the following formula

$$D = \frac{ct}{2}$$

D is the distance from the sensor to the water surface, $c \approx 343$ m s^{-1} is the speed of sound in air, and t is the transit time for the ultrasonic pulse to reach the target and return to the sensor.

Dropouts

The ultrasonic probes have a sensing range from 3 cm to 30 cm (Banner, 2013). There are limitations to which extent the ultrasonic probes can measure an inclined surface, however. At the minimum sensing range $s_{min} = 3$ cm the maximum target inclination angle is $\alpha = 10°$, and it decreases to a maximum target inclination angle of approximately $\alpha = 5°$ at the maximum sensing range $s_{max} = 30$ cm. If the target has a larger inclination angle than this, the signal from the probe reflects off the target at such large angle that it cannot return to the sensor. This is problematic when measuring steep waves, and dropouts in the measured surface elevation appear at locations where the waves are particularly steep. This often occurs between the crests and the troughs of the waves. The software Labview is programmed to set the value of the surface elevation to 10 (the upper limit of the measuring window) when dropouts occur, and the dropouts can then later be removed with a filter. The filter also needs to take care of high frequent noise which is common for all digital and electronic measuring devices. In section 5.3.3 the filter that was used is presented in more detail.

5.3 Surface elevation

5.3.1 Startup effects

When logging the surface elevation with Labview, the program was triggered by starting the wave generator. Hence, the probes started recording as soon as the wave paddle started moving. Since the array with the ultrasonic probes was placed in different distances from the wave generator, it took some time before the waves reached the array. Figure 5.9 shows the first 20 s recorded by three probes fairly close to each other, measuring the surface elevation near the wave generator. In the following, when post processing and analysing the data gained from our experiments, the first minute of the time series was discarded to avoid transient startup effects.

5.3.2 Repeatability

Three repetitions were performed for each experimental run, and the repeatability of the data could easily be checked. Let us say the goal was to to check repeatability for run A and run B. Due to inconsistency of the probes, dropouts and other types of noise occurred at different times and location for each run. This meant repeatability could only be checked for data points that were not been removed by filtering, neither for run A nor run B. As explained in Section 5.3.3, when the data is filtered, the data points which are identified as noise are replaced by NaNs in the time series. To check the repeatability it was therefore necessary to loop through all the data points for the two runs, and compare the values for pairs with no NaNs. The correlation between the two runs was calculated using the following formula:

$$Co = \frac{\langle (x_i - y_i)^2 \rangle}{\langle x_i^2 + y_i^2 \rangle} \tag{5.1}$$

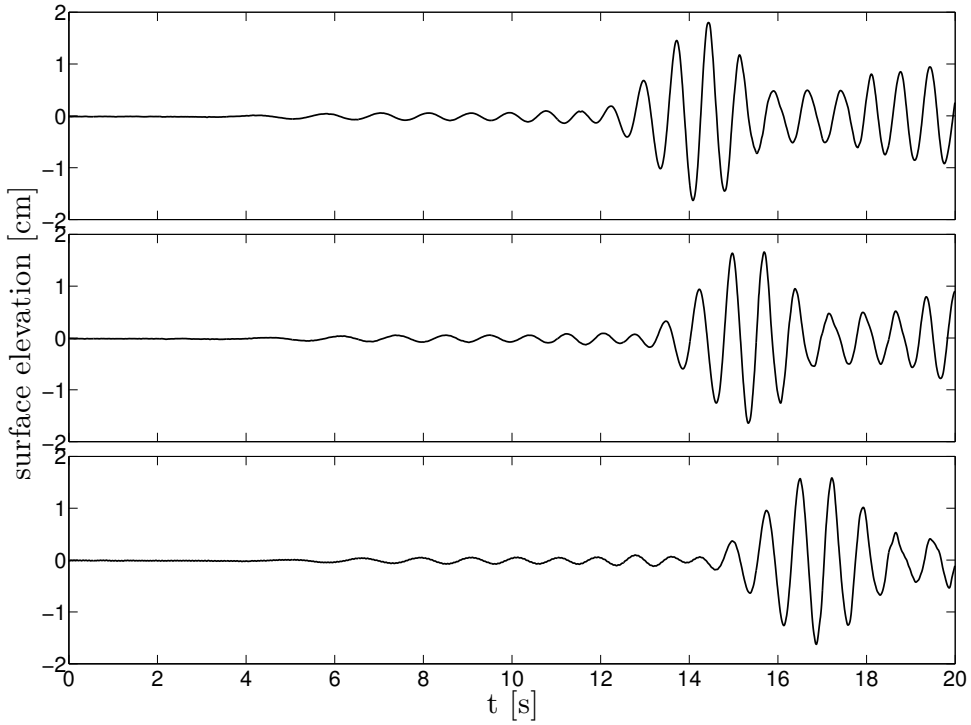

Figure 5.9: Startup effects

If $Co = 0$, the two runs were perfectly correlated, and if $Co = 1$, they were uncorrelated. The correlation factor needed to be as low as possible, as this corresponded to good repeatability. For the experiments conducted in this thesis, the correlation factor turned out having a magnitude proportional to $\frac{1}{100}$, see values in Tables B.3 and B.4. This means that repeatability was very good, and data from only one run per case will be considered for post-processing and analysis of experimental results.

5.3.3 Filters

There were mainly two kinds of noise in the measured data from the probes. As described in Section 5.2.2, dropouts occurred because the reflected signal from the water surface was not always reflected back to the probe. The surface elevation was then set to a default value of 10 cm, which was the upper limit of the measuring window set for the probes. The other kind was a high-frequency noise, with only positive contributions to the surface elevation. This noise might have come from the connections in the system, because there is not much grounding in the DAQ-card to which the probes were connected.

To remove dropouts a filter which was first developed by Tore Magnus Taklo, `RemoveDropouts`, was adapted. The filter has an upper and an inner threshold as input arguments, which is used to check which data points to remove. Mainly, the filter is supposed to remove values of the surface elevation measured to be higher than the upper threshold. These data points are set to be NaNs (Not a Number). Also, if the difference in value for two neighbouring points is higher than an inner threshold, then one of the data points is assumed to be wrong. So this is also set

to NaN. The filter `RemoveDropouts` is included as Appendix A.3.1.

The high frequent noise is removed by a filter called `RemovePeaks`, developed by the author together with Anne Raustøl, inspired by a filter first developed by Odin Gramstad. The filter is based on the MATLAB function `findpeaks`, which finds local maxima in the input. A threshold can be given as a name-value pair argument to this function, and peaks are then returned that exceed their neighbours by at least the value of the threshold. `RemovePeaks` sets the value of these local maxima to NaNs. `RemovePeaks` is included as Appendix A.3.2.

The experiments were conducted with a relatively high steepness ϵ, which caused a lot of dropouts. In fact, the measured data had so many dropouts that it complicated the filtering process, and the two filters described above were not sufficient to get rid of all the noise. An additional filter had to be used. The problem is clusters where more than one data point has dropped out and is located above the rest. If a single point has dropped out, `RemoveDropouts` might catch it. But if two or more points have dropped out, close to each other, `RemoveDropouts` will only get rid of one of them. This happens because the difference between one dropout-point and the next does not exceed the inner threshold. The PhD student Jostein Kolaas was of great help when addressing this issue. In 2009 he developed a MATLAB function, `mlsmax`, for removing noise from results from experiments with PIV. The documentation for this function is included as Appendix A.3.3. The function computes multivariate moving least squares approximation of the input with variance/confidence interval estimates (also known as local regression), and it returns interpolated data. It also returns the indicies for at which locations in the input it finds something wrong. The function is very long and somewhat complicated, and we have not had time to study it in detail. To verify that `mlsmax` has the desired effect, it is necessary to plot the filtering process step by step.

An example is given in Figure 5.10, where 14 s out of 900 s for one of the experimental runs are considered. This example was taken from a probe which was particularly problematic, and had all the different kinds of noise. On top the raw data can be seen, which has a lot of dropouts. Second from the top the "normal" dropouts, as well as high-frequent noise, have been removed. There are still a few data points that are problematic, these can be seen clearly because black crosses have been used for plotting. These points are then removed using the function mlsmax, and the second plot from the bottom shows the data after these particular points are removed. In the bottom plot the data has been interpolated, this is necessary to be able to calculate statistical properties like variance, skewness and kurtosis of the measured data. This way is has been confirmed that `mlsmax` does not generate or remove any troughs and crests, and that it seems to interpolate in a very good way. Although it is not optimal to use a "black box" like this one to remove noise from experimental data, plotting the filtering step by step and inspecting have made us certain that mlsmax has the desired effect.

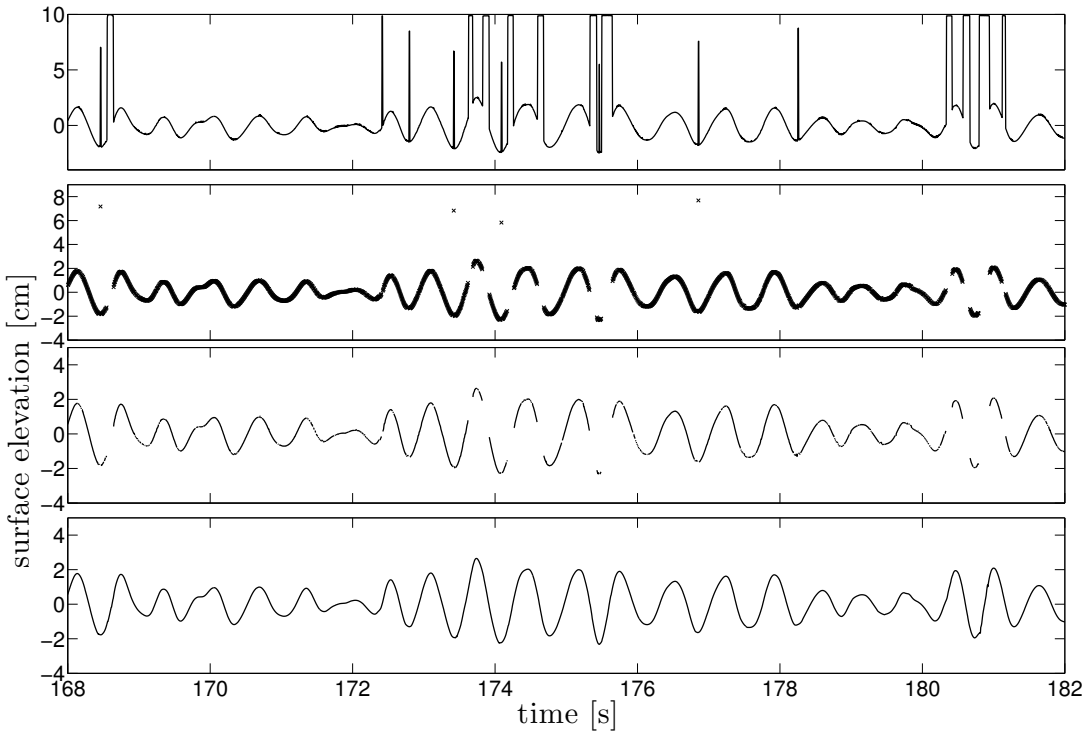

Figure 5.10: Filtering step by step.

Chapter 6

Experimental results

The experimental setup was designed for studying two crossing wave trains with the same peak period T_p, characteristic frequency ω_c and wave number k_c. Opposite directioned wave trains were obtained by inserting a reflecting wall at the far end of the wave tank.

6.1 Experimental conditions

For the experiments a peak period $T_p = 0.7$ s was chosen, which corresponded to a peak wavelength of $\lambda_p = 0.77$ m. For a water depth of 0.5 m this left us in a "deeper" domain with $k_p h \simeq 4.11$.

The goal was to compare crossing and non-crossing sea for two different steepnesses; $\epsilon = 0.1$ and $\epsilon = 0.06$. Three input series for the wave generator were created, with different amplitudes for the back and forth movement of the wave paddle. This gave different steepnesses for crossing and non-crossing sea (runs with reflecting wall and absorbing beach, respectively). To obtain crossing sea, the reflecting wall was always located in the same position, just in front of the absorbing beach. This leads to different amplitudes for the incoming and reflected wave trains of the crossing sea.

Time series	Crossing (C)	Non-crossing (NC)
I	0.1341	0.0910
II	0.0998	0.0661
III	0.0648	0.0437

Table 6.1: Time series with measured steepness.

Table 6.1 shows that time series I (NC) and II (C) had measured values for the steepness $\simeq 0.1$. Correspondingly, time series II (NC) and III (C) had a steepness $\simeq 0.06$. This means results can be compared of experimental runs for these pairs of time series. Experiments corresponding to the higher steepness are defined as *case 1* and to the the lower steepness as *case 2* (see Table 6.2).

As described in Section 5.2.2, the array with $M = 16$ equispaced probes could be moved along the tank. Three different locations were chosen for the array,

case	Crossing (C)	Non-crossing (NC)
1	0.0998	0.0910
2	0.0648	0.0661

Table 6.2: Definition of case 1 and case 2 with measured steepness

with the middle of the tank as a reference point. This gave measurements from 48 different locations along the tank. The 48 probes spanned from $x = 3.705$ m to $x = 17.805$ m, with a Δx of 0.30 m. $x = 0$ was taken to be the position of the wave generator (see Figure 5.8).

6.2 Results

The following refers to case 1 and case 2 as described in Table 6.2.

6.2.1 Point estimates with bootstrap confidence intervals

After filtering the data, by the method described in Section 5.3.3, point estimates for variance, skewness and kurtosis were calculated for all probes using the MATLAB functions *var*, *skewness* and *kurtosis*. The measured time series were 15 min long, and with $\Delta t = 0.005$ s this means 180000 samples were generated for each probe for each run. After removing the first minute to avoid transient start-up effects, $N = 168000$ samples were left for each probe. Bootstrapping was performed as described in Section 2.4, with N draws and N repetitions, and 95% confidence intervals were obtained. Point estimates for variance, skewness and kurtosis, with confidence intervals, are plotted as a function of x in Figure 6.1a for case 1, and Figure 6.1b for case 2.

Results show that the variance decreases along the tank, because of dissipation of the waves. The dissipation is especially prominent for the case of non-crossing sea, with an absorbing beach in the far end of the wave tank.

The skewness is found to be non-zero and positive.

Results show that for case 1, corresponding to a steepness $\epsilon \simeq 0.1$, the kurtosis is larger than three everywhere along the tank, both for crossing and non-crossing sea. Case 2, $\epsilon \simeq 0.06$, also has a kurtosis larger than three everywhere along the tank for the case of non-crossing sea, while crossing sea has a few values below three. For case 2, non-crossing sea, the kurtosis increases along the tank, while for case 2, crossing sea, as well as both crossing and non-crossing sea for case 1, the values of the kurtosis seem to be more stable. Note that the values of the kurtosis are generally higher for the non-crossing sea than crossing sea. It also seems like the difference in the values of the kurtosis between crossing and non-crossing sea are larger for case 2, with the lowest steepness, than for case 1.

6.2.2 Comparison with statistics for a narrowband wave train

In Sections 3.3 and 3.4 the expressions for the theoretical skewness and kurtosis were found, for a narrowband process, to second and third order, respectively. In Figures 6.2 and 6.3 theoretical values for skewness and kurtosis are plotted together with the values found from experiments, for case 1 and case 2, respectively. Theoretical values were found only for the case of non-crossing sea, as the values for crossing sea requires an extensive analysis (see Section 3.5).

6.2.3 Exceedance probability

In Figures 6.4 and 6.5 the exceedance probability of the wave height, Pe, is shown. $Pe = 1 - F$, where F is the cumulative distribution function. Values of the wave height found using the Hilbert transform are compared with the theoretical wave heights given by the Rayleigh distribution. Three probes are considered (out of 48) for each of the cases 1 and 2. For case 2, probe 40, seen in Figure 6.5c, the measured wave heights for crossing sea never cross the freak wave limit, $H > 2H_s = 8\sigma$, but drops down on the lower side of the theoretical values. This means that no freak waves were measured in this time series.

The freak wave probability, $Pe(8\sigma)$, is shown in Figures 6.6a and 6.6b for case 1 and case 2, respectively. It is shown that the freak wave probability seems to vary in the same manner as the kurtosis. For crossing sea, case 2, some probes have a freak wave probability of zero.

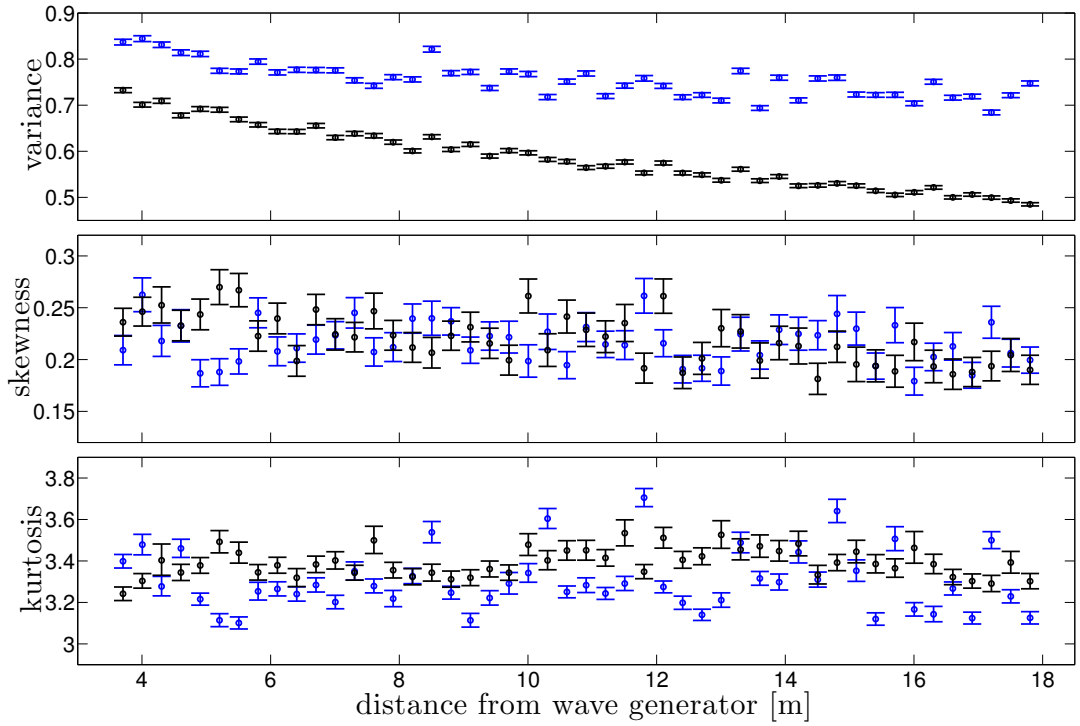

(a) case 1: $\epsilon \simeq 0.1$

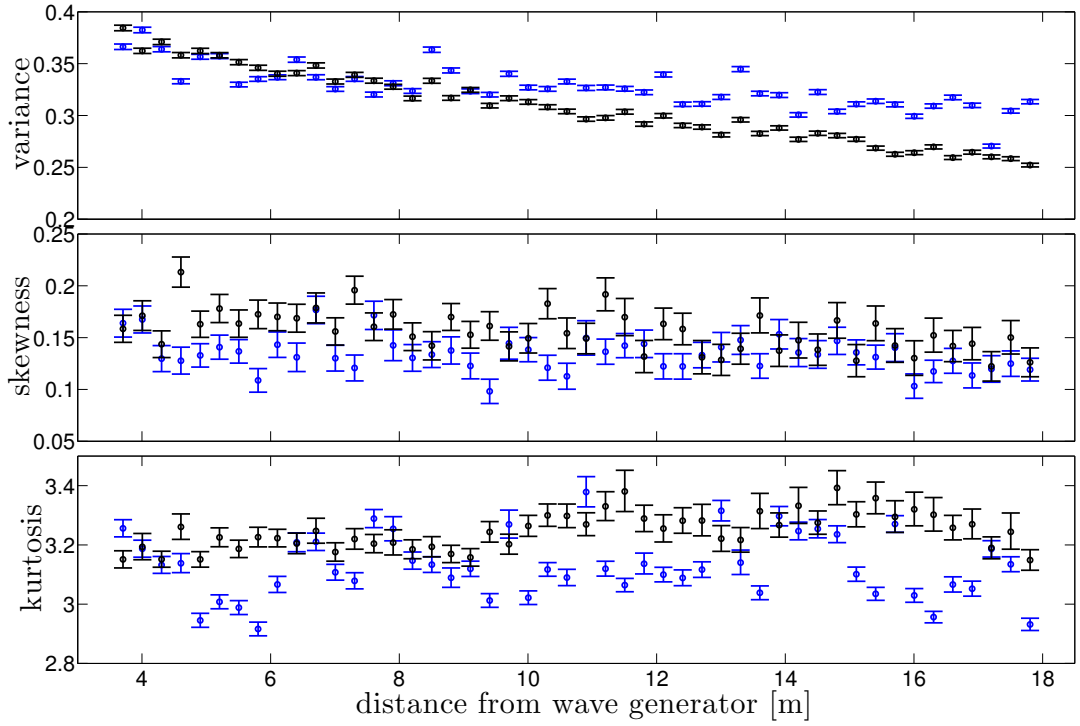

(b) case 2: $\epsilon \simeq 0.06$

Figure 6.1: Point estimates with bootstrap confidence intervals. Crossing sea (blue), non-crossing sea (black).

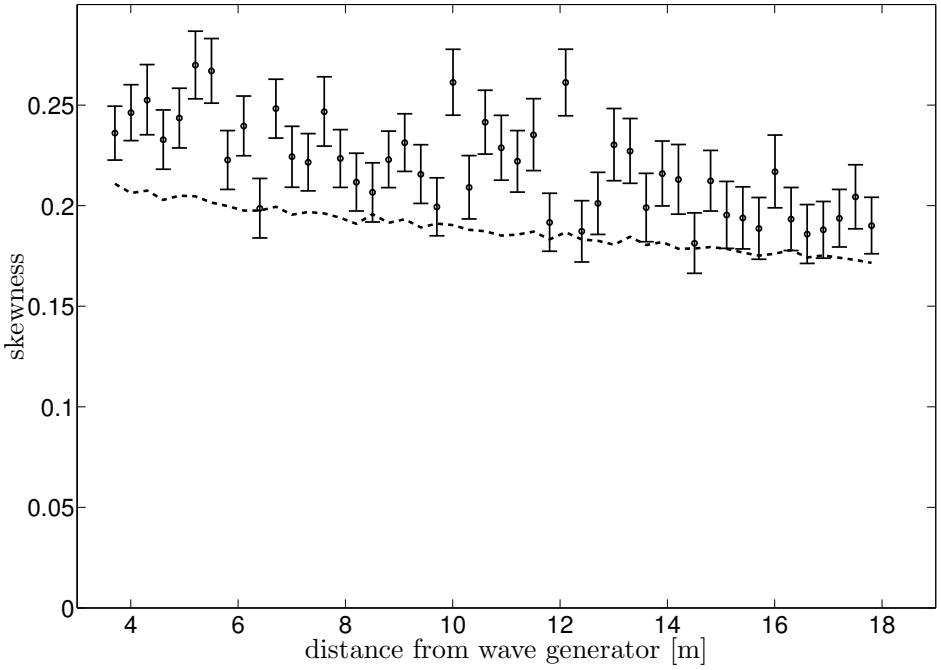

(a) case 1: $\epsilon \simeq 0.1$

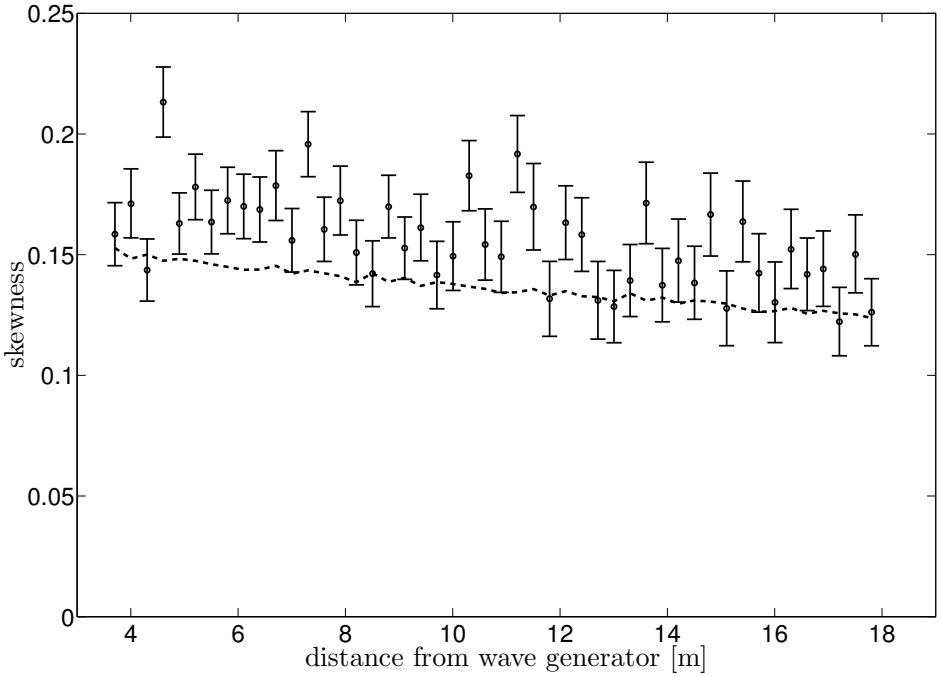

(b) case 2: $\epsilon \simeq 0.06$

Figure 6.2: Point estimates for skewness for non-crossing sea, with bootstrap confidence intervals. The dotted line represents the theoretical value from equation (3.13).

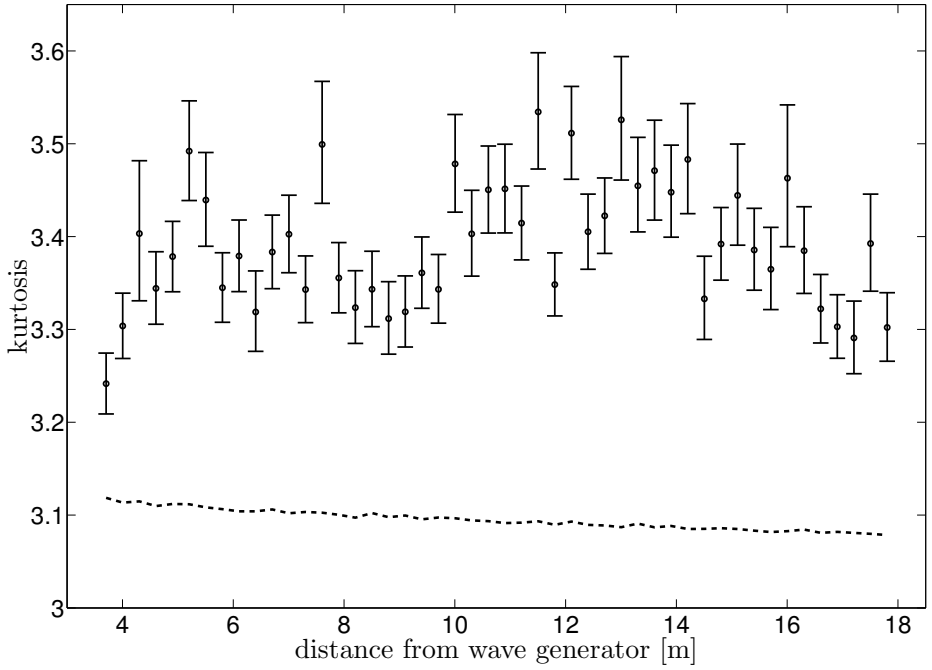

(a) case 1: $\epsilon \simeq 0.1$

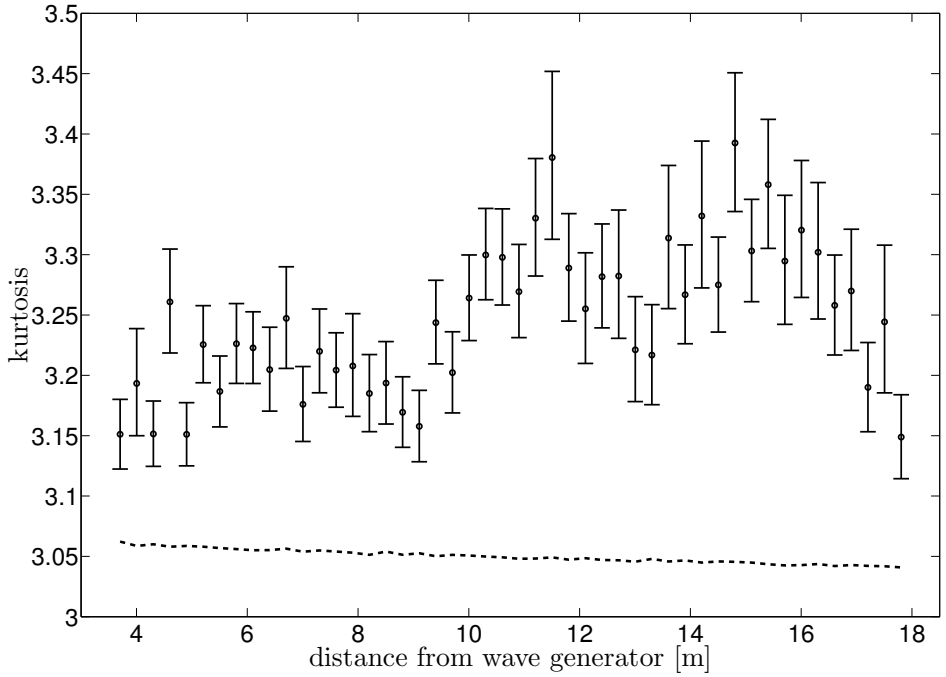

(b) case 2: $\epsilon \simeq 0.06$

Figure 6.3: Point estimates for kurtosis of non-crossing sea, with bootstrap confidence intervals. The dotted line represents the theoretical value from equation (3.21).

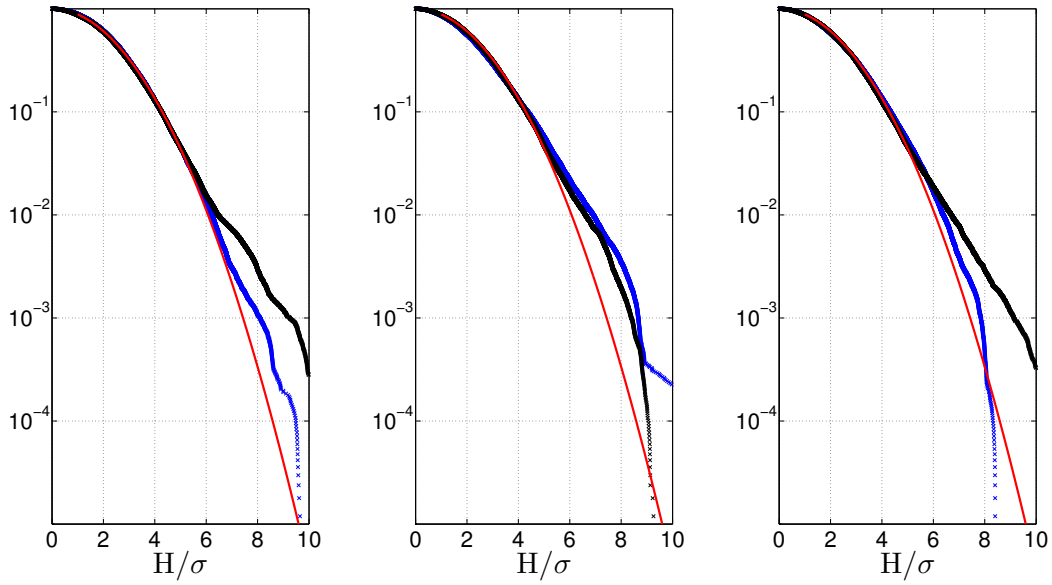

(a) Probe 6 (b) Probe 28 (c) Probe 29

Figure 6.4: Exceedance probability case 1: $\epsilon \simeq 0.1$. Crossing (blue), non-crossing (black) and theoretical (red).

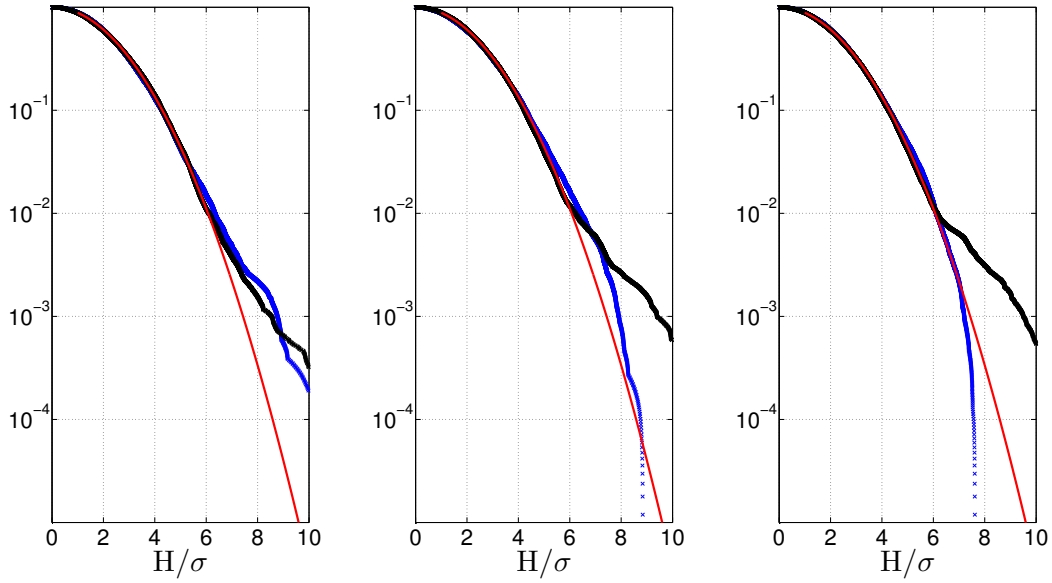

(a) Probe 15 (b) Probe 36 (c) Probe 40

Figure 6.5: Exceedance probability case 2: $\epsilon \simeq 0.06$. Crossing (blue), non-crossing (black) and theoretical (red).

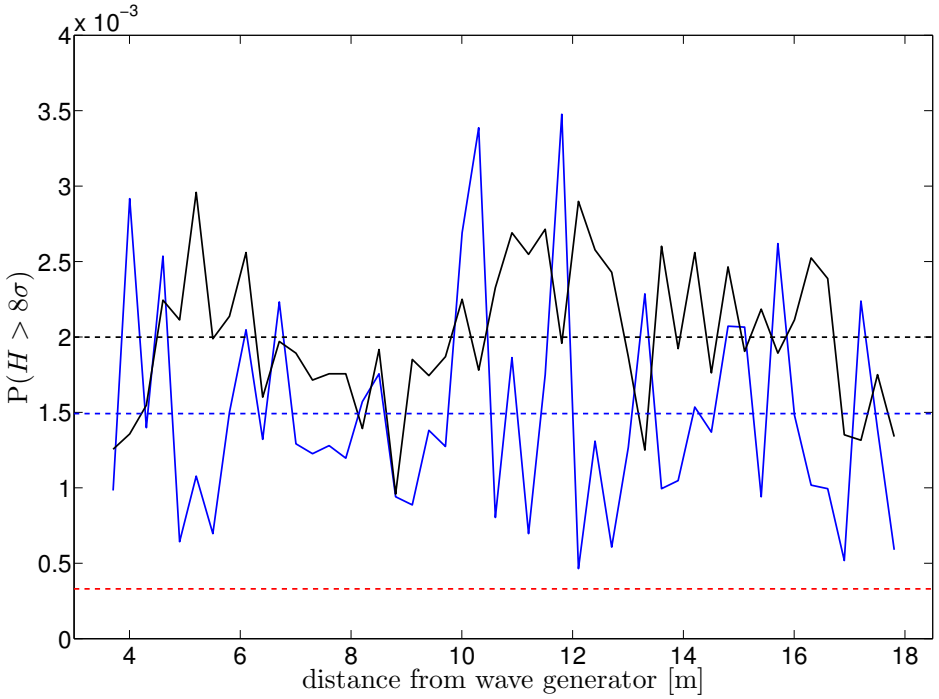

(a) case 1: $\epsilon \simeq 0.1$

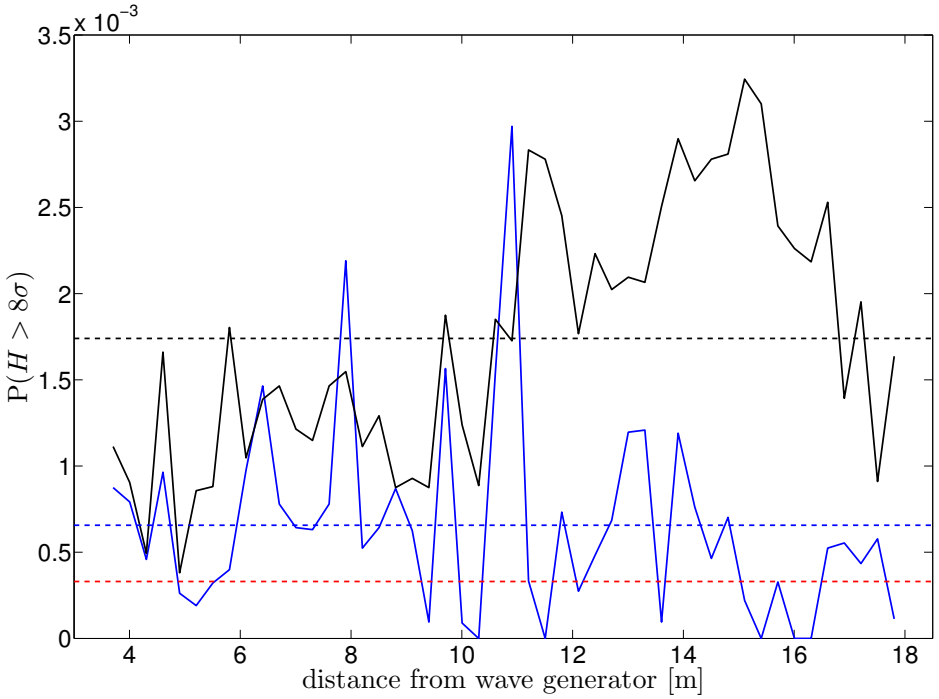

(b) case 2: $\epsilon \simeq 0.06$

Figure 6.6: Freak wave probability, the probability that the wave height exceeds $2H_s$. Theoretical value from Rayleigh distribution (red dotted line). Crossing sea (blue solid line) with mean value (blue dotted line). Non-crossing sea (black solid line) with mean value (black dotted line).

Chapter 7

Discussion and conclusion

A stability analysis of two coupled nonlinear Schrödinger equations has shown that two Stokes waves travelling in opposite directions were less subject to modulational instability than a single travelling Stokes wave. Laboratory experiments, where irregular waves generated by a JONSWAP spectrum have been studied, have revealed a tendency for a special case of crossing sea to have lower kurtosis than non-crossing sea. These observations contradict what has been a widespread mindset, namely that crossing sea has a higher occurrence of freak waves than non-crossing sea.

The following discussion refers to the results found in Chapter 6.

7.1 Experimental results

7.1.1 Point estimates

The variance was shown to decrease along the tank, due to dissipation of the waves. The variance can be considered a measure of the energy density in the tank, thus the results showed less loss of energy for the case with reflecting wall compared to the case with absorbing beach. Since the energy density is proportional to the amplitude squared, a larger amplitude gives higher values for the variance. This was seen clearly as the variance for case 1 was higher than for case 2.

The skewness was found to be non-zero and positive, the values being significantly higher for case 1 than case 2. Positive skewness indicates that the tail on the right side of the probability density function is longer or fatter than the tail on the left side. Hence, for the measured time series, we expect a higher occurrence of large positive values of the surface elevation, than large negative values.

It was shown that the kurtosis was higher than three everywhere along the tank for case 1, for both crossing and non-crossing sea. For case 2 the kurtosis was below three at some locations for crossing sea, but higher than three everywhere for non-crossing sea. Generally the measured values for the kurtosis were higher for case 1 compared to case 2. Note that the kurtosis increased along the tank for non-crossing sea, case 2. This growth represents the dynamic development of the Schrödinger equation, which exchanges energy between different modes. For case 1, crossing sea, as well as both crossing and non-crossing sea for case 2, the nonlinearities are so strong that the dynamical development happens instantly

and in such a manner that it looks as if the values of the kurtosis have stabilised. The kurtosis is a measure of how much weight a probability distribution has on its tails. The normal distribution has a kurtosis of three, and a kurtosis higher than three means a distribution is expected to have a higher occurrence of extreme events than Gaussian statistics anticipates.

A kurtosis larger than three, together with positive skewness, indicates that the probability distribution for the measured surface elevation has a higher occurrence of large positive values than what is normal. A higher occurrence of freak waves is expected in the measured surface elevation, for both crossing and non-crossing sea, than anticipated by a normal distribution. Since the kurtosis is higher for non-crossing sea than crossing sea, a higher occurrence of freak waves is expected in non-crossing sea compared with crossing sea.

7.1.2 Comparison with theoretical values

Deviations were shown between theoretical and experimental values of both the skewness and kurtosis, being most significant for the latter. The deviations may be caused by many factors, one of them being the fact that the theoretical values are found assuming that the process is narrowbanded (see Sections 3.3 and 3.4). Another reason might be that the theoretical expressions have only static terms, and do not take into consideration the dynamical development of the Schrödinger equation, the exchange of energy between modes and frequencies of the wave trains. Theoretical values for both skewness and kurtosis are functions of the steepness ϵ, which decreases along the tank due to dissipation. This does not correspond well to the dynamical development of the governing equation. This is especially clear for non-crossing sea for the lowest steepness, case 2, where the dynamic development leads to the kurtosis increasing along the tank.

7.1.3 Exceedance probability

In Chapter 2 it was shown that when assuming that the surface elevation is narrowbanded and Gaussian distributed, the crest heights and wave heights are Rayleigh distributed. For the experiments waves were generated from a JONSWAP spectrum, which is not narrowbanded. For a finite-width wave spectrum, the use of the Hilbert transform to calculate wave heights might be problematic. For crossing sea consisting of two irregular wave trains, each generated from a finite-width spectrum, the use of the Hilbert transform to calculate wave heights is probably even more problematic. For the work in this thesis it was assumed, however, that the Hilbert envelope does in fact give the distribution for "true" crest heights and wave heights even though the process is not narrowbanded, and therefore the Hilbert transform was chosen for the approximation of wave heights from experimental data.

Because of nonlinearities, the surface elevation is not perfectly Gaussian, and the wave heights estimated by the Hilbert transform, are not perfectly Rayleigh distributed. Hence, the deviation between theoretical and measured values seen in the exceedance probability plots can be interpreted as a measure of the nonlinearities of the wave systems.

Neither crossing nor non-crossing sea had systematic deviations for the wave heights from the theoretical values given by the Rayleigh distribution. An example was given of the exceedance probability of a probe that had not measured any freak waves. This must be seen in correspondence to both the kurtosis and the freak wave probability for this probe. While the kurtosis is connected to the distribution of the surface elevation, the occurrence of freak waves (and the freak wave probability) is related to the distributions of wave heights or crest heights. The freak wave probability for the particular probe that did not measure any freak waves was zero, and the kurtosis was below three. Other probes, however, also had a freak wave probability of zero, but a kurtosis higher than three. This might be an indication that the measured time series were not long enough in order for the freak waves to appear. For very long time series a better correspondence between kurtosis and freak wave probability can be assumed.

7.2 General discussion

Crossing sea has been studied for the special case of two wave systems propagating in opposite directions, with the same characteristic frequency ω_c and wave number k_c. Statistical properties of this sea state have been compared to non-crossing sea, the same wave system propagating in only one direction. It was shown that the kurtosis was higher than three for crossing as well as non-crossing sea. This means that both sea states have a higher occurrence of extreme events than what is anticipated by Gaussian statistics. The experimental results also showed that kurtosis of a non-crossing sea generally is higher than that of a crossing sea.

A stability analysis was performed for two coupled nonlinear Schrödinger equations describing the propagation of two Stokes waves in opposite directions. The stability analysis showed that both the instability domain and the growth rates were reduced for a two-wave system compared with a one-wave system. Even though the behaviour of crossing Stokes waves cannot be compared directly to the behaviour of irregular waves generated from a JONSWAP spectrum, the result of the stability analysis gives an indication that crossing sea is less unstable than non-crossing sea. This corresponds with the experimental results showing that the kurtosis generally is lower for crossing sea than non-crossing sea.

Previous works have been focused on the angle between two wave systems in a crossing sea, trying to map which effect the angle between two systems has had on the occurrence of freak waves. Different angles between crossing Stokes waves were studied by Okamura (1984); Onorato *et al.* (2006); Gramstad & Trulsen (2011), while Onorato *et al.* (2010); Toffoli *et al.* (2011) performed numerical and experimental investigations of irregular wave trains generated from realistic ocean wave spectra, crossing at different angles. The work in this thesis represents a new approach; comparing directly the non-crossing and crossing seas made up by the same irregular wave systems. This way we can distinguish between how much of the excess kurtosis that comes from the fact that the wave systems are strongly nonlinear in themselves, and how much that comes from the nonlinear interactions due to crossing.

More work is needed to broaden the understanding of whether or not crossing

sea enhances the occurrence of freak waves. The experimental results should be supported qualitatively with numerical simulations. The effect of different characteristic wave numbers, frequencies and amplitudes for the crossing wave trains should be investigated. More focus should be given at comparing crossing and non-crossing sea, not only searching for the angle between crossing wave trains that give the highest probability of freak waves. It is necessary to investigate whether or not non-crossing sea is just as, or even more, dangerous than crossing sea.

The work presented in this thesis has shown the importance and value of combining theory and experiments. By considering a special case of crossing sea experimentally, a new behaviour has been seen for crossing of irregular wave trains. The observed behaviour differs from what was expected based on previous works, both theoretically and experimentally.

7.3 Conclusion

This work presented a theoretical and experimental investigation on the statistical properties of the surface elevation in a special case of crossing sea conditions. The special case considered was the case of two irregular wave trains propagating in opposite directions, with the same characteristic frequency ω_c and wave number k_c. The modulational instability of two crossing Stokes waves, according to two coupled nonlinear Schrödinger equations describing the problem, was investigated. The stability analysis showed that the unstable domain of the perturbation was reduced in the case of a crossing sea compared to a non-crossing sea, at the same time as the growth rates were reduced. Such behaviour is usually interpreted as an indication that the occurrence of extreme events is reduced. Experimental results showed that the kurtosis, a measure of the probability of the occurrence of extreme events, was generally lower for crossing sea than non-crossing sea. Results of both the stability analysis and the experiments were in contradiction with the widespread mindset that crossing sea is more dangerous than non-crossing sea. The work presented in this thesis has demonstrated the need of further investigation, in order to fully understand the occurrence of freak waves in crossing sea with counterpropagating wave systems.

Bibliography

Alber, I. E. 1978 The effects of randomness on the stability of two-dimensional surface wave trains. *Proc. R. Soc. Lond.* **363**, 525–546.

Banner, Engineering Corp. 2013 *U-GAGE S18U Series Sensors with Analog Output*. Minneapolis USA.

Boukhanovsky, A. V. & Guedes Soares, C. 2009 Modelling of multi peaked directional wave spectra. *Appl. Ocean Res.* **31**, 132–141.

Bunnik, T. 2010 *Benchmark workshop on numerical wave modelling - description of test cases*. MARIN.

Cavaleri, L., Bertotti, L., Torrisi, L., Bitner-Gregersen, E., Serio, M. & Onorato, M. 2012 Rogue waves in crossing seas: The louis majesty accident. *J. Geophys. Res.* **117**, C00J10.

Devore, J. L. & Berk, K. N. 2007 *Modern Mathematical Statistics with Applications*. Thompson Brooks/Cole.

Dysthe, K., Krogstad, H. E. & Muller, P. 2008 Oceanic Rogue Waves. *Annu. Rev. Fluid Mech.* **40**, 287–310.

Gramstad, O. & Trulsen, K. 2011 Fourth-order coupled nonlinear Schrödinger equations for gravity waves on deep water. *Phys. Fluids* **23**, 062102.

Grönlund, A., Eliasson, B. & Marklund, M. 2009 Evolution of rogue waves in interacting wave systems. *Europhys. Lett.* **86**, 24001.

Grue, J., Clamond, D. & Jensen, A. 2003 Kinematics of extreme waves in deep water. *Appl. Ocean Res.* **25**, 355–366.

Guedes Soares, C. 1984 Representation of double-peaked sea wave spectra. *Ocean Eng.* **11**, 185–207.

Guedes Soares, C. 1991 On the occurrence of double peaked wave spectra. *Ocean Eng.* **18**, 167–171.

Hasselmann, K., Barnett, T.P., Bouws, E., Carlson, H., Cartwright, D.E., Enke, K., Ewing, J.A., Gienapp, H., Hasselmann, D.E., Kruseman, P., A., Meerburg, Muller, P., Olbers, D.J., Richter, K., Sell, W. & Walden, H. 1973 Measurements of Wind-Wave Growth and Swell decay during the Joint North Sea Wave Project (JONSWAP). Deutches Hydrographiches Institut, Hamburg.

Krogstad, H. E. & Arntsen, Ø.A. 2006 Linear Wave Theory: Part B. Norwegian Univeristy of Science and Technology.

Lechuga, A. 2006 Were freak waves involved in the sinking of the Tanker "Prestige"? *Nat. Hazards Earth Syst. Sci.* **6**, 973–978.

Mori, N. & Janssen, P. A. E. M. 2006 On Kurtosis and Occurence Probability of Freak Waves. *J. Phys. Oceanogr.* **36**, 1471–1483.

Ochi, M. K. 1998 *Ocean Waves: The Stochastic Approach*. Cambridge University Press.

Okamura, M. 1984 Instabilities of Wearly Nonlinear Standing Gravity Waves. *J. Phys. Soc. Jpn.* **53** (11), 3788–3796.

Onorato, M., Osborne, A. R. & Serio, M. 2006 Modulational Instability in Crossing Sea States: A Possible Mechanism for the Formation of Freak Waves. *Phys. Rev. Lett.* **96**, 014503.

Onorato, M., Proment, D. & Toffoli, A. 2010 Freak waves in crossing seas. *Eur. Phys. J. Special Topics* **185**, 45–55.

Osborne, Alfred 2015 *The Sinking of Prestige: Were Rouge Waves Responsible?*. Elsevier.

Shukla, P. K., Kourakis, I., Eliasson, B., Marklund, M. & Stenflo, L. 2006*a* Instability and Evolution of Nonlinearly Interacting Water Waves. *Phys. Rev. Lett.* **97**, 094501.

Shukla, P. K., Marklund, M. & Stenflo, L. 2006*b* Modulational Instability of Nonlinearly Interacting Incoherent Sea States. *JETP Lett.* **84**, 645–649.

Srokosz, M. A. & Longuet-Higgins, M. S. 1986 On the skewness of sea-surface elevation. *J. Fluid Mech.* **164**, 497–497.

Toffoli, A., Bitner-Gregersen, E. M., Osborne, A. R., Serio, M., Monbaliu, J. & Onorato, M. 2011 Extreme wave in random cross in seas: Laboratory experiments and numerical simulations. *Geophys. Res. Lett.* **38**, L06605.

Trulsen, K. 2006 *Tsunamis, rogue waves, internal waves and internal tides*, chap. Weakly nonlinear and stochastic properties of ocean wave fields. Application to an extreme wave event, pp. 49–106. Springer Wien NewYork.

Trulsen, K., Zeng, H. & Gramstad, O. 2012 Laboratory Evidence of freak waves provoked by non-uniform bathymetry. *Phys. Fluids* **24**, 097101.

Zakharov, V. E. 1968 Stability of periodic waves of finite amplitude on the surface of a deep fluid. *J. Appl. Mech. Tech. Phy.* **9**, 86–94.

List of Figures

List of Tables

Appendix A

Experimental setup

A.1 Creating input files for the wave generator

An input file for the wave generator consists of an array of voltage values. It is generated from a MATLAB script developed by Tore Magnus Taklo. The scan rate is chosen to be $SR = 50\ \mathrm{s}^{-1}$, which is the number of values the wave generator will be given per second. A JONSWAP spectrum is defined, with a peak enhancement factor $\gamma = 3.3$ (see Section 2.2.1). The spectrum is then normalised by the area under the curve. Amplitudes are found from the spectrum, using the fact that $S \sim a^2$. Components of the surface elevation is found by multiplying the amplitudes by a cosine with a random phase. The desired surface elevation η is a superposition of all these components connected to all the amplitudes from the JONSWAP spectrum, $\eta = \sum_j a_j \cos(\omega_j t + n\pi r)$ where r is a random number between 0 and 1. Now that we have found the desired surface elevation for our wave train, we need to convert this into an electrical voltage input for the wave generator. We choose a small amplitude, AV, which is multiplied with the surface elevation η. Since the equilibrium position for the wave generator is $EQ = 5.5$ V, we need to add this value to all the entries in the input array. We define the input array as $\eta_V = AV\eta + EQ$. Because of the equilibrium position of the wave generator, we need the time series to start and end at this value. This is done by setting the very first and very last entries of the time series to 5.5 V, and setting about one second in the beginning and the end to NaNs. These points are then interpolated to fit the boundary values, so that we end up with an array of voltage values that start and end with the equilibrium

A.2 Calibrating the ultrasonic probes

The U-GAGE S18U sensor is equipped with TEACH-mode programming which makes it easy to program for an arbitrary window for measurements. There are lights on the probe that indicate if the sensor is measuring values outside its sensing range. The sensing range of the probe is 3 cm to 30 cm, so if we want a window of ± 10 cm it can be smart to use a distance of 15 cm to the mean water level as the zero-level for the probe. To program the sensor, we place it in this zero-level, and hold the TEACH button for a couple of seconds until the LED light turns red. We

then move the probe to its Near limit, for a window of ±10 cm that would be a distance of 5 cm above the mean water level. We push the button again, and the LED light starts blinking. We then move the probe to the Far limit, in this case 25 cm above the mean water level, and push the button again. The LED light is now yellow, and when we have moved the probe back down to its starting point it is ready for use. This calibration, with the Near limit first, gives us a positive output slope for the surface elevation.

We do however need to make sure that the conversion between the electrical voltage registered by the probe, and the output values for the surface elevation (in centimetres) is correct. This can be done by moving a probe to its Far limit, and then moving it with steps of 1 cm all the way down to the Near limit. We track the signal from the probe in WaveLab and check if physically moving the probe 1 cm closer to the surface is logged as exactly a 1 cm displacement by the software. We conduct this conversion check for two of the probes (probe 11 and probe 15, which are the ones who are easiest to adjust), and since we get good results we assume that the conversion for the rest of the probes is correct too. See Figure A.1 for the run with probe 11.

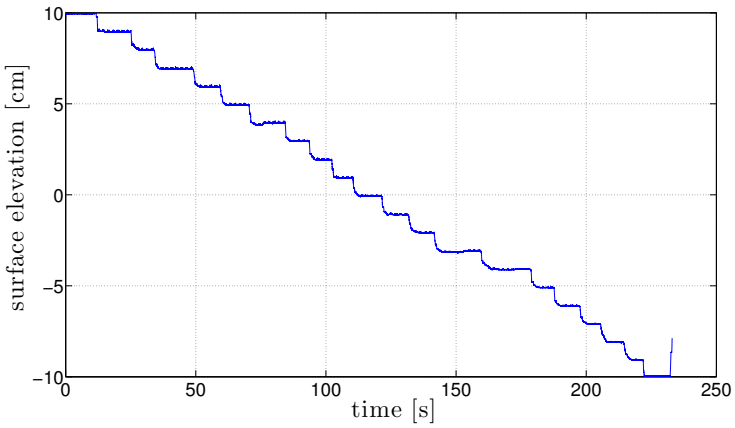

Figure A.1: Test of conversion between V and cm

A.3 Filters

The following three filters have been used for post-processing of the experimental data.

A.3.1 RemoveDropouts

```
function eta_out=RemoveDropouts(eta,ProbeNo,UpperThreshold, ...
                                        InnerThreshold)
% eta is a matrix containing time in the first column
% and surface elevation data in the remaning columns
% ProbeNo gives the probe you want to look at, a scalar

for i=1:length(eta)-1
    % Criteria for dropouts.
    if abs(eta(i+1,ProbeNo+1)-eta(i,ProbeNo+1))>InnerThreshold ...
        || abs(eta(i,ProbeNo+1))>UpperThreshold
        % Dropout data points are set to not a number (NaN).
        eta(i,ProbeNo+1) = NaN;
    end
end

eta_out=eta(:,ProbeNo+1);

end
```

A.3.2 RemovePeaks

```
function [etaOut] = RemovePeaks(etaIn, Threshold)
%etaIn is a vector for which we wish to remove sharp peaks
%(fast oscillating noise)

npr = 1; %no of peaks rmv in each run of loop
counter = 0;
npT = 0; %total no of peaks removed
etaOut = etaIn;

while npr > 0
    counter = counter + 1;

    [~, indices] = findpeaks(etaOut,'threshold',Threshold);
    etaOut(indices) = NaN;

    npr = sum(indices); %no of peaks rmv in this pass
    npT = npT + npr;

    fprintf('Pass no: %2d, removed %6d peaks. \n', counter, npr)

end
fprintf('Total no of peaks removed: %6d \n',npT)
end
```

A.3.3 `mlsmax` documentation

```
function [Pf,Pfres,Pfvar,Delta,Root,DiagSS2,dof]= ...
    mlsmax(epoints,dsites,f,Pfres,Delta,Root,order,nlocal)
% Computes multivariate moving least squares approximation of f
% with variance / confidence interval estimates.
% (This is method also known as local Regression)
%
% Usage:
%
%  [Pf,Pfres,Pfvar,Delta,Root,DiagSS2,dof] =
%      MLS(epoints,dsites,f,order,nlocal,csrbf)
% or
%
%  [Pf,Pfres,Pfvar,Delta,Root,DiagSS2,dof] =
%       MLS(epoints,dsites,f,Pfres,Delta,Root,order,nlocal,csrbf)
%
% Inputs  - epoints - List of evaluation points
%           dsites  - List of data sites for the function f
%           f       - Function values taken at data sites
%                     (may be a vector)
%           Pfres   - returned from previous execution of mls
%                     (avoid recompution)
%           Delta   - returned from previous execution of mls
%           Root    - returned from previous execution of mls
%           order   - Order of local polynomial
%                     (0 - constant, 1 - linear etc.)
%           nlocal  - Number of points within Support radius
%           csrbf   - Radial basis function with compact support.
%                    (uses Wendeland's phi(3,1) as default.)
%
% Outputs - Pf      - MLS approximation of f and its derivatives
%         - Pfres   - Residuals
%                     (evaluating of MLS approximation at dsites)
%         - Pfvar   - Variance function esimate and its derivatives
%         - Delta   - diag(S1*S1'-2*S1)
%         - Root    - Root of k-D tree created from dsites
%         - DiagSS2 - diag(S2*S2') (see Note 3)
%         - dof     - degrees of freedom (see Note 3)
%
% NOTE 1: This function uses ANN: A Library for Approximate Nearest
% Neighbor Searching (http://www.cs.umd.edu/~mount/ANN)
%
% NOTE 2: If Root is return as output, the user is responsible
% removing the k-D tree from memory using
%
%   ANNkd_tree_delete(Root)
%
% NOTE 3: If the errors are normally distributed, then
% confidence intervals for the true mean can be constructed as
%
%   Pf = Pf +- c*sqrt(Pfvar.*DiagSS2). * check this for multivariate
```

```
%
% The constant c can be chosen from the Student's t distribution
% with degrees of freedom equal to dof.
%
% References:
%
% G.E. Fasshauer
% Meshfree approximation method with matlab
% World Scientific Publishing, 2007
%
% Loader, C.
% Smoothing: Local Regression Techniques
% in Handbook of Computational Statistics
% Springer Heidelberg (2004, pages 539–563)
%
% D. Ruppert and M.P. Wand
% Multivariate locally weighted least–squares regression
% Annals of statistics (1994, volume 22, pages 1346–1370)
%
% D. Ruppert, M.P. Wand, U. Holst and O. Hossjer
% Local polynomial variance–function estimation
% Technometrics (1997, volume 39, pages 262–273)
%
% Writen by Jostein Kolaas (2009)

    .
    .
    .

end
```

Appendix B

Bootstrap intervals and repeatability

B.1 Width of confidence intervals

The maximum and minimum widths of the confidence intervals for the point estimates of variance, skewness and kurtosis are shown in Tables B.1 and B.2 for case 1 and case 2, respectively.

	Kurtosis		Skewness		Variance	
Time series	max	min	max	min	max	min
I S	0.1527	0.0656	0.0362	0.0268	0.0105	0.0070
II V	0.1155	0.0541	0.0350	0.0243	0.0127	0.0099

Table B.1: Confidence intervals for case 1: $\epsilon \simeq 0.1$

	Kurtosis		Skewness		Variance	
Time series	max	min	max	min	max	min
II S	0.1391	0.0524	0.0358	0.0254	0.0054	0.0035
III V	0.1021	0.0386	0.0332	0.0216	0.0054	0.0038

Table B.2: Confidence intervals for case 2: $\epsilon \simeq 0.06$

B.2 Repeatability

The repeatability is represented by a correlation factor Co, given by equation (5.1). The correlation factors that describe repeatability between two runs are given in Tables B.3 and B.4.

Runs	Crossing sea	Non-crossing sea
01/02	0.0091	0.0160
02/03	0.0074	0.0248
01/03	0.0168	0.0387

Table B.3: Max correlation factor, case 1: $\epsilon \simeq 0.1$

Runs	Crossing sea	Non-crossing sea
01/02	0.0449	0.0092
02/03	0.0024	0.0049
01/03	0.0346	0.0173

Table B.4: Max correlation factor, case 2: $\epsilon \simeq 0.06$

Appendix C

Pre-project

A pre-project for this master thesis was conducted in December 2013 - January 2014. The attached project has been corrected since it was handed in in January.

A factor $\frac{1}{2}$ was missing in the last terms of the series expansions in Section C.2.1.6, which led to one term on the right hand side in each of the equations (C.46) and (C.47) also missing a factor $\frac{1}{2}$. Also, in the expression for the surface elevation to second order, equation (C.45), the factor multiplying the parenthesis was $\frac{1}{2}$, but should be $\frac{1}{4}$.

Redoing the calculations in Section C.3 led to the same coupled nonlinear Schrödinger equations (C.63) and (C.64) as originally found. One explanation might be a miscalculation the first time the equations were derived. More likely, however, the two factors $\frac{1}{2}$ may have ended up cancelling each other out so that the correct equations were found the first time.

Prosjekt på 6 studiepoeng for

Lisa Bæverfjord Rye

Spesiell modell for kryssende sjø – to bølgesystemer med samme karakteristiske frekvens og motsatt retning

Veileder: Karsten Trulsen

Utlevert: 13.desember 2013
Innlevert: 20.januar 2014

Sammendrag

Jeg ønsker å beskrive kryssende sjø i det spesielle tilfellet at to bølgefelt med samme karakteristiske frekvens ω_c og samme karakteristiske bølgetall k_c forplanter seg i motsatt retning. Jeg vil bestemme alle koeffisienter i andre ordens uttrykk for overflatehevning og hastighetspotensial, både de for resonante og ikke-resonante bidrag. Ønsker å si noe om enkelte av koeffisientene i overflatehevningen kan settes lik null ved å pålegge passende krav på tilsvarende koeffisienter i hastighetspotensialet samt løsbarhetsbetingelser på første-ordens koeffisientene. Deretter ønsker jeg å etablere nøyaktig hvordan de koblede ikke-lineære Schrödinger-likningene ser ut, og gjøre rede for om disse likningene er utledet og studert tidligere.

Innhold

C.1 Innledning

Eksistensen av to simultane bølgesystemer på havoverflaten er vel dokumentert av bøyemålinger [1, 2] og hindcastdata [3]. En vanlig tilnærming for å studere et enkelt system av to ikkelineære vannbølger er applikasjonen av ikkelineære Schrödingerlikninger (NLS). For smalbåndede tyngdebølger er den mest grunnleggende tilnærmingen den kubiske NLS-likningen som ble utledet for dypt vann av Zakharov [4]. Det er velkjent at den kubiske NLS-likningen feiler i beskrivelsen av viktige aspekter av den ikkelineære utviklingen av et bølgefelt.

Jeg ønsker å beskrive kryssende sjø i det spesielle tilfellet at to bølgefelt med samme karakteristiske frekvens ω_c og samme karakteristiske bølgetall k_c forplanter seg i motsatt retning. Dette er ikke et smalbåndet problem, altså kan man for eksempel ikke anta at størrelser som bølgehøyde og kamhøyde er Rayleigh-fordelt. Derimot er dette det mest bredbåndede tilfellet man kan studere med to bølgekomponenter i to dimensjoner!

Det er to mål med dette prosjektet. Ved å begynne med Euler-likningene for inkompressibel væske som har virvelfri bevegelse, og å bruke perturbasjonsteori og flerskalaanalyse, ønsker jeg først å bestemme alle andreordens bidrag til overflatehevningen. Dette er verdifullt fordi det på lang sikt ville være interessant å diskutere envelope, bølgehøyde, kamhøyde, bølgestatistikk og forekomst av freake bølger i kryssende sjø. Det andre målet er å komme frem til to koblede ikkelineære Schrödingerlikninger, som beskriver en slik bølgebevegelse med ikkelineære effekter opp til og med tredje orden.

Dersom jeg bruker en karakteristisk steilhet ϵ som ordningsparameter kan jeg tenke meg at bølgefeltet er satt sammen av bidrag til forskjellige ordener (η er overflatehevningen)

$$\eta = \eta_1 + \epsilon\eta_2 + \epsilon^2\eta_3 + ...$$

hvor første ordens lineære del av bølgefeltet er satt sammen av to bølgefelt som forplanter seg mot høyre og venstre

$$\eta_1 = \eta_{1,h} + \eta_{1,v}$$

hvor

$$\eta_{1,h} = \frac{1}{2}B_h e^{i(k_c x - \omega_c t)} + c.c$$

og

$$\eta_{1,v} = \frac{1}{2}B_v e^{i(-k_c x - \omega_c t)} + c.c.$$

C.c. representerer den komplekskonjugerte. Til andre orden vil bølgefeltet ha komponenter til venstre og høyre (både første og andre harmonisk), et nullte harmonisk bidrag, samt to ledd som representerer en stående svingning i rom og en stående

svingning i tid. Det vil se omtrent slik ut:

$$\eta_2 = B_{2,0} + \frac{1}{2}\left(B_{2,h}e^{i(k_c x-\omega_c t)} + B_{2,v}e^{i(-k_c x-\omega_c t)} + B_{2,2h}e^{2i(k_c x-\omega_c t)} + c.c.\right) + \frac{1}{2}\left(B_{2,2v}e^{2i(-k_c x-\omega_c t)} + B_{2,2x}e^{2ik_c x} + B_{2,2t}e^{2i\omega_c t} + c.c.\right)$$

hvor k_c og ω_c er karakteristiske størrelser.

Jeg har begrenset meg til å se på kun *én* koordinat, altså en teori som egner seg utmerket for å studere eksperiment i en smal laboratorietank, men som neppe er pålitelig ute på åpent hav. Jeg har til hensikt å bestemme alle $B_{2,?}$, som er langsomme funskjoner av tid og rom for å beskrive modulasjon rundt den karakteristiske bølgen. Jeg skal også undersøke om jeg kan sette $B_{2,0}$, $B_{2,h}$, $B_{2,v}$, $B_{2,2x}$ og $B_{2,2t}$ til null ved å pålegge passende krav på de tilsvarende koeffisientene i hastighetspotensialet samt løsbarhetsbetingelser på koeffisientene i overflatehevningen. Jeg antar at hastighetsfeltet er virvelfritt og kan representeres ved et potensial ϕ (på samme form som η, med bidrag både for høyre og venstre). Deretter skal jeg bestemme løsbarhetsbetingelsene til tredje orden. De skal se omtrent slik ut

$$\frac{\partial B_h}{\partial t} + \frac{1}{2}\frac{\partial B_h}{\partial x} + \frac{i}{8}\frac{\partial^2 B_h}{\partial x^2} + \frac{i}{2}|B_h|^2 B_h + \alpha|B_v|^2 B_h = 0$$
$$\frac{\partial B_v}{\partial t} - \frac{1}{2}\frac{\partial B_v}{\partial x} + \frac{i}{8}\frac{\partial^2 B_v}{\partial x^2} + \frac{i}{2}|B_v|^2 B_v + \beta|B_h|^2 B_v = 0$$

og det er α og β som skal bestemmes. Til slutt skal jeg lese relevante artikler og gjøre rede for om disse likningene er utledet og studert tidligere, og i såfall sammenlikne mine resultater med tidligere resultater.

C.2 Full løsning til andre orden

C.2.1 Euler-likningene

Jeg begynner med Euler-likningene for inkompressibel væske med virvelfri bevegelse. Siden hastighetsfeltet er antatt virvelfritt kan det representeres ved et potensial ϕ. Jeg har to overflatekrav (kinematisk og dynamisk), feltlikning (Laplace likning er oppfylt i fluidet siden inkompressibelt og virvelfritt) og et bunnkrav.

$$\frac{\partial \eta}{\partial t} + \frac{\partial \phi}{\partial x}\frac{\partial \eta}{\partial x} - \frac{\partial \phi}{\partial z} = 0 \qquad @z = \eta \tag{C.1}$$
$$\frac{\partial \phi}{\partial t} + g\eta + \frac{1}{2}\left(\nabla\phi\right)^2 = 0 \qquad @z = \eta \tag{C.2}$$
$$\nabla^2\phi = 0 \qquad \text{for } -\infty < z < \eta \tag{C.3}$$
$$\frac{\partial \phi}{\partial z} = 0 \qquad \text{for } z \to -\infty \tag{C.4}$$

C.2.1.1 Skaleringsparametre

$$\begin{aligned}
\eta &\sim a \\
x, z &\sim \frac{1}{k_c} \\
t &\sim \frac{1}{\omega_c} \\
\phi &\sim \frac{a\omega_c}{k_c} \\
\frac{\partial}{\partial x} &= k_c \frac{\partial}{\partial x^*} \\
\frac{\partial}{\partial z} &= k_c \frac{\partial}{\partial z^*} \\
\frac{\partial}{\partial t} &= \omega_c \frac{\partial}{\partial t^*}
\end{aligned}$$

a er en karakteristisk amplitude for overflatehevningen.

C.2.1.2 Skalerer kinematisk randbetingelse

$$\begin{aligned}
\frac{\partial \eta}{\partial t} + \frac{\partial \phi}{\partial x}\frac{\partial \eta}{\partial x} - \frac{\partial \phi}{\partial z} &= 0 \\
a\omega_c \frac{\partial \eta^*}{\partial t^*} + a^2\omega_c k_c \frac{\partial \phi^*}{\partial x^*}\frac{\partial \eta^*}{\partial x^*} - a\omega_c \frac{\partial \phi^*}{\partial z^*} &= 0
\end{aligned}$$

Deler på ω_c og multipliserer med k_c. Jeg har funnet ut hvilken orden hvert av leddene har! Går tilbake til dimensjonelle størrelser, og $\epsilon = ak_c$ er nå en formell pertubasjonsparameter.

$$\epsilon \frac{\partial \eta}{\partial t} + \epsilon^2 \frac{\partial \phi}{\partial x}\frac{\partial \eta}{\partial x} - \epsilon \frac{\partial \phi}{\partial z} = 0 \quad @z = \epsilon\eta \tag{C.5}$$

C.2.1.3 Skalerer dynamisk randbetingelse

$$\begin{aligned}
\frac{\partial \phi}{\partial t} + g\eta + \frac{1}{2}\left(\nabla\phi\right)^2 &= 0 \\
\frac{a\omega_c}{k_c}\omega_c \frac{\partial \phi^*}{\partial t^*} + ga\eta^* + \frac{1}{2}\left(\left(k_c \frac{\partial}{\partial x^*}\frac{a\omega_c}{k_c}\phi^*\right)^2 + \left(k_c \frac{a\omega_c}{k_c}\frac{\partial \phi^*}{\partial z^*}\right)^2\right) &= 0
\end{aligned}$$

Forkorter

$$\frac{a\omega_c^2}{k_c}\frac{\partial \phi^*}{\partial t^*} + ga\eta^* + \frac{1}{2}\left(a^2\omega_c^2\left(\frac{\partial \phi^*}{\partial x^*}\right)^2 + a^2\omega_c^2\left(\frac{\partial \phi^*}{\partial z^*}\right)^2\right) = 0$$

Deler på ω_c^2 og multipliserer med k_c^2.

$$ak_c\frac{\partial\phi^*}{\partial t^*}+\frac{agk_c^2}{\omega_c^2}\eta+\frac{\epsilon^2}{2}\left(\left(\frac{\partial\phi^*}{\partial x^*}\right)^2+\left(\frac{\partial\phi^*}{\partial z^*}\right)^2\right)=0 \quad @z^*=\epsilon\eta^*$$

Antar at den lineære dispersjonsrelasjonen $\omega_c^2=gk_c$ er oppfylt, så jeg står igjen med ϵ i første og andre ledd og ϵ^2 i det siste. Har nå funnet ut hvilken orden hvert av leddene i den dynamiske randbetingelsen har, og jeg kan skrive opp den dynamiske randbetingelsen (C.2) med ϵ som formell perturbasjonsparameter:

$$\epsilon\frac{\partial\phi}{\partial t}+\epsilon g\eta+\frac{\epsilon^2}{2}\left(\left(\frac{\partial\phi}{\partial x}\right)^2+\left(\frac{\partial\phi}{\partial z}\right)^2\right)=0 \quad @z=\epsilon\eta \tag{C.6}$$

C.2.1.4 Skalerer Laplace likning

$$\begin{aligned}\nabla^2\phi&=0\\ \frac{\partial^2\phi}{\partial z^2}+\frac{\partial^2\phi}{\partial x^2}&=0\\ k_ca\omega_c\frac{\partial^2\phi^*}{\partial(z^*)^2}+k_ca\omega_c\frac{\partial^2\phi^*}{\partial(x^*)^2}&=0\\ \epsilon\frac{\partial^2\phi}{\partial z^2}+\epsilon\frac{\partial^2\phi}{\partial x^2}&=0 \quad \text{for} -\infty<z<\epsilon\eta\end{aligned} \tag{C.7}$$

C.2.1.5 Skalerer bunnkravet

$$\begin{aligned}\frac{\partial\phi}{\partial z}&=0\\ k_c\frac{a\omega_c}{k_c}\frac{\partial\phi^*}{\partial z^*}&=0\\ \epsilon\frac{\partial\phi}{\partial z}&=0 \quad \text{for } z\to-\infty\end{aligned} \tag{C.8}$$

C.2.1.6 Rekkeutvikling

Rekkeutvikler (C.5) og (C.6) om $z=0$

$$\begin{aligned}\left.\frac{\partial\phi}{\partial t}\right|_{z=\epsilon\eta}&=\left.\frac{\partial\phi}{\partial t}\right|_{z=0}+\epsilon\eta\left.\frac{\partial^2\phi}{\partial z\partial t}\right|_{z=0}+\frac{\epsilon^2\eta^2}{2}\left.\frac{\partial^3\phi}{\partial z^2\partial t}\right|_{z=0}+\mathcal{O}(\epsilon^3)\\ \left.\frac{\partial\phi}{\partial x}\right|_{z=\epsilon\eta}&=\left.\frac{\partial\phi}{\partial x}\right|_{z=0}+\epsilon\eta\left.\frac{\partial^2\phi}{\partial z\partial x}\right|_{z=0}+\frac{\epsilon^2\eta^2}{2}\left.\frac{\partial^3\phi}{\partial z^2\partial x}\right|_{z=0}+\mathcal{O}(\epsilon^3)\\ \left.\frac{\partial\phi}{\partial z}\right|_{z=\epsilon\eta}&=\left.\frac{\partial\phi}{\partial z}\right|_{z=0}+\epsilon\eta\left.\frac{\partial^2\phi}{\partial z^2}\right|_{z=0}+\frac{\epsilon^2\eta^2}{2}\left.\frac{\partial^3\phi}{\partial z^3}\right|_{z=0}+\mathcal{O}(\epsilon^3)\end{aligned}$$

(C.5) til og med tredje orden

$$\epsilon\frac{\partial\eta}{\partial t}+\epsilon^2\frac{\partial\eta}{\partial x}\frac{\partial\phi}{\partial x}+\epsilon^3\eta\frac{\partial\eta}{\partial x}\frac{\partial^2\phi}{\partial z\partial x}-\epsilon\frac{\partial\phi}{\partial z}-\epsilon^2\eta\frac{\partial^2\phi}{\partial z^2}-\frac{\epsilon^3\eta^2}{2}\frac{\partial^3\phi}{\partial z^3}=0$$

(C.6) til og med tredje orden

$$\begin{aligned}&\epsilon\frac{\partial\phi}{\partial t}+\epsilon^2\eta\frac{\partial^2\phi}{\partial z\partial t}+\frac{\epsilon^3\eta^2}{2}\frac{\partial^3\phi}{\partial z^2\partial t}+\epsilon g\eta\\&+\frac{\epsilon^2}{2}\left(\left(\frac{\partial\phi}{\partial x}\right)^2+\left(\frac{\partial\phi}{\partial z}\right)^2\right)+\epsilon^3\eta\left(\frac{\partial^2\phi}{\partial z^2}\frac{\partial\phi}{\partial z}+\frac{\partial^2\phi}{\partial z\partial x}\frac{\partial\phi}{\partial x}\right)=0\end{aligned}$$

C.2.1.7 Flerskalaanalyse

Det er to ulike og helt uavhengige grunner til at en flerskalaanalyse må benyttes. Hadde jeg betraktet to monokromatiske bølger, for eksempel Stokes-bølger, som propagerer i motsatt retning, måtte jeg tatt med en langsom skala for å få noe fornuftig ut av løsbarhetsbetingelsen. Perturbasjonsanalysen bryter sammen dersom du ikke har en langsom modulasjon å putte inn i løsbarhetsbetingelsen. Den andre grunnen er at for å kunne beskrive et irregulært bølgefelt slik som det jeg ønsker å se på, som har båndbredde ulik 0, må langsomme skalaer benyttes. Hvis jeg hadde antatt at modulasjonen av bølgefeltet var på samme skala som bærebølgen, hadde jeg ikke lenger hatt noen karakteristisk frekvens. Altså må den komplekse amplituden B_h være en funksjon av t_1, hvor t_1 er en langsom skala i forhold til bærebølgens frekvens ω_c. Denne langsomme skalaen er knyttet til båndbredden δ. Deretter gjør jeg en umotivert antagelse om at den langsomme skalaen er koblet til steilheten, ved å si at $\delta=\epsilon$.

$$\begin{aligned}x_0&=x,\quad x_1=\epsilon x,\quad x_2=\epsilon^2x,...\\t_0&=t,\quad t_1=\epsilon t,\quad t_2=\epsilon^2t,...\\\frac{\partial}{\partial x}&=\frac{\partial}{\partial x_0}+\epsilon\frac{\partial}{\partial x_1}+\epsilon^2\frac{\partial}{\partial x_2}+...\\\frac{\partial}{\partial t}&=\frac{\partial}{\partial t_0}+\epsilon\frac{\partial}{\partial t_1}+\epsilon^2\frac{\partial}{\partial t_2}+...\end{aligned}$$

I tillegg benytter jeg en pertubasjonsutvikling av ϕ og η, med steilheten ϵ som parameter [5]

$$\begin{aligned}\phi&=\phi_1+\epsilon\phi_2+\epsilon^2\phi_3+...\\\eta&=\eta_1+\epsilon\eta_2+\epsilon^2\eta_3+...\end{aligned}$$

C.2.2 Første ordens problem, skalert og rekkeutviklet

$$\frac{\partial \eta_1}{\partial t_0} - \frac{\partial \phi_1}{\partial z} = 0 \qquad @z = 0 \tag{C.9}$$

$$\frac{\partial \phi_1}{\partial t_0} + g\eta_1 = 0 \qquad @z = 0 \tag{C.10}$$

$$\frac{\partial^2 \phi_1}{\partial z^2} + \frac{\partial^2 \phi_1}{\partial x_0^2} = 0 \qquad \text{for} - \infty < z < 0 \tag{C.11}$$

$$\frac{\partial \phi_1}{\partial z} = 0 \qquad \text{for } z \to -\infty \tag{C.12}$$

C.2.2.1 Løsning

Laplace likning (C.11) og bunnkrav (C.12) gjør at jeg kan anta en løsning for ϕ_1 på formen

$$\phi_1 = \phi_{1,h} + \phi_{1,v}$$

hvor

$$\phi_{1,h} = \frac{1}{2} a_h e^{i(k_c x_0 - \omega_c t_0) + k_c z} + c.c$$
$$\phi_{1,v} = \frac{1}{2} a_v e^{i(-k_c x_0 - \omega_c t_0) + k_c z} + c.c$$

Tilsvarende, for η_1

$$\eta_1 = \eta_{1,h} + \eta_{1,v}$$

hvor

$$\eta_{1,h} = \frac{1}{2} B_h e^{i(k_c x_0 - \omega_c t_0)} + c.c$$
$$\eta_{1,v} = \frac{1}{2} B_v e^{i(-k_c x_0 - \omega_c t_0)} + c.c.$$

Eliminerer η_1 fra (C.10) og får at

$$\frac{\partial^2 \phi_1}{\partial t_0^2} + g\frac{\partial \phi_1}{\partial z} = 0 \quad @z = 0$$

Dette gir dispersjonsrelasjonen

$$\omega_c^2 = g k_c \tag{C.13}$$

som må være oppfylt for bølger som går både mot høyre og venstre.

Relasjoner mellom $\mathbf{a_h}$ og $\mathbf{B_h}$:
Kan bruke enten (C.9) eller (C.10), og får at

$$a_h = \frac{-i\omega_c}{k_c} B_h \tag{C.14}$$

$$a_v = \frac{-i\omega_c}{k_c} B_v \tag{C.15}$$

B_h og B_v er amplitudene for overflatehevningen for bølger som går henholdsvis mot høyre og venstre. Disse kan måles i laben.

C.2.3 Andre ordens problem, skalert og rekkeutviklet

$$\frac{\partial \eta_2}{\partial t_0} - \frac{\partial \phi_2}{\partial z} = -\frac{\partial \eta_1}{\partial t_1} - \frac{\partial \phi_1}{\partial x_0}\frac{\partial \eta_1}{\partial x_0} + \eta_1 \frac{\partial^2 \phi_1}{\partial z^2} \qquad @z = 0 \tag{C.16}$$

$$\frac{\partial \phi_2}{\partial t_0} + g\eta_2 = -\frac{\partial \phi_1}{\partial t_1} - \eta_1 \frac{\partial^2 \phi_1}{\partial z \partial t_0} - \frac{1}{2}\left((\frac{\partial \phi_1}{\partial x_0})^2 + (\frac{\partial \phi_1}{\partial z})^2 \right) \qquad @z = 0 \tag{C.17}$$

$$\frac{\partial^2 \phi_2}{\partial z^2} + \frac{\partial^2 \phi_2}{\partial x_0^2} = -2\frac{\partial^2 \phi_1}{\partial x_0 \partial x_1} \qquad \text{for } -\infty < z < 0 \tag{C.18}$$

$$\frac{\partial \phi_2}{\partial z} = 0 \qquad \text{for } z \to -\infty \tag{C.19}$$

C.2.3.1 Høyresidene

Fra første ordens problem har jeg at

$$\phi_1 = \frac{1}{2} a_h e^{i(k_c x_0 - \omega_c t_0) + k_c z} + \frac{1}{2} a_v e^{i(-k_c x_0 - \omega_c t_0) + k_c z} + c.c$$

$$\eta_1 = \frac{1}{2} B_h e^{i(k_c x_0 - \omega_c t_0)} + \frac{1}{2} B_v e^{i(-k_c x_0 - \omega_c t_0)} + c.c$$

Dette kan jeg bruke for å finne høyresidene i likningssystemet for andre orden (C.16) - (C.19). Jeg får følgende likningssystem

$$\begin{aligned}\frac{\partial \eta_2}{\partial t_0} - \frac{\partial \phi_2}{\partial z} &= -\frac{1}{2}\frac{\partial B_h}{\partial t_1}e^{i(k_c x_0 - \omega_c t_0)} - \frac{1}{2}\frac{\partial B_v}{\partial t_1}e^{i(-k_c x_0 - \omega_c t_0)} \\ &\quad - \frac{1}{2}B_h^2 i k_c \omega_c e^{2i(k_c x_0 - \omega_c t_0)} - \frac{1}{2}B_v^2 i k_c \omega_c e^{2i(-k_c x_0 - \omega_c t_0)} + ... \qquad \text{(C.20)} \\ \frac{\partial \phi_2}{\partial t_0} + g\eta_2 &= -\frac{1}{2}\frac{\partial a_h}{\partial t_1}e^{i(k_c x_0 - \omega_c t_0)} - \frac{1}{2}\frac{\partial a_v}{\partial t_1}e^{i(-k_c x_0 - \omega_c t_0)} \\ &\quad + \frac{1}{4}B_h^2\omega_c^2 e^{2i(k_c x_0 - \omega_c t_0)} + \frac{1}{2}B_h B_v \omega_c^2 e^{-2i\omega_c t_0} \\ &\quad + \frac{1}{4}B_v^2\omega_c^2 e^{2i(-k_c x_0 - \omega_c t_0)} + \frac{1}{2}\omega_c^2 B_v B_h e^{-2i\omega_c t_0} + ... \qquad \text{(C.21)} \\ \frac{\partial^2 \phi_2}{\partial z^2} + \frac{\partial^2 \phi_2}{\partial x_0^2} &= -i\frac{\partial a_h}{\partial x_1}k_c e^{i(k_c x_0 - \omega_c t_0)} + i\frac{\partial a_v}{\partial x_1}k_c e^{i(-k_c x_0 - \omega_c t_0)} \qquad \text{(C.22)} \\ \frac{\partial \phi_2}{\partial z} &= 0 \qquad \text{(C.23)}\end{aligned}$$

C.2.3.2 Fokuserer på $B_{2,2h}$

Antar ϕ_{22} har formen

$$\begin{aligned}\phi_{22} &= \phi_{2,2h} + \phi_{2,2v} \\ &= \frac{1}{2}A_{2,2h}e^{2i(k_c x_0 - \omega_c t_0)} + \frac{1}{2}A_{2,2v}e^{2i(-k_c x_0 - \omega_c t_0)} + c.c\end{aligned}$$

Setter inn i Laplace likning (C.22) (som ikke har noen andre ordens andre harmoniske inhomogeniteter) og benytter bunnkravet (C.19). Får at

$$\begin{aligned}A_{2,2h} &= a_{2,2h}e^{2k_c z} \\ \Rightarrow \phi_{2,2h} &= \frac{1}{2}a_{2,2h}e^{2i(k_c x_0 - \omega_c t_0) + 2k_c z}\end{aligned}$$

Tilsvarende har jeg at

$$\eta_{22} = \frac{1}{2}B_{2,2h}e^{2i(k_c x_0 - \omega_c t_0)} + \frac{1}{2}B_{2,2v}e^{2i(-k_c x_0 - \omega_c t_0)} + c.c$$

Setter dette inn i (C.20) og (C.21), og får to likninger med to ukjente

$$\begin{bmatrix} -i\omega_c & \frac{1}{2}g \\ -k_c & -i\omega_c \end{bmatrix}\begin{bmatrix} a_{2,2h} \\ B_{2,2h} \end{bmatrix} = \begin{bmatrix} \frac{1}{4}\omega_c^2 B_h^2 \\ -\frac{1}{2}ik_c\omega_c B_h^2 \end{bmatrix}$$

Finner den inverse av matrisa på venstre side, får et uttrykk for $a_{2,2h}$ og $B_{2,2h}$

$$\begin{bmatrix} a_{2,2h} \\ B_{2,2h} \end{bmatrix} = \frac{1}{-\omega_c^2 + \frac{1}{2}gk_c}\begin{bmatrix} -i\omega_c & -\frac{1}{2}g \\ k_c & -i\omega_c \end{bmatrix}\begin{bmatrix} \frac{1}{4}\omega_c^2 B_h^2 \\ -\frac{1}{2}ik_c\omega_c B_h^2 \end{bmatrix}$$

Dette gir at

$$a_{2,2h} = 0 \tag{C.24}$$

$$B_{2,2h} = \frac{1}{2} k_c B_h^2 \tag{C.25}$$

C.2.3.3 Fokuserer på $B_{2,2v}$

Tilsvarende som for $B_{2,2h}$ får jeg at

$$a_{2,2v} = 0 \tag{C.26}$$

$$B_{2,2v} = \frac{1}{2} k_c B_v^2 \tag{C.27}$$

C.2.3.4 Fokuserer på $B_{2,h}$

Antar

$$\phi_{2,h} = \frac{1}{2} A_{2,h} e^{i(k_c x_0 - \omega_c t_0)} + c.c$$

Setter inn i Laplace likning (C.22), som har et inhomogent bidrag på høyre side. Får da at

$$A_{2,h} = a_{2,h} e^{k_c z} - i \frac{\partial a_h}{\partial x_1} z e^{k_c z} \tag{C.28}$$

Får igjen to likninger i to ukjente

$$\begin{bmatrix} -k_c & -i\omega_c \\ -i\omega_c & g \end{bmatrix} \begin{bmatrix} a_{2,h} \\ B_{2,h} \end{bmatrix} = \begin{bmatrix} -\frac{\omega_c}{k_c} \frac{\partial B_h}{\partial x_1} - \frac{\partial B_h}{\partial t_1} \\ \frac{i\omega_c}{k_c} \frac{\partial B_h}{\partial t_1} \end{bmatrix} \tag{C.29}$$

Matrisa på venstre side har en egenverdi $\lambda = 0$, dvs at de to likningene kan reduseres til en. Multipliserer øverste rad med $-i\omega_c$ og nederste rad med k_c, og legger de to likningene sammen. Da får jeg

$$g k_c B_{2,h} - \omega_c^2 B_{2,h} = i\omega_c \frac{\partial B_h}{\partial t_1} + \frac{i\omega_c^2}{k_c} \frac{\partial B_h}{\partial x_1} + i\omega_c \frac{\partial B_h}{\partial t_1}$$

Siden den lineære dispersjonsrelasjonen (C.13) er oppfylt er venstresiden 0, og jeg får løsbarhetsbetingelsen

$$\begin{aligned} 2i\omega_c \frac{\partial B_h}{\partial t_1} + \frac{i\omega_c^2}{k_c} \frac{\partial B_h}{\partial x_1} &= 0 \\ \Rightarrow \frac{\partial B_h}{\partial t_1} + \frac{\omega_c}{2k_c} \frac{\partial B_h}{\partial x_1} &= 0 \end{aligned} \tag{C.30}$$

som forteller oss at den komplekse envelopen forflytter seg med gruppehastigheten til den karakteristiske bølgen. I tillegg får jeg fra nederste rad i (C.29) en relasjon mellom $a_{2,h}$ og $B_{2,h}$ (hvor en av koeffisientene kan velges fritt):

$$a_{2,h} = -\frac{ig}{\omega_c} B_{2,h} - \frac{1}{k_c}\frac{\partial B_h}{\partial t_1}$$

Jeg skal velge $B_{2,h} = 0$, da er $a_{2,h}$ entydig bestemt

$$a_{2,h} = -\frac{1}{k_c}\frac{\partial B_h}{\partial t_1} \tag{C.31}$$

C.2.3.5 Fokuserer på $B_{2,v}$

Tilsvarende som for $B_{2,h}$ får jeg at

$$\frac{\partial B_v}{\partial t_1} - \frac{\omega_c}{2k_c}\frac{\partial B_v}{\partial x_1} = 0 \tag{C.32}$$

Jeg velger også $B_{2,v} = 0$, da blir

$$a_{2,v} = -\frac{1}{k_c}\frac{\partial B_v}{\partial t_1} \tag{C.33}$$

C.2.3.6 Fokuserer på $B_{2,0}$

Antar

$$\phi_{2,0} = A_{2,0}(z)$$

så $\phi_{2,0}$ er ikke en funksjon av x_0. Setter inn i Laplace likning (C.18), får at

$$\begin{aligned} \frac{\partial^2 A_{2,0}}{\partial z^2} &= 0 \\ \Rightarrow A_{2,0} &= c_1 z + c_2 \end{aligned}$$

hvor c_1 og c_2 er konstanter. For å oppfylle bunnkravet (C.19) må $c_1 = 0$, altså er $A_{2,0}$ en konstant slik jeg kjenner den. Høyresiden i den kinematiske overflatebetingelsen (C.16) har ingen nullte harmonisk komponent, og blir nå

$$\begin{aligned} \frac{\partial \eta_{2,0}}{\partial t_0} &= 0 \\ \Rightarrow \eta_{2,0} &= B_{2,0}(x_1, t_1) \end{aligned}$$

Det dynamiske overflatekravet (C.17) er

$$\frac{\partial \phi_{2,0}}{\partial t_0} + g\eta_{2,0} = 0$$

og siden $\frac{\partial \phi_{2,0}}{\partial t_0} = 0$ får jeg at

$$B_{2,0} = 0 \tag{C.34}$$

C.2.3.7 Fokuserer på $B_{2,2t}$

Antar

$$\phi_{2,2t} = A_{2,2t} e^{2i\omega_c t_0} \tag{C.35}$$

og

$$\eta_{2,2t} = B_{2,2t} e^{2i\omega_c t_0} \tag{C.36}$$

Høyresiden i Laplace likning (C.18) har ingen bidrag på formen $e^{2i\omega_c t_0}$, og sammen med bunnkravet gir dette at $\phi_{2,2t}$ ikke er en funksjon av z. Kinematisk randbetingelse blir da

$$\begin{aligned} \frac{\partial \eta_{2,2t}}{\partial t_0} &= 2i\omega_c B_{2,2t} e^{2i\omega_c t_0} = 0 \\ &\Rightarrow B_{2,2t} = 0 \\ &\Rightarrow \eta_{2,2t} = 0 \end{aligned} \tag{C.37}$$

Dynamisk randkrav:

$$\frac{\partial \phi_{2,2t}}{\partial t_0} + g\eta_{2,2t} = \omega_c^2 B_h^* B_v^* e^{2i\omega_c t_0} \tag{C.38}$$

(C.37) $\Rightarrow$ (C.38):

$$\begin{aligned} 2i\omega_c A_{2,2t} e^{2i\omega_c t_0} &= \omega_c^2 B_h^* B_v^* e^{2i\omega_c t_0} \\ \Rightarrow A_{2,2t} &= -\frac{i}{2}\omega_c B_h^* B_v^* \\ \Rightarrow \phi_{2,2t} &= -\frac{i}{2}\omega_c B_h^* B_v^* e^{2i\omega_c t_0} \end{aligned} \tag{C.39}$$

C.2.3.8 Fokuserer på $B_{2,2x}$

Antar

$$\phi_{2,2x} = A_{2,2x} e^{2ik_c x_0} \tag{C.40}$$

og

$$\eta_{2,2x} = B_{2,2x} e^{2ik_c x_0}$$

Høyresiden i Laplace likning (C.18) har ingen bidrag på formen $e^{2ik_c x_0}$. Setter (C.40) inn i (C.18), og får at

$$\begin{aligned} \frac{\partial^2 \phi_{2,2x}}{\partial z^2} - 4k_c^2 \phi_{2,2x} &= 0 \\ \Rightarrow A_{2,2x} &= a_{2,2x} e^{2k_c z} \\ \Rightarrow \phi_{2,2x} &= a_{2,2x} e^{2ik_c x_0 + 2k_c z} \end{aligned} \tag{C.41}$$

Kinematisk randbetingelse (bruker at $\eta_{2,2x}$ ikke er en funksjon av t_0):

$$\begin{aligned} -\frac{\partial \phi_{2,2x}}{\partial z} &= -2k_c a_{2,2x} e^{2ik_c x_0} = \frac{k_c^2}{2}\left(a_h B_v^* + a_v^* B_h\right) e^{2ik_c x_0} = 0 \\ \Rightarrow a_{2,2x} &= 0 \end{aligned} \tag{C.42}$$

hvor jeg har brukt at

$$a_v^* = \frac{i\omega_c}{k_c} B_v^*$$

Bruker (C.42), dynamisk randbetingelse blir

$$\begin{aligned} gB_{2,2x} &= \frac{i}{4}\omega_c k_c \left(a_h B_v^* + B_h a_v^*\right) = 0 \\ \Rightarrow B_{2,2x} &= 0 \end{aligned} \tag{C.43}$$

C.2.4 Oppsummering av andre ordens løsning

$$\begin{aligned} \phi_2 = a_{2,0} &- \frac{i}{2}\omega_c B_h B_v^* e^{2i\omega_c t_0} - \frac{1}{2k_c}\left(\frac{\partial B_h}{\partial t_1} + \omega_c \frac{\partial B_h}{\partial x_1} z\right) e^{i(k_c x_0 - \omega_c t_0) + k_c z} \\ &- \frac{1}{2k_c}\left(\frac{\partial B_v}{\partial t_1} + \omega_c \frac{\partial B_v}{\partial x_1} z\right) e^{i(-k_c x_0 - \omega_c t_0) + k_c z} + c.c \end{aligned} \tag{C.44}$$

$$\eta_2 = \frac{1}{4} k_c \left(B_h^2 e^{2i(k_c x_0 - \omega_c t_0)} + B_v^2 e^{2i(-k_c x_0 - \omega_c t_0)}\right) + c.c \tag{C.45}$$

Har bestemt koeffisienter for både resonante og ikke-resonante ledd til andre orden. Jeg har vist at det ikke kan finnes ledd av typen $e^{2ik_c x_0}$, da både $B_{2,2x}$ og $a_{2,2x}$ er 0. Dette leddet ville ha tilsvart stående svingninger i rommet.
Jeg har vist at det fins bidrag på formen $e^{2i\omega_c t_0}$ som tilsvarer stående svingninger i tid. I neste del skal jeg undersøke om disse påvirker løsbarhetsbetingelsen til 3.orden.

Jeg har vist at $B_{2,h}$ og $B_{2,v}$ kan settes lik null dersom man pålegger passende krav på de tilsvarende koeffisientene i hastighetspotensialet samt løsbarhetsbetingelser på koeffisientene i overflatehevningen. I tillegg har jeg funnet at $B_{2,0}$ er null, og $a_{2,0}$ er en konstant slik jeg kjenner den (dette kan endre seg når jeg går til en høyere orden, eller innfører langsomme og raske skalaer også i z).

C.3 Løsbarhetsbetingelsen til tredje orden

C.3.1 3.ordens problem, skalert og rekkeutviklet

$$\begin{aligned}
\frac{\partial \eta_3}{\partial t_0} - \frac{\partial \phi_3}{\partial z} = &-\frac{\partial \eta_2}{\partial t_1} - \frac{\partial \eta_1}{\partial t_2} - \frac{\partial \eta_1}{\partial x_0}\frac{\partial \phi_2}{\partial x_0} - \frac{\partial \eta_2}{\partial x_0}\frac{\partial \phi_1}{\partial x_0} \\
&- \frac{\partial \eta_1}{\partial x_0}\frac{\partial \phi_1}{\partial x_1} - \frac{\partial \phi_1}{\partial x_0}\frac{\partial \eta_1}{\partial x_1} + \frac{\eta_1^2}{2}\frac{\partial^3 \phi_1}{\partial z^3} \\
&- \eta_1 \frac{\partial \eta_1}{\partial x_0}\frac{\partial^2 \phi_1}{\partial z \partial x_0} + \eta_1 \frac{\partial^2 \phi_2}{\partial z^2} + \eta_2 \frac{\partial^2 \phi_1}{\partial z^2} \qquad @z = 0 \qquad \text{(C.46)} \\
\frac{\partial \phi_3}{\partial t_0} + g\eta_3 = &- \frac{\partial \phi_1}{\partial t_2} - \frac{\partial \phi_2}{\partial t_1} - \eta_2 \frac{\partial^2 \phi_1}{\partial z \partial t_0} - \eta_1 \frac{\partial^2 \phi_1}{\partial z \partial t_1} \\
&- \eta_1 \frac{\partial^2 \phi_2}{\partial z \partial t_0} - \frac{\eta_1^2}{2}\frac{\partial^3 \phi_1}{\partial z^2 \partial t_0} \\
&- \frac{\partial \phi_1}{\partial z}\frac{\partial \phi_2}{\partial z} - \frac{\partial \phi_1}{\partial x_0}\frac{\partial \phi_1}{\partial x_1} - \frac{\partial \phi_1}{\partial x_0}\frac{\partial \phi_2}{\partial x_0} \\
&- \eta_1 \left(\frac{\partial^2 \phi_1}{\partial z^2}\frac{\partial \phi_1}{\partial z} + \frac{\partial^2 \phi_1}{\partial z \partial x_0}\frac{\partial \phi_1}{\partial x_0} \right) \qquad @z = 0 \qquad \text{(C.47)} \\
\frac{\partial^2 \phi_3}{\partial z^2} + \frac{\partial^2 \phi_3}{\partial x_0^2} = &-2\frac{\partial^2 \phi_2}{\partial x_0 \partial x_1} - 2\frac{\partial^2 \phi_1}{\partial x_2 \partial x_0} - \frac{\partial^2 \phi_1}{\partial x_1^2} \qquad \text{for} - \infty < z < 0 \qquad \text{(C.48)} \\
\frac{\partial \phi_3}{\partial z} = &\ 0 \qquad \text{for } z \to -\infty \qquad \text{(C.49)}
\end{aligned}$$

C.3.2 Snarvei for å finne løsbarhetsbetingelsen til n-te orden

Jeg trenger en snarvei for å finne løsbarhetsbetingelsene til tredje orden (ikkelineær Schrödingerlikning) uten å måtte løse Poissons likning (C.48). Ser på n-te ordens problemet, første harmonisk, spesialtilfellet for *én* bølge (indeks 1 representerer enten høyre eller venstre).

$$\frac{\partial \phi_{n,1}}{\partial t_0} - \frac{\partial \phi_{n,1}}{\partial z} = F_{n,1} \qquad @z = 0 \qquad \text{(C.50)}$$

$$\frac{\partial \phi_{n,1}}{\partial t_0} + g\eta_{n,1} = G_{n,1} \qquad @z = 0 \qquad \text{(C.51)}$$

$$\frac{\partial^2 \phi_{n,1}}{\partial z^2} + \frac{\partial^2 \phi_{n,1}}{\partial x_0^2} = H_{n,1} \qquad \text{for} - \infty < z < 0 \qquad \text{(C.52)}$$

$$\frac{\partial \phi_{n,1}}{\partial z} = I_{n,1} \qquad \text{for } z \to -\infty \qquad \text{(C.53)}$$

Eliminerer $\eta_{n,1}$ fra (C.51), multipliserer (C.52) med $\phi_{1,1}$ og integrerer fra $-\infty$ til 0 dz:

$$\frac{\partial^2\phi_{n,1}}{\partial t_0^2} + g\frac{\partial\phi_{n,1}}{\partial z} = -i\omega_c G_{n,1} - gF_{n,1}$$

$$\int_{-\infty}^{0} \phi_{1,1}\frac{\partial^2\phi_{n,1}}{\partial z^2}\ \mathrm{dz} + \int_{-\infty}^{0} \phi_{1,1}\frac{\partial^2\phi_{n,1}}{\partial x_0^2}\ \mathrm{dz} = \int_{-\infty}^{0} \phi_{1,1}H_{n,1}\ \mathrm{dz} \tag{C.54}$$

Bruker delvis integrasjon på første ledd i (C.54) to ganger, får at

$$\int_{-\infty}^{0} \phi_{1,1}\frac{\partial^2\phi_{n,1}}{\partial z^2}\ \mathrm{dz} = \phi_{1,1}\left[-F_{n,1} - \frac{i\omega_c}{g}G_{n,1} - \frac{1}{g}\frac{\partial^2\phi_{n,1}}{\partial t_0^2}\right]_{z=0} + \frac{1}{g}\frac{\partial^2\phi_{1,1}}{\partial t_0^2}\phi_{n,1} + \int_{\infty}^{0} \frac{\partial^2\phi_{1,1}}{\partial z^2}\phi_{n,1}\ \mathrm{dz} \tag{C.55}$$

Forkorter, og bruker første ordens Laplace likning (C.11) på siste ledd, første ledd i (C.54) blir da

$$\int_{-\infty}^{0} \phi_{1,1}\frac{\partial^2\phi_{n,1}}{\partial z^2}\ \mathrm{dz} = \phi_{1,1}\left[-F_{n,1} - \frac{i\omega_c}{g}G_{n,1}\right]_{z=0} - \int_{\infty}^{0} (ik_c)^2\phi_{1,1}\phi_{n,1} \tag{C.56}$$

Siste ledd i (C.56) kansellerer med andre ledd i (C.54), og jeg får en integrallikning som kan benyttes til å finne løsbarhetsbetingelsene for n-te orden

$$\int_{-\infty}^{0} \phi_{1,1}H_{n,1}\ \mathrm{dz} = -\phi_{1,1}\left[F_{n,1} + \frac{i\omega_c}{g}G_{n,1}\right]_{z=0} \tag{C.57}$$

Eksempel: Løsbarhetsbetingelse til andre orden
Finner løsbarhetsbetingelsen for en bølge som forplanter seg mot høyre

$$-i\omega_c\eta_{2,h} - \frac{\partial\phi_{2,h}}{\partial z} = -\frac{\partial\eta_{1,h}}{\partial t_1} = -\frac{1}{2}\frac{\partial B_h}{\partial t_1} = F_{2,h} \tag{C.58}$$

$$-i\omega_c\phi_{2,h} + g\eta_{2,h} = -\frac{\partial\phi_{1,h}}{\partial t_1} = -\frac{1}{2}\frac{\partial a_h}{\partial t_1} = \frac{i\omega_c}{2k_c}\frac{\partial B_h}{\partial t_1} = G_{2,h} \tag{C.59}$$

$$-2\frac{\partial^2\phi_{1,h}}{\partial x_0\partial x_1} = -ik_c\frac{\partial a_h}{\partial x_1} = -\omega_c\frac{\partial B_h}{\partial x_1} = H_{2,h} \tag{C.60}$$

Setter dette inn i (C.57)

$$-\int_{-\infty}^{0}\left(\frac{a_h\omega_c}{2}\frac{\partial B_h}{\partial x_1}e^{2k_cz}\right)\mathrm{dz} = -\frac{a_h}{2}e^0\left[-\frac{1}{2}\frac{\partial B_h}{\partial t_1}+\frac{i\omega_c}{g}\frac{i\omega_c}{2k_c}\frac{\partial B_h}{\partial t_1}\right]$$

$$\Rightarrow \frac{\partial B_h}{\partial t_1}+\frac{\omega_c}{2k_c}\frac{\partial B_h}{\partial x_1}=0 \tag{C.61}$$

som er det samme som (C.30).

C.3.3 Løsbarhetsbetingelse til tredje orden

Jeg kan altså finne løsbarhetsbetingelsen til tredje orden ved å finne F_{31}, G_{31} og H_{31}, og benytte likning (C.57). Jeg ser først på bølgen som forplanter seg mot høyre.
I den kinematiske randbetingelsen (C.46) vil høyresiden ha resonante bidrag fra $\frac{\partial\eta_1}{\partial t_2}$,$\frac{\partial\eta_2}{\partial x_0}\frac{\partial\phi_1}{\partial x_0}$, $\frac{\eta_1^2}{2}\frac{\partial^3\phi_1}{\partial z^3}$, $\eta_2\frac{\partial^2\phi_1}{\partial z^2}$ og $\eta_1\frac{\partial^2\phi_1}{\partial z\partial x_0}\frac{\partial\eta_1}{\partial x_0}$. Jeg får at

$$F_{3,1} = -\frac{1}{2}\frac{\partial B_h}{\partial t_2}+\frac{1}{16}i\omega_c k_c^2 B_h^2 B_h^* - \frac{3}{8}i\omega_c k_c^2 B_h B_v B_v^*$$

Går frem på tilsvarende måte for den dynamiske randbetingelsen (C.47) og finner at

$$G_{3,1} = \frac{i\omega_c}{2k_c}\frac{\partial B_h}{\partial t_2}+\frac{1}{2k_c}\frac{\partial^2 B_h}{\partial t_1^2}-\frac{9}{16}\omega_c^2 k_c B_h^2 B_h^* + \frac{1}{8}\omega_c^2 k_c B_h B_v B_v^*$$

Setter inn i (C.57) og får at høyresiden blir

$$H.S. = -\frac{i\omega_c}{2k_c}B_h\frac{\partial B_h}{\partial t_2}-\frac{1}{4k_c}B_h\frac{\partial^2 B_h}{\partial t_1^2}+\frac{1}{4}\omega_c^2 k_c B_h^3 B_h^* + \frac{1}{8}B_h^2 B_v B_v^*$$

Finner resonante bidrag fra høyresiden i Poissons likning (C.48), og disse gir

$$H_{3,1} = \left(i\frac{\partial^2 B_h}{\partial t_1\partial x_1}+i\omega_c z\frac{\partial^2 B_h}{\partial x_1^2}-\omega_c\frac{\partial B_h}{\partial x_2}+\frac{i\omega_c}{2k_c}\frac{\partial^2 B_h}{\partial x_1^2}\right)e^{k_cz}$$

Venstresiden i (C.57) blir

$$V.S. = \frac{\omega_c}{4k_c^2}B_h\frac{\partial^2 B_h}{\partial t_1\partial x_1}+\frac{i\omega_c^2}{4k_c^2}B_h\frac{\partial B_h}{\partial x_2}$$

Kombinerer disse, og løsbarhetsbetingelsen blir

$$\begin{aligned}&\frac{\omega_c}{4k_c^2}B_h\frac{\partial^2 B_h}{\partial t_1\partial x_1}+\frac{i\omega_c^2}{4k_c^2}B_h\frac{\partial B_h}{\partial x_2}+\frac{i\omega_c}{2k_c}B_h\frac{\partial B_h}{\partial t_2}\\ &+\frac{1}{4k_c}B_h\frac{\partial^2 B_h}{\partial t_1^2}-\frac{1}{4}\omega_c^2 k_c B_h^3 B_h^*-\frac{1}{8}B_h^2 B_v B_v^*=0\\ \Rightarrow\ &\frac{\partial B_h}{\partial t_2}+\frac{\omega_c}{2k_c}\frac{\partial B_h}{\partial x_2}-\frac{i}{2k_c}\frac{\partial^2 B_h}{\partial t_1\partial x_1}-\frac{i}{2\omega_c}\frac{\partial^2 B_h}{\partial t_1^2}+\frac{i}{2}\omega_c k_c^2|B_h|^2 B_h+\frac{i}{4}\omega_c k_c^2|B_v|^2 B_h=0\end{aligned} \tag{C.62}$$

Jeg husker løsbarhetsbetingelsen fra andre orden, (C.30). Multipliserer denne med ϵ og legger den sammen med ϵ^2(C.62), da kan jeg kombinere for eksempel leddene som inneholder $\frac{\partial B_h}{\partial t_2}$ og $\frac{\partial B_h}{\partial t_1}$ slik at jeg får $\frac{\partial B_h}{\partial t}$. På samme måte kan jeg trekke ϵ^2 inn i $\frac{\partial^2 B_h}{\partial t_1 \partial x_1}$, og står igjen med $\frac{\partial^2 B_h}{\partial t \partial x}$. Jeg finner et uttrykk for $\frac{\partial B_h}{\partial t_1}$ som jeg kan sette inn igjen i likningen (iterasjon). På den måten kan jeg eliminere t-avhengighet fra kryssleddet $\frac{\partial B_h}{\partial x \partial t}$ samt leddet $\frac{\partial^2 B_h}{\partial t^2}$ og står igjen med følgende

$$\frac{\partial B_h}{\partial t} + \frac{\omega_c}{2k_c}\frac{\partial B_h}{\partial x} + \frac{i\omega_c}{8k_c^2}\frac{\partial^2 B_h}{\partial x^2} + \frac{i}{2}\omega_c k_c^2 |B_h|^2 B_h + \frac{i}{4}\omega_c k_c^2 |B_v|^2 B_h = 0 \qquad \text{(C.63)}$$

På samme måte kan jeg finne en løsbarhetsbetingelse for bølgen for forplanter seg mot venstre.

$$\frac{\partial B_v}{\partial t} - \frac{\omega_c}{2k_c}\frac{\partial B_v}{\partial x} + \frac{i\omega_c}{8k_c^2}\frac{\partial^2 B_v}{\partial x^2} + \frac{i}{2}\omega_c k_c^2 |B_v|^2 B_v + \frac{i}{4}\omega_c k_c^2 |B_h|^2 B_v = 0 \qquad \text{(C.64)}$$

Dette er de to koblede ikkelinære Schrödinger-likningene som beskriver kryssende sjø i det spesielle tilfellet at to bølgefelt med samme karakteristiske frekvens ω_c og samme karakteristiske bølgetall k_c forplanter seg i motsatt retning.

C.4 Sammenlikning med tidligere arbeider

Det er interessant å gå til litteraturen for å sammenlikne både de andre ordens koeffisientene jeg har funnet, samt koeffisiente i de koblede ikkelineære Schrödinger-likningene med tidligere arbeider. I artiklene jeg har studert er det ingen som nevner noe om hvordan koeffisientene for andre orden ser ut. Derimot er disse oppgitt i Trulsen [5], men jeg har dessverre ikke tid til å gå i detalj på denne sammenlikningen nå. Når det gjelder de koblede Schrödinger-likningene er disse utledet/listet opp i flere artikler, for ulike varianter av problemet som studeres i dette prosjektet.

C.4.1 Gramstad og Trulsen

Gramstad og Trulsen [6] studerer problemet hvor to todimensjonale bølgesystemer har ulike bølgetall og/eller retninger. De opererer med bølgetall $\mathbf{k_a}$ og $\mathbf{k_b}$, $\mathbf{k_{a+b}} = \mathbf{k_a} + \mathbf{k_b}$, $k_{a+b} \neq k_a + k_b$ (og tilsvarende for ω). For mitt problem tilsvarer dette

$$k_a = k_c = -k_b \Rightarrow k_{a+b} = 0, k_{a-b} = 2k_c$$
$$\omega_a = \omega_b = \omega_c \Rightarrow \omega_{a+b} = 2\omega_c, \omega_{a-b} = 0.$$

Følgende likningssystem finnes (med min notasjon)

$$\frac{\partial A}{\partial t} + \frac{1}{2}\frac{\omega_c}{k_c}\frac{\partial A}{\partial x} + \frac{i\omega_c}{8k_c^2}\frac{\partial^2 A}{\partial x^2} + ik_c^3|A|^2 A + iE|B|^2 A = 0$$
$$\frac{\partial B}{\partial t} - \frac{1}{2}\frac{\omega_c}{k_c}\frac{\partial B}{\partial x} + \frac{i\omega_c}{8k_c^2}\frac{\partial^2 B}{\partial x^2} + ik_c^3|B|^2 B + iE|A|^2 B = 0$$

hvor E kan finnes uttykt ved $\omega_a,\ \omega_b,\ \omega_{a+b}$ og ω_{a-b}. I mitt tilfelle blir $E = \frac{1}{2}k_c^3$, og det endelige likningssystemet blir

$$\frac{\partial A}{\partial t} + \frac{1}{2}\frac{\omega_c}{k_c}\frac{\partial A}{\partial x} + \frac{i\omega_c}{8k_c^2}\frac{\partial^2 A}{\partial x^2} + ik_c^3|A|^2A + \frac{i}{2}k_c^3|B|^2A = 0$$
$$\frac{\partial B}{\partial t} - \frac{1}{2}\frac{\omega_c}{k_c}\frac{\partial B}{\partial x} + \frac{i\omega_c}{8k_c^2}\frac{\partial^2 B}{\partial x^2} + ik_c^3|B|^2B + \frac{i}{2}k_c^3|A|^2B = 0$$

Sammenligner definisjonen av A og B med min definisjon av B_h og B_v. Jeg har at

$$\sqrt{\frac{2k}{\omega}}A_G = B_R$$
$$A_G = \sqrt{\frac{\omega}{2k}}B_R$$

Dersom dette settes inn i likningen kan det vises at koeffisienten foran det første ikkelineære leddet i likningene blir $\frac{i}{2}\omega_c k_c^2$, som er det samme som jeg fikk i mine løsbarhetsbetingelser. Foran det ikkelineære kryssleddet står det $\frac{i}{4}\omega_c k_c^2$ som også stemmer med mine resultater! Altså har jeg bekreftet at koblingskoeffisientene α og β fra innledningen ser slik ut:

$$\alpha = \beta = \frac{i}{4}\omega_c k_c^2$$

C.4.2 Roskes

Roskes sin artikkel fra 1976 [7] omhandler følgende koblede ikkelineære Schrödinger-likninger:

$$A_{1t} = i\gamma_1 A_{1xx} + iA_1\left(\beta_{11}|A_1|^2 + \beta_{12}|A_2|^2\right)$$
$$A_{2t} = i\gamma_2 A_{2xx} + iA_2\left(\beta_{21}|A_1|^2 + \beta_{22}|A_2|^2\right)$$

Roskes har studert to bølgekomponeneter (A_1 og A_2) som vekselvirker på dypt vann, i det tilfellet at modulasjoner oppstår i den retningen projeksjonene av gruppehastigheten overlapper. Jeg ser for meg A og B som to bølger som begge beveger seg i positiv x-retning, men med ulike vinkler til x-aksen. X-retningen vil da være den retningen hvor projeksjoner av gruppehastigheten overlapper, og altså den retning hvor det finnes modulasjoner. Problemet jeg studerer tilsvarer å øke vinkelen mellom de to bølgekomponentene, helt til den ene beveger seg i positiv y-retning og den andre i negativ y-retning (vinkelen mellom de to komponentene er da π).

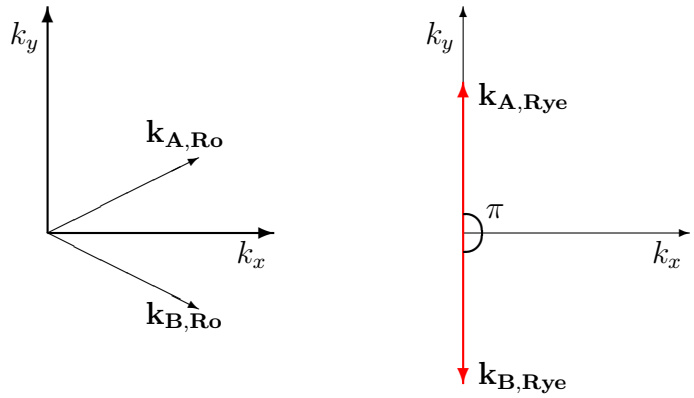

Så retningen for modulasjonene som kan tillates i Roskes problem vil være på tvers av aksen som mine to bølgekomponenter forplanter seg langs. Dette kan også sees lett fordi det ikke finnes noe ledd av typen A_{iyy} i Roskes likninger for overflatehevningen, det finnes kun A_{ixx}. Og siden hans x-retning svarer til min y-retning finnes det altså ingen modulasjoner i forplantningsretningen for mitt tilfelle, og jeg kan ikke bruke Roskes resultater som sammenligningsgrunnlag for mine egne. En annen observasjon når det gjelder Roskes sine likninger er at de heller ikke inneholder ledd av typen A_x eller A_y. Dette betyr enten at han har valgt et koordinatsystem som beveger seg med gruppehastigheten, eller at bølgefeltet er uniformt. Det fremgår ikke av artikkelen hvilken av disse to forklaringene som er den rette. Koeffisientene for de ikkelineære leddene i Roskes sitt likningssystem er $\beta_{11} = -\frac{1}{2}\omega k_c^2$ og $\beta_{12} = \omega k_c$. Når disse leddene flyttes over på andre siden (og løsbarhetsbetingelsen får en form jeg kan sammenlikne med mine resultater, blir koeffisienten på det første ikkelineære leddet riktig, mens det for kryssleddet avviker fra mine resultater med et fortegn og en faktor fire.

C.4.3 Onorato, Osborne og Serio

En annen artikkel som det er populært å refere til er den av Onorato et al. [8]. Her er det studert et tilfelle med to bølgekomponenter A og B som propagerer i ulike retninger. De propagerer på en slik måte at x-komponenten av bølgetallet er den samme for de to bølgene, mens y-komponenten har samme tallverdi, men er henholdsvis positiv og negativ. Altså er bølgetallsvektorene $\mathbf{k}^{(A)} = (k, l)$ og $\mathbf{k}^{(B)} = (k, -l)$. Onorato et.al kommer frem til følgende likningssystem:

$$\begin{aligned}
&\frac{\partial A}{\partial t} + C_x\frac{\partial A}{\partial x} + C_y\frac{\partial A}{\partial y} - i\alpha\frac{\partial^2 A}{\partial x^2} \\
&\quad - i\beta\frac{\partial^2 A}{\partial y^2} + i\gamma\frac{\partial^2 A}{\partial x\partial y} + i\left(\xi|A|^2 + 2\zeta|B|^2\right)A = 0 \\
&\frac{\partial B}{\partial t} + C_x\frac{\partial B}{\partial x} - C_y\frac{\partial B}{\partial y} - i\alpha\frac{\partial^2 B}{\partial x^2} \\
&\quad - i\beta\frac{\partial^2 B}{\partial y^2} - i\gamma\frac{\partial^2 B}{\partial x\partial y} + i\left(\xi|B|^2 + 2\zeta|A|^2\right)B = 0
\end{aligned}$$

og koeffisientene er definert på følgende måte

$$\kappa = \sqrt{k^2 + l^2}, \quad C_y = \frac{\omega(\kappa)}{2\kappa^2} l, \quad \beta = \frac{\omega(\kappa)}{8\kappa^4}(2k^2 - l^2),$$
$$\xi = \frac{1}{2}\omega(\kappa)\kappa^2\zeta = \frac{\omega(\kappa)}{2\kappa}\frac{k^5 - k^3l^2 - 3kl^4 - 2k^2\kappa + 2k^2l^2\kappa + 2l^4\kappa}{(k - 2\kappa)\kappa}$$

Her er det noe muffens med definisjonene av ξ og ζ. Problemet jeg har studert er et spesialtilfelle av det Onorato et al. har studert, ved at $k = 0$, og $l = \pm k_c$. Deres x er altså min y (som for Roskes), og jeg har derfor sett bort fra koeffisientene som er knyttet til den x-deriverte. Hvis jeg regner ut ξ fra den nederste likningen, får jeg $\xi = -\frac{1}{2}\omega l^2$ og $\zeta = -1$. Dette kan ikke stemme fordi dimensjonen på ζ (og det siste leddet i likningene) blir feil! Min teori er at det er en trykkfeil i artikkelen, og at ζ skal stå på neste linje. I såfall blir $\xi = \frac{1}{2}\omega(\kappa)l^2$ og $\zeta = -\xi$. Da blir dimensjonene og koeffisienten på det første ikkelineære leddet riktig i forhold til mine resultater, mens koeffisienten for kryssleddet avviker med et fortegn og en faktor fire. Jeg vet selvsagt ikke med sikkerhet at det er dette som burde stått i definisjonene av ξ og ζ, det eneste som er sikkert er at slik det er presentert i artikkelen må det være feil. Jeg synes det er bekymringsfullt at flere senere artikkelforfattere har refert til og kopiert dette likningssystemet, uten å påpeke denne finurligheten i Onoratos definisjoner av koeffisientene. Dette er gjort av blant andre Shukla et al. [10, 11] og Toffoli et al. [9] og Grönlund et al. [12] (både [11] og [12] har gjort samme antagelse som meg på hvordan ξ og ζ er definert, men uten å kommentere en eventuell trykkfeil i artikkelen likningene er hentet fra) .

C.5 Konklusjon

Jeg har beskrevet kryssende sjø i det spesielle tilfellet at to bølgefelt med samme karakteristiske frekvens ω_c og samme karakteristiske bølgetall k_c forplanter seg i motsatt retning. Jeg har bestemt alle $B_{2,?}$, som er langsomme funskjoner av tid og rom for å beskrive modulasjon rundt den karakteristiske bølgen.

Jeg har vist at det ikke kan finnes ledd av typen $e^{2ik_cx_0}$, da både $B_{2,2x}$ og $a_{2,2x}$ er 0. Dette leddet ville ha tilsvart stående svingninger i rommet. Jeg har vist at det fins bidrag på formen $e^{2i\omega_ct_0}$ som tilsvarer stående svingninger i tid. Jeg har vist at $B_{2,h}$ og $B_{2,v}$ kan settes lik null dersom man pålegger passende krav på de tilsvarende koeffisientene i hastighetspotensialet samt løsbarhetsbetingelser på koeffisientene i overflatehevningen. I tillegg har jeg funnet at $B_{2,0}$ er null, og $a_{2,0}$ er en konstant slik jeg kjenner den.

Jeg har funnet løsbarhetsbetingelser til tredje orden for bølger som forplanter seg mot høyre

$$\frac{\partial B_h}{\partial t} + \frac{\omega_c}{2k_c}\frac{\partial B_h}{\partial x} + \frac{i\omega_c}{8k_c^2}\frac{\partial^2 B_h}{\partial x^2} + \frac{i}{2}\omega_c k_c^2 |B_h|^2 B_h + \frac{i}{4}\omega_c k_c^2 |B_v|^2 B_h = 0$$

og mot venstre

$$\frac{\partial B_v}{\partial t} - \frac{\omega_c}{2k_c}\frac{\partial B_v}{\partial x} + \frac{i\omega_c}{8k_c^2}\frac{\partial^2 B_v}{\partial x^2} + \frac{i}{2}\omega_c k_c^2 |B_v|^2 B_v + \frac{i}{4}\omega_c k_c^2 |B_h|^2 B_v = 0$$

Har også sammenlignet disse med tidligere arbeider, og funnet at mine resultater samsvarer med Gramstad og Trulsen [6].

Det som åpenbart gjenstår er å få full klarhet i om det faktisk er noe muffens med Onorato et al. [8] sine definisjoner av koeffisientene for de ikkelineære leddene, og å sammenlikne hans likninger med mine. Det hadde også vært bra å sammenlikne koeffisientene for de andre ordens bidragene jeg fant med tidligere arbeider (Trulsen [5]).

Referanser

[1] C. Guedes Soares, *Representation of double-peaked sea wave spectra.* Ocean Eng., **18**, 185 (1984).

[2] C. Guedes Soares, *On the occurrence of double peaked wave spectra.* Ocean Eng., **11**, 167 (1991).

[3] A.V. Boukhanovsky and C. Guedes Soares, *Modelling of multipeaked directional wave spectra.* Appl. Ocean Res., **31**, 132 (2009).

[4] V.E. Zakharov *Stability of periodic waves of finite amplitude on the surface of a deep fluid.* J. Appl. Mech. Tech. Phys., **9**, 190 (1968).

[5] K. Trulsen, *Tsunamis, rogue waves, internal waves and internal tides.* Springer Wien New York, chapter: Weakly nonlinear and stochastic properties of ocean wave fields. Application to an extreme wave event, pp. 49-106 (2006).

[6] O. Gramstad and K. Trulsen, *Fourth-ordered coupled nonlinear Schödinger equations for gravity waves on deep water.* Phys. Fluids, **23**, 062102 (2011).

[7] G. J. Roskes, *Nonlinear multiphase deepwater wavetrains.* Phys. Fluids, **19**, 1253 (1976).

[8] M. Onorato, A.R. Osborne and M. Serio, *Modulational instability in crossing sea states: A possible mechanism for the formation of freak waves.* Phys. Rev. Lett., **96**, 014503 (2006).

[9] A. Toffoli, E.M. Bitner-Gregersen, A.R. Osborne, M. Serio, J. Monbaliu and M. Onorato, *Extreme waves in random crossing seas: Laboratory experiments and numerical simulation.* Geophysical Research Letters, **38**, L06605(2011).

[10] P.K. Shukla, M. Marklund and L. Stenflo, *Modulational instability of nonlinearly interacting incoherent sea states.* JETP Letters, **84**, No.12, pp. 645-649 (2006).

[11] P.K. Shukla, I. Kourakis, B. Eliasson, M. Marklund and L. Stenflo, *Instability and evolution of nonlinearly interacting water waves.* Phys. Rev. Lett., **97**, 094501 (2006).

[12] A. Grönlund, B. Eliasson and M. Marklund, *Evolution of rouge waves in interacting wave systems*. Europhysics Letters, **86**, 24001 (2009).